



# Modelling of Thermal Resistance and Some Other Comfort Parameters of Socks in Wet State

## Dissertation Thesis

*Study programme:*

P3106 Textile Engineering

*Study branch:*

Textile Technics and Materials Engineering

*Author:*

**Tariq Mansoor, M.Sc.**

*Thesis Supervisor:*

prof. Ing. Luboš Hes, DrSc.

Department of Textile Evaluation



# Declaration

I hereby certify, I, myself, have written my dissertation as an original and primary work using the literature listed below and consulting it with my thesis supervisor and my thesis counsellor.

I acknowledge that my bachelor dissertation is fully governed by Act No. 121/2000 Coll., the Copyright Act, in particular Article 60 – School Work.

I acknowledge that the Technical University of Liberec does not infringe my copyrights by using my dissertation for internal purposes of the Technical University of Liberec.

I am aware of my obligation to inform the Technical University of Liberec on having used or granted license to use the results of my dissertation; in such a case the Technical University of Liberec may require reimbursement of the costs incurred for creating the result up to their actual amount.

At the same time, I honestly declare that the text of the printed version of my dissertation is identical with the text of the electronic version uploaded into the IS/STAG.

I acknowledge that the Technical University of Liberec will make my dissertation public in accordance with paragraph 47b of Act No. 111/1998 Coll., on Higher Education Institutions and on Amendment to Other Acts (the Higher Education Act), as amended.

I am aware of the consequences which may under the Higher Education Act result from a breach of this declaration.

July 2, 2020

Tariq Mansoor, M.Sc.

## **Preface**

This dissertation is the result of my own work and includes nothing which is the outcome of work done in collaboration. The presented work was undertaken at the Department of Textile Evaluation, Technical University of Liberec, Czech Republic. No other part of this dissertation has been submitted for a degree to this or any other university. This dissertation contains approximately 33325 words, 55 figures and 32 tables.

**Tariq Mansoor, M.Sc.**

**Student ID: T15000566**

## **Abstract**

A human foot may exhibit a sweat rate of about 30g and in some cases even up to 50g per hour in a hot environment [1][2]. The average sweat rate reaches around 10g/h per foot during heavy exercise in a cold environment. This sweat rate may reach to 30g/h per foot during very high levels of exercise. During common occupational exposures, the sweat rates are expected to lie between 3-6g/h [3][4]. The thermal resistance of wet fabrics gets substantially reduced due to the considerably higher thermal conductivity of the absorbed water as compared to that of air. Keeping high thermal resistance of their socks is important for people working under wet conditions to be protected from trench foot and hypothermia like issues. Thermal resistance prediction is also very important for product development of different textiles.

In the study, an algebraic model and its experimental verification were executed to investigate the effect of moisture content on the thermal resistance of sock fabrics and the results were mutually in good agreement. The results show that increasing moisture content in the studied sock fabrics caused a significant reduction in their thermal resistance. Along with the model and its experimental verification, a novel method to measure thermal resistance and comfort properties of various knitted socks samples under real conditions of their use (it means under extension and in wet state) was proposed.

Generally, any level of moisture largely influences all thermophysiological properties of textile fabrics. Therefore, plain knitted socks with different fibre composition were wetted to a saturated level, and then stepwise their moisture content was reduced. When achieving the required moisture content, the socks samples characteristics were determined by the Alambeta testing instrument (as regards thermal resistance and thermal absorptivity), and by the Permetest tester (as for relative water vapor permeability) and by the Horizontal Plate Friction Analyzer (to get the coefficient of friction in the wet state).

Moreover, various skin models were also utilized to get thermal resistance values of dry samples for the comparison. One of these thermal models was a special thermal model of the human foot. The experimental results from this model well correlated with the results from the Permetest skin model.

Three different existing mathematical models for the thermal resistance of dry fabrics were modified for predicting thermal resistance of knits used in socks under wet conditions. Volume porosity values of the studied fabrics, used in these thermal models, were determined both by means of semi-empirical approach and by a micro-tomography procedure. The results from both ways are in very good agreement for all the socks at a 95% confidence level.

In the above-mentioned models, the prediction of thermal resistance presents newly a combined effect of the real filling coefficient and thermal conductivity of the so-called “wet” polymers instead of dry polymers. With these modifications, the used models predicted the thermal resistance at different moisture levels with a significantly high coefficient of correlation.

Along with thermal resistance, the thermal absorptivity of the sock fabrics in a wet state (this time experimentally only) was first time investigated in the Thesis. This parameter increases with the increasing moisture content of materials, this time of textile fabrics. It characterises thermal contact feeling from dry to cool, cold, and wet feelings of any objects. The results of this study show that thermal absorptivity values of the studied dry fabrics range from 80 to 180 [ $\text{Ws}^{1/2}\text{m}^{-2}\text{K}^{-1}$ ]. As thermal conductivity and capacity of water are much higher than that of fibres and air entrapped in the textile structure is partly replaced by water and thermal absorptivity of wetted fabrics increases. In these thermal absorptivity measurements, the effect of an extension of socks during their practical use was also newly respected.

As already mentioned, moisture in textiles also significantly affects (reduces) the vapor permeability of fabrics. Because the measurement of the vapor permeability of wet textiles by conventional commercial instruments is difficult (the measurement takes too long, so that the moisture evaporates during the measurement), there are very few relevant publications. Given that vapor permeability is the second main parameter of thermo-physiological comfort of textiles, in the last part of the work the influence of moisture on the vapor permeability of socks was also studied experimentally by using the original methodology developed several years ago at the Faculty of Textiles TU Liberec. It was found that the effective relative vapor permeability of wet sock knits made of synthetic fibers is higher than the vapor permeability of wet knits made of natural materials.

In the (appendix 3) of the study, the newly developed (upgraded) models of thermal resistance of wetted fabrics were successfully applied on some knitted and woven fabrics of different composition. The next research in this area will follow.

### **Keywords**

Thermal resistance; mathematical modelling; relative water vapor permeability; thermal absorptivity; plain socks; moisture content; filling coefficient; volume porosity; coefficient of friction.

## Abstrakt

Lidská noha může v horkém prostředí za hodinu vytvořit 30 gramů, někdy dokonce až 50 gramů potu. Průměrná produkce potu při intenzivním cvičení v chladu činí kolem 10 g/h na nohu. Intenzita pocení může dosáhnout až 30 g/h na nohu při velmi vysokých úrovni cvičení, zatímco během běžných pracovních aktivit bude produkce potu ležet mezi 3-6 g/h [3][4]. Tepelný odpor vlhkých textilií se podstatně snižuje díky mnohokrát vyšší tepelné vodivosti absorbované vody ve srovnání s tepelnou vodivostí vzduchu. Zachování vysokého tepelného odporu ponožek je důležité pro osoby pracující ve vlhkých podmínkách, aby byli chráněni před zákopy a problémy s podchlazením. Predikce tepelného odporu je také velmi důležitá při vývoj různých ochranných a sportovních textilií.

Ke zkoumání vlivu obsahu vlhkosti ponožkových textilií na jejich tepelný odpor byl v této práci sestaven matematický (algebraický) model a vypočtené výsledky byly v dobré shodě s výsledky experimentálními. Výsledky ukazují, že zvyšující se obsah vlhkosti ve studovaných textiliích vedl k podstatnému snížení jejich tepelného odporu. Ve zmíněném matematickém modelu, ale při proměrování tepelného modelu vzorků byly nově respektovány (realizovány) konkrétní podmínky užívání ponožek v praxi, tj. kromě vlivu vlhkosti bylo při výpočtech i měření simulováno prodloužení ponožek při jejich nošení.

Obecně, jakékoli úrovně absorbovaná v textiliích významně ovlivňuje všechny parametry jejich termo-fyziologického komfortu. Proto byly hladké ponožkové úplety s různým složením vláken navlhčeny na maximální úroveň a postupně vysoušeny na požadovaný obsah vlhkosti. Takto připravené vzorky ponožek byly poté proměřovány přístrojem Alambeta (pro zjištění jejich tepelného odporu a tepelné jímavosti), dále byl použit i přístroj Permetest typu Skin model (pro stanovení relativní propustnosti vzorků pro vodní páru) a na zahraničním pracovišti byl k relativně novým měřením použit Horizontální deskovým analyzátořem tření (pro zjištění součinitele tření ponožkových textilií ve vlhkém stavu).

Kromě toho byly tepelné odpory nezavlhčených vzorků ponožek pro možnost porovnání výsledků měřeny i na jiných tzv. Skin modelech s různou geometrií. Jedním z nich byl tepelný model lidské nohy. Výsledky z tohoto modelu velmi dobře korelují s výsledky získaných pomocí malého Skin modelu Permetest.

Pro predikci tepelného odporu vlhké textilie byly původním způsobem modifikovány tři různé již existující matematické modely pro suché textilie. Tyto modely sestavené pro predikci tepelného odporu ponožkových textilií jsou nově založeny na kombinovaném účinku skutečného koeficientu objemového zaplnění a tepelné vodivosti tzv. vlhkého vlákenného polymeru namísto polymeru suchého. Hodnoty objemové porozity textilií, nezbytné ke konstrukci uvedených tepelných modelů, byly zjištěny semi-empirickým postupem a také pomocí tzv. mikro-tomografie. Výsledky obou postupů způsobů jsou pro všechny ponožkové textilie na 95% úrovni spolehlivosti prakticky shodné. Algebraické modely, sestavené na základě výše uvedených postupů a modifikací umožňují stanovení a predikci tepelných odporů všech zkoumaných ponožkových textilií při relativně rozsáhlém stupni zavlhčení s významně vysokým součinitelem korelace.

Vedle tepelných odporů, byl v této práci také poprvé experimentálně studován vliv vlhkosti na tepelnou jímavost ponožkových textilií. Tento parametr roste se zvyšováním obsahu vlhkosti v materiálech, v našem případě plošných textiliích a postupně může charakterizovat suchý, teplý chladný a mokrá tepelně – kontaktní vjem. Výsledky této studie ukazují, že hodnoty tepelné jímavosti zkoumaných nezavlhčených suchých tkanin se pohybují od 80 do 180 [ $Ws^{1/2}m^{-2}K^{-1}$ ]. Ve vlhké textilií je vzduch o nízké tepelné vodivosti částečně nahrazen vodou o cca 25 x vyšší tepelné vodivosti a vysoké tepelné kapacitě, takže výsledná tepelná vodivost vlhké textilie podstatně vzroste. Jak již bylo uvedeno, při měření tepelných odporů bylo (prakticky ověřeném) prodloužením vzorku simulováno prodloužení ponožek při jejich nošení. Tento přístup byl nově aplikován i při hodnocení tepelné jímavosti zavlhčených ponožkových textilií.

Jak již bylo uvedeno, vlhkost v textiliích také významně ovlivňuje (snižuje) paropropustnost plošných textilií. Vzhledem k tomu, že měření paropropustnosti vlhkých textilií klasickými komerčními přístroji je obtížné (měření trvá příliš dlouho, takže vlhkost se při měření odpaří), příslušných publikací je velmi málo. Vzhledem k tomu, že paropropustnost je druhým hlavním parametrem termo-fyziologického komfortu textilií, byl v poslední části práce vliv vlhkosti na paropropustnost ponožkových úpletů rovněž systematicky experimentálně studován, a to pomocí originální metodiky vyvinuté před několika lety na fakultě textilní TU Liberec. Bylo zjištěno, že efektivní relativní paropropustnost vlhkých ponožkových úpletů ze syntetických vláken je vyšší než paropropustnost vlhkých úpletů z přírodních materiálů.

V (příloze 3) práce jsou nově vytvořené modely tepelného odporu vlhkých ponožkových úpletů také s dobrými výsledky použity ke stanovení tepelného odporu vybraných tkanin z různých vlákenných materiálů. Výzkum v této oblasti bude pokračovat.

### **Klíčová slova**

Teplotní odolnost; matematické modelování; relativní propustnost pro vodní páru; tepelná nasákavost; holé ponožky; Obsah vlhkosti; plnicí koeficient; objemová pórovitost; koeficient tření.

## **Acknowledgement**

First and foremost, I'm thankful to my God who gave me the capability, courage, and opportunity to complete my Ph.D. thesis, a very long journey full of hardships. The list of those that I would like to acknowledge seems to be endless. However, there are those who provided support, without which this thesis would not have been possible. I would like to thank my parents, wife, and children for their sincere love, enormous support, and patience, for being away from them during the last four years.

I would like to thank my respected supervisor prof. Ing. Luboš Hes, DrSc., the person who helped me to see it through to the end. I'm thankful for his continued encouragement, advice; a prompt response, inclusion, patience, support, invaluable guidance and confidence in my abilities.

It is a great pleasure to thank all those people who helped me during this journey. I will always be grateful to all members of the Textile Evaluation Department in general and especially doc. Ing. Vladimír Bajzík, Ph.D. Without the help of all these people, this thesis would have never been completed.

I will always be grateful to Mr. Navid Fazil COO Interloop Limited Pakistan and Prof. Zenun Skenderi Ph.D. (Faculty of Textile Technology, University of Zagreb Croatia), as well as dean's office of the faculty especially Mrs. Bohumila Keilová and Mrs. Hana Musilova. Last, but certainly not least, I am thankful to the Faculty of Textile Engineering for their financial assistance.

# Contents

Preface .....	i
Abstract .....	ii
Abstrakt .....	v
Acknowledgement.....	viii
Contents.....	ix
List of Figures .....	xiii
List of Tables.....	xvi
List of symbols/ abbreviations .....	xviii
Dissertation outline .....	xx
<i>1 Introduction .....</i>	<i>1</i>
<i>2 Purpose and aim of the thesis.....</i>	<i>4</i>
<i>2.1 Overview of the current state of problem.....</i>	<i>8</i>
2.1.1 Thermal resistance .....	8
2.1.2 Maxwell–Eucken2 (ME2)’s modified model .....	13
2.1.3 Schuhmeister’s modified model .....	14
2.1.4 Militky’s modified model.....	14
2.2 Porosity.....	15
2.3 Thermal absorptivity .....	16
2.4 Relative water vapor permeability .....	17
2.5 Coefficient of friction.....	19
<i>3 Materials and Methods.....</i>	<i>21</i>
3.1 Fibre fineness .....	21
3.2 Yarn linear density, twist & porosity .....	21
3.3 Socks samples .....	25

3.4	Fibre quantitative analysis.....	31
3.5	Volume socks porosity by model .....	31
3.6	3D porosity of socks by micro-tomography scanning .....	32
3.7	Sample preparation for testing .....	32
3.8	Testing equipments/ methods.....	34
3.8.1	Alambeta (equivalent to ISO 8301).....	34
3.8.2	Permetest .....	36
3.8.3	Thermal foot model .....	37
3.8.4	Averaging thermal conductivity & filling coefficient calculations .....	38
3.8.5	Validation of the models.....	40
3.8.6	Frictional characteristics of socks in wet conditions .....	41
4	<i>Results and discussions</i> .....	43
4.1	Socks porosity .....	43
4.1.1	Volume porosity of socks by model & micro-tomography (MCT).....	43
4.2	Effect of moisture content on thermal resistance .....	50
4.3	Assumptions for theoretical models.....	51
4.3.1	Effect of moisture content on cotton socks (P1).....	52
4.3.2	Effect of moisture content on viscose socks (P2).....	55
4.3.3	Effect of moisture content on polyester socks (P3).....	58
4.3.4	Effect of moisture content on polyamide socks (P4).....	61
4.3.5	Effect of moisture content on polypropylene socks (P5) .....	64
4.3.6	Effect of moisture content on wool socks (P6).....	66
4.3.7	Effect of moisture content on acrylic socks (P7).....	69
4.4	Effect of moisture content on thermal absorptivity.....	71
4.5	Effect of moisture content on RWVP .....	72
4.6	Effect of extension on comfort properties.....	74
4.6.1	Effect of extension on thermal resistance.....	75

4.6.2	Effect of extension on thermal absorptivity .....	75
4.6.3	Effect of extension on RWVP .....	76
4.7	Effect of moisture content on coefficient of friction.....	77
4.8	Thermal resistance comparison among different skin models .....	82
5	<i>Conclusion</i> .....	85
6	<i>References</i> .....	88
	Author's publications .....	100
	Author's publications in international conferences.....	101
	<i>Appendixes</i> .....	102
	Appendix 1 .....	102
	Specifications of the Thermal Foot Model [158] .....	102
	Appendix 2 .....	103
	Specifications of the wooden Leg (Salzmann MST Switzerland).....	103
	Appendix 3 .....	104
	Validation of models for other fabrics.....	104
	Appendix 4 .....	105
	GSM and thickness of the plain (single jersey) socks without extension .....	105
	Appendix 5 .....	105
	Coding for thermal resistance prediction in Matlab/ Freemmat .....	105
	Appendix 6 .....	108
	Appendix 7 .....	110
	Appendix 8 .....	113
	Appendix 9 .....	116
	Appendix 10 .....	118
	Appendix 11 .....	121
	Appendix 12 .....	124
	Appendix 13 .....	127

Appendix 14 .....	129
Socks biaxial extension on the wooden leg .....	129
Appendix 15 .....	130
Sock's washing recipe .....	130

## List of Figures

Figure 1. A Ju Wie model diagram .....	9
Figure 2. A model of wetted parallel fiber assemblies (1) Swelled fiber, (2) Water, (3) Saturated air .....	11
Figure 3. The geometry of a porous medium .....	15
Figure 4. Cooling flow from the surface & through the fabric .....	18
Figure 5. Yarn images for diameter measurement .....	24
Figure 6. Knitting style of plain (single jersey) sock construction .....	26
Figure 7. Sock images by macroscopic camera (without extension) .....	27
Figure 8. Sock images by macroscopic camera (with extension) .....	29
Figure 9. Working scheme of micro-tomography .....	32
Figure 10. Schematic illustration of (a) Circle marking, (b) Socks loading on dummy foot, and (c) Embroidery hoop respectively .....	33
Figure 11. Schematic illustration of hysteresis loop showing the paths of the isobar, isostere and isotherm curves .....	33
Figure 12. Worn sock situation inside the shoe .....	34
Figure 13. Time dependence heat flow after contact .....	35
Figure 14. (a) Assembled foot manikin (b) The layout of surface segments.....	37
Figure 15. (a) A semi-permeable membrane of $2.9 \text{ m}^2\text{paW}^{-1}$ glued (b) Open spaces between segments are covered with paper tape .....	38
Figure 16. Horizontal plate friction analyzer (a) Drawing (b) Real situation.....	42
Figure 17. 2D scanned images conversion into 3D images by using NRecon .....	43
Figure 18. Color coded images by CTVox .....	44
Figure 19. Pore size ranges distribution (P1).....	46
Figure 20. Pore size ranges distribution (P2).....	47
Figure 21. Pore size ranges distribution (P3).....	47
Figure 22. Pore size ranges distribution (P4).....	48

Figure 23. Pore size ranges distribution (P5).....	48
Figure 24. Pore size ranges distribution (P6).....	49
Figure 25. Pore size ranges distribution (P7).....	49
Figure 26. Vouolume porosity (micro-tomography vs theoretical).....	50
Figure 27. Schematic presentation of (a) Segmental mass & volume, and (b) Volumetric change during wetting .....	51
Figure 28. Predicted & experimental thermal resistance: P1 (cotton 80%, polyester 18.20%, elastane 1.8%) .....	53
Figure 29. Coefficient of determination predicted & experimental thermal resistance: P1 (cotton 80%, polyester 18.20%, elastane 1.8%).....	53
Figure 30. Predicted & experimental thermal resistance: P2 (viscose 81.08%, polyester 17.22% & elastane 1.77%) .....	56
Figure 31. Coefficient of determination predicted & experimental thermal resistance: P2 (viscose 81.08%, polyester 17.22% & elastane 1.77%).....	56
Figure 32. Predicted & experimental thermal resistance: P3 (polyester 98.38% & elastane 1.62%) .....	59
Figure 33. Coefficient of determination predicted & experimental thermal resistance: P3 (polyester 98.38% & elastane 1.62%) .....	59
Figure 34. Predicted & experimental thermal resistance: P4 (polyamide nylon 70%, polyester 26.54% & elastane 2.63%) .....	62
Figure 35. Coefficient of determination predicted & experimental thermal resistance: P4 (polyamide nylon 70%, polyester 26.54% & elastane 2.63%).....	62
Figure 36. Predicted & experimental thermal resistance: P5 (polypropylene 65.22%, polyester 31.65% & elastane 3.13%) .....	64
Figure 37. Coefficient of determination predicted & experimental thermal resistance: P5 (polypropylene 65.22%, polyester 31.65% & elastane 3.13%).....	65
Figure 38. Predicted & experimental thermal resistance: P6 (wool 76.19%, 21.67% polyester & elastane 2.14%) .....	67
Figure 39. Coefficient of determination predicted & experimental thermal resistance: P6 (wool 76.19%, 21.67% polyester & elastane 2.14%).....	67

Figure 40. Predicted & experimental thermal resistance: P7 (acrylic 81.25%, 17.06% polyester & elastane 1.69%).....	69
Figure 41. Coefficient of determination predicted & experimental thermal resistance: P7 (acrylic 81.25%, 17.06% polyester & elastane 1.69%).....	70
Figure 42. Effect of moisture content on thermal absorptivity.....	72
Figure 43. Effect of moisture content on RWVP.....	74
Figure 44. Effect of extension on thermal resistance.....	75
Figure 45. Effect of extension on thermal absorptivity.....	76
Figure 46. Effect of extension on relative water vapour permeability.....	77
Figure 47. (a) Effect of moisture content on coefficient of friction (b) Average COF at different moisture levels (P1).....	78
Figure 48. (a) Effect of moisture content on coefficient of friction (b) Average COF at different moisture levels (P2).....	78
Figure 49. (a) Effect of moisture content on coefficient of friction (b) Average COF at different moisture levels (P3).....	79
Figure 50. (a) Effect of moisture content on coefficient of friction (b) Average COF at different moisture levels (P4).....	80
Figure 51. (a) Effect of moisture content on coefficient of friction (b) Average COF at different moisture levels (P5).....	80
Figure 52. (a) Effect of moisture content on coefficient of friction (b) Average COF at different moisture levels (P6).....	81
Figure 53. (a) Effect of moisture content on coefficient of friction (b) Average COF at different moisture levels (P7).....	82
Figure 54. Thermal resistance comparison (TFM Vs Alameta).....	83
Figure 55. Thermal resistance comparison (TFM Vs Permetest).....	84

## List of Tables

Table 1. Experimental fibre fineness results .....	21
Table 2. Yarn specification .....	22
Table 3. Constant values for (Eq.27) .....	22
Table 4. Constant values for (Eq.28) .....	23
Table 5. Yarn diameter results .....	25
Table 6. Yarn porosity results .....	25
Table 7. Sock samples specifications.....	26
Table 8. Insole sample specifications .....	31
Table 9. Thermal skin models comparison .....	38
Table 10. Filling coefficients .....	39
Table 11. Different fibres properties.....	40
Table 12. Summary output P1 (ME-2 Mod. Vs Experimental).....	54
Table 13. Summary output P1 (Militky Mod. Vs Experimental) .....	54
Table 14. Summary output P1 (Schuhmeister Mod. Vs Experimental) .....	55
Table 15. Summary output P2 (ME-2 Mod. Vs Experimental).....	57
Table 16. Summary output P2 (Militky Mod. Vs Experimental) .....	57
Table 17. Summary output P2 (Schuhmeister Mod. Vs Experimental) .....	58
Table 18. Summary output P3 (ME-2 Mod. Vs Experimental).....	60
Table 19. Summary output P3 (Militky Mod. Vs Experimental) .....	60
Table 20. Summary output P3 (Schuhmeister Mod. Vs Experimental) .....	61
Table 21. Summary output P4 (ME-2 Mod. Vs Experimental).....	63
Table 22. Summary output P4 (Militky Mod. Vs Experimental) .....	63
Table 23. Summary output P4 (Schuhmeister Mod. Vs Experimental) .....	63
Table 24. Summary output P5 (ME-2 Mod. Vs Experimental).....	65
Table 25. Summary output P5 (Militky Mod. Vs Experimental) .....	66

Table 26. Summary output P5 (Schuhmeister Mod. Vs Experimental) .....	66
Table 27. Summary output P6 (ME-2 Mod. Vs Experimental).....	68
Table 28. Summary output P6 (Militky Mod. Vs Experimental) .....	68
Table 29. Summary output P6 (Schuhmeister Mod. Vs Experimental) .....	69
Table 30. Summary output P7 (ME-2 Mod. Vs Experimental).....	70
Table 31. Summary output P7 (Militky Mod. Vs Experimental) .....	71
Table 32. Summary output P7 (Schuhmeister Mod. Vs Experimental) .....	71

## List of symbols/ abbreviations

Symbol	Description	Units
b	Thermal absorptivity	$W s^{1/2} m^{-2} K^{-1}$
c	Specific heat	$J kg^{-1} K^{-1}$
$F_a$	Filling coefficient of the air	-
$F_w$	Filling coefficient of the wet water	-
$F_{wet\ polymer}$	Filling coefficient of the wet polymer	-
GSM	Gram per meter square / areal density	$gm^{-2}$
h	Thickness	mm
P	Power	W
q	Heat Flow	$W m^{-2}$
$q_0$	Heat flow without sample	$W m^{-2}$
$q_s$	Heat flow with sample	$W m^{-2}$
$R^2$	Coefficient of determination	-
$R_{ct}$	Thermal resistance	$m^2 K W^{-1}$
$R_{ct0}$	Thermal resistance without sample	$m^2 K W^{-1}$
$R_{ctn}$	Thermal resistance with sample	$m^2 K W^{-1}$
RWVP	Relative water vapor permeability	%
SSD	Sum of squares of deviation	-
SSE	Sum of squares of errors	-
TFM	Thermal foot model	-
$t_a$	Ambient temperature	$^{\circ}C$
$\alpha$	Coefficient of convection	$W m^{-2} K^{-1}$
$\lambda$	Thermal conductivity	$W m^{-1} K^{-1}$
$\lambda_a$	Thermal conductivity of the air	$W m^{-1} K^{-1}$
$\lambda_w$	Thermal conductivity of the water	$W m^{-1} K^{-1}$
$\lambda_{fib1}$	First fibre thermal conductivity	$W m^{-1} K^{-1}$
$\lambda_{fib2}$	Second fibre thermal conductivity	$W m^{-1} K^{-1}$
$\lambda_{wet\ polymer}$	Thermal conductivity of the wet polymer	$W m^{-1} K^{-1}$
$\lambda_{fab}$	Thermal conductivity of the fabric (socks)	$W m^{-1} K^{-1}$
$F_w$	Water filling coefficient	-
$F_a$	Air filling coefficient	-

$F_{fib1}$	First fibre filling coefficient	-
$F_{fib2}$	Second fibre filling coefficient	-
	Pretension	mg
	Fibre fineness	dtex
CV	Coefficient of variation	%
$N_{ec}$	English count number (indirect system)	-
$N_m$	Metric count number (indirect system)	-
D	Denier count (direct system)	-
dtex	Deci tex count (direct system)	-
TPI	Twist per inches	-
$\emptyset$	Packing density	-
	Fibre/ yarn diameter (micro meter)	$\mu\text{m}$
$\varepsilon$	Porosity	%
$\rho_0$	Fibre density	$\text{kgm}^{-3}$
$\rho$	Fabric density	$\text{kgm}^{-3}$
a	Thermal diffusivity	$\text{ms}^{-1}$
$q_{dyn}$	Dynamic (transient) heat flow	$\text{Wm}^{-2}$
$q_{steady}$	Steady state heat flow	$\text{Wm}^{-2}$
	Convection air velocity	$\text{ms}^{-1}$
$R_{et}$	Evaporation resistance	$\text{m}^2\text{paW}^{-1}$
ME	Maxwell-Eucken	-
$\mu$	Coefficient of friction (COF)	
	Frictional force	N
$\beta_1$	Slope	-
$\beta_2$	Intercept	-
EMT	Effective medium theory	-
Mod.	Modified	-

## **Dissertation outline**

**Chapter 1** provides a detailed introduction about the dissertation theme that contains current state of the problem and research objectives. **Chapter 2** provides state of the art and discusses related work in previous literatures. The main body of the dissertation is in chapter 3 and chapter 4. **Chapter 3** describes the experimental conditions, materials, methods, equipment, characterizations, modulations and formulas that modified during the research work. **Chapter 4** explains a detailed theoretical, experimental, and statistical analysis of the results derived from different models and experiments. In the end, **Chapter 5** concludes the dissertation and suggests some avenues for further research

# Chapter 1

## *1 Introduction*

Consumers believe comfort as one of the most essential features in their purchase of apparel; therefore companies lean to focal point on their apparel's comfort. Comfort is an amusing condition of physiological and psychosomatic accord among a human being and the surrounding [5]. Thermo-physiological and sensorial are the two major components of the clothing comfort that unite to generate a subjective sensitivity of satisfaction. Thermo-physiological narrates the method how clothing protects and transfers a metabolic heat and mass [6][7], whereas the sensorial deals with the interaction of the wearer's senses and clothing [8][9]. Ventilation, convection, conduction, and radiation are ways of dry heat transfer, whereas several complex processes like sorption and desorption, wicking, evaporation, wet conduction, and condensation involve in wet heat transfer [10][11][12]. Heat transfer due to conduction mostly depends on fibre's thermal conductivity, volume, orientation to the heat flow direction, and fabric construction [13][14].

Garments required not only physiological comfort but also the ability to maintain the sensation and well-being of the wearer during their work. For example when soldiers, fire-fighters, mountain climbers, medical rescuers, or the marathon runners will be more comfortable if their clothing has suitable protection, along with optimum thermophysiological comfort or if their lives and health are in danger by some means due to improper clothes. Unlike general perception about garments (often used in wet state) due to sweat sorption because of damp or rainy weather influences their comfort properties. Thus, the thermophysiological comfort has two main components: thermal resistance and the active cooling in the wet state [15].

Thermal-wet comfort is the strongest perception among tactile and pressure comfort perceived by subjects during exercise [16]. Thermal comfort is mainly dependent on the moisture spread by textile layers, which is related to fibre and yarn characteristics, fabric construction, and finish. The scope of their link to comfort perception in clothing is also affected by garment cutting, design, and fitting. Thermal resistance and water vapor resistance are basic comfort properties [11]. Thermal conductivity and resistance of the fabrics can be evaluated in different ways: experimental method, analytical solution method, and numerical method [17]. It is well recognized that the fabric insulation may be lowered

substantially if the clothing becomes wet probably due to rain penetration. Most of the weather garments generally include a water repellent outer layer. Conversely, clothing is also exposed to moisture from inside due to body perspiration [18]. Moisture in this way leads to condensation of water in the fabric layers, particularly under cold weather conditions. As air is replaced by water molecules, there is a substantial reduction in thermal resistance of the wet fabric observed due to approximately 25 times higher thermal conductivity of water than air [19].

Most of the studies on thermal resistance/conductivity in the wet state to date are experimental and reported a reduction in thermal resistance by increasing the moisture content [20][21][22][23][24]. Bogusławska and Hes have reported a 50% reduction in the thermal resistance between 10 to 20% moisture content in different fabrics [25]. Oğlakcioğlu and Marmarali measured the thermal resistance of cotton knitted fabric in the wet state. They found that the wetted fabrics indicated lower thermal insulation and cooler feeling [22]. Clothing thermal insulation decreases during perspiration, and the amount of reduction varies from 2 to 8%, as related to water accumulation within clothing ensembles [23]. Another study on footwear reported about 19-25% (30-37% in toes) reduction of thermal insulation during sweating [24]. Kalev Kuklane et al. measured the effect of different sweat rates on thermal insulation and found a strong negative correlation. Furthermore, he found that 30% of the total moisture can stay in socks [26]. Wet heat loss results in dry and wet states through thermal manikins are presented from different laboratories. They have observed the condensation within the clothing increased the conductivity of the wet clothing layers [27]. This study will provide a quantitative prediction of the insulation loss with the addition of water in socks.

Thermal absorptivity is another important parameter that is adversely affected by moisture content. It is an objective measurement of the warm-cool sensation and a surface-related attribute of fabrics. A higher value leads to cool, cold, and wet effects; the lowest value has a dry to warm feeling at first contact with the skin. The surface character of the fabric greatly influences this sensation [28]. This warm-cool feeling is also a thermal contact property that is characterized as the maximum heat flux ( $q_{max}$ ) proposed by Kawabata and Hes respectively [29][30]. It is measured, when the fabric touches the human skin for a short time, normally, less than two seconds [30][31][32]. Fabric structural parameters affect the thermal contact feeling measurement [33]. A lot of theoretical (dry state) [34] and experimental (dry and wet states) [35][36][37][33] investigations for thermal absorptivity were reported by the

literature. The areal density of knitted fabrics has a positive correlation with the number of contact points between the human skin and the textile material. It causes to increase the thermal absorptivity [38]. Thermal absorptivity depends also on the fabric surface profile: Smoother surface leads to more contact between the human skin and the textile material [33][39][40]. The characterization of surface profile depends on its definition. “This is generally expressed as the relative height of the major peaks to the valleys” [41] or is “a measure of positive and negative vertical difference from the mean line” [42].

The area of contact between two adjacent bodies promotes the heat flow through conduction. More contact area points will increase the warm-cool feeling through a raise in heat transfer with higher thermal absorptivity. The wet fabric has significantly higher thermal absorptivity as compared to dry one [43][20]. The thermal absorptivity of the common textile products was experimentally investigated by various researches. As per Asif et al. it varies from 20 to 900 [ $Ws^{1/2}m^{-1}K^{-1}$ ], corresponds to dry and wet cotton fabrics [44]. Thermal absorptivity of dry fabrics range 20-300 [ $Ws^{1/2}m^{-1}K^{-1}$ ] reported in the literature and these values increase between 150 and 300 [ $Ws^{1/2}m^{-1}K^{-1}$ ] when the fabrics get wet [45][46].

Water vapour permeability also significantly affected by humidity. Ruckman has studied the effect of moisture regain on water vapour permeability of fabrics without taking into consideration the evaporation of water [47]. Hes and Dolezal reported that as the moisture content of fabric increases, water vapour permeability decreases, but the total relative water vapour permeability (RWVP) increases due to the evaporation of water from the fabric surface [48]. Hes & Araujo simulated the effect of air gaps between the skin and wet fabric on the resulting cooling flow and found that water vapour permeability decreased when the layers of 2mm and 4mm thickness were introduced without any dependence on the fabric moisture content [49]. Water vapour transportability is deteriorated significantly by the higher moisture content. A decrease of 70-80% is observed for wool and wool/viscose blended fabrics, which is caused by exchanging the air pores by water. It means that the physiological properties of the wet fabrics are subject to abrupt changes, significantly affects the quality of the apparel [25].

## Chapter 2

### *2 Purpose and aim of the thesis*

This study deals with the thermal comfort properties of socks in the wet state. Sock insulation is linked to the material thickness and trapped air (porosity) in between the fibres. The increase in the insulation of footwear may not be obvious for the shoes only. It depends on the sock's insulation as well because low insulation shoes can get comparatively more insulation from socks than shoes. Footwear insulation is a vital feature for feet warmth; on the other hand, the sweat generation due to the motion of subjects can strongly affect the foot temperatures. Mostly the cold feet sensation is associated with low skin temperatures due to sweating [50].

Sweating is the reaction of an organism to overheating [51] and primarily a way of thermoregulation by discharging the water from the eccrine glands [52]. Even the well-insulated footwear will start feeling cold on wetting. Socks are made of fabrics where the absorbed moisture can strongly influence their thermal comfort properties since a human foot could generate up to 30-50 grams of sweat per hour in a hot environment [1][2]. At a high physical activity, it could be 30g/h even in the cold environment [3][4]. The work by Smith also verifies Fogarty's findings [1] with an average sweat rate of 27.6g/h [53]. The most recent study reports this range with shoes ( $10.3 \pm 3.6$  g/h) compared to nude ( $12.6 \pm 3.7$  g/h) for a single foot [54]. These sweat rates are quoted just for information, however, the research aims to study the consequences of sweat rates rather than sweat generation. Due to these high sweat rates, the thermal resistance may substantially decrease. Prolonged damp and cold conditions can cause injuries like a trench foot. The trench foot, however, does not require a freezing temperature; it can occur at a hot temperature as well [55].

By using Alambeta fast working tester there were made measurements of thermal resistance and thermal absorptivity of plain surface socks consisting of cotton, viscose, polyester, nylon, polypropylene, wool, and acrylic fibre, with the same plaiting yarn polyester covered elastane, without any special finishing (commercial state). The measurements were executed at different levels of moisture content. Additionally, in these experiments, the extension of socks in their practical use was also observed by using an additional device which made the experiments very realistic. Alambeta testing corresponded well to the use of socks inside a shoe (boundary conditions of first-order). In the next step, the focus was placed on the

development of a mathematical model for the prediction of thermal resistance of plain socks in the wet state. Following models have been tried for the prediction of thermal conductivity/resistance in the wet state. The model's selection criteria based on the assumption that the addition of water changes the volumes and ultimately thermal conduction. These prediction models aren't customized for textiles only but they are being used in the fields of food technology, soil sciences, and civil engineering as well. The first four models involved the moisture effect, but the rest of them are applied by the combined approach of water and polymer components for the determination of thermal conductivity instead of dry polymer.

- ❖ Mangat parallel/ series models [56][19]
- ❖ R.S Hollies model (parallel model) [18]
- ❖ S. Naka model (three parameters model series/ parallel) [57]
- ❖ Dias and Delkumburewatte (three parameters series model) [58]
- ❖ Fricke's model (100% Series) [59]
- ❖ Ju Wei model (considered polymer + air in parallel and air in series) [60]
- ❖ Schuhmeister model (considered 30 % parallel+ 70% series) [61]
- ❖ Baxter model (considered 21 % parallel+ 79% series) [62]
- ❖ Militky (considered 50 % parallel+ 50% series) [63][64]
- ❖ Maxwell Eucken-1 and Maxwell Eucken-2(dispersed and continuous phases) [65][66]

Above all models were compared with the experimental data. Unfortunately, none of these models was offering a good correlation with the experimental data from the wetted socks except Maxwell Eucken-2, Schuhmeister and Militky's models. The solution was based on modifications of these models has done by adopting a combined approach of water and polymer components for determination of thermal conductivity and introduction of linear changes of the filling coefficient (volume ratio) with the increasing moisture. In this way, the predicted thermal resistance of all samples at different moisture levels with the coefficient of determination  $R^2$  ranging from 0.7691 to 0.9535. Based on the knowledge of the fibre composition (thermal conductivity of the used polymer), fabric areal density and thickness,

these original models can predict the thermal resistance of the studied socks at any moisture regain up to 100%.

In addition to thermal resistance, thermal absorptivity also determined experimentally (wet state) by using Alambeta. The results were treated statistically and presented in diagrams. Very interesting results were also achieved when measuring thermal resistance of socks subject to the heat transfer by the convection on their free surface where the socks are worn free, not inside a shoe (boundary condition of 3rd order). A special thermal foot model installed in the laboratory of the Textile faculty in Zagreb (Croatia) was used. It was discovered that the gaps between the heated elements of this commercial device were the source of measuring errors. Consequently, this was fixed by a semi-permeable membrane on the foot model to avoid the turbulence effects. After this improvement, the samples measured on this model had good repeatability. Then these results were compared with the results achieved on the Permetest skin model (which works on similar principle). Both devices showed very good correlations.

In addition to thermophysiological comfort, interface of fabrics with the human senses is an important comfort property as textile materials are in contact with the skin [67]. When a fabric is moved along the skin, the perception of the fabric roughness or smoothness is induced. The friction during this contact is the key factor for the perception of unevenness or smoothness. The smooth surface fabrics mostly have the lower friction. Presence of the moisture between the friction interfaces can change the fabric roughness perception. The friction of skin increases, with the increase of the moisture content, and it can activate more feel receptors by bringing discomfort [68]. The information about friction is very essential for the protection of feet against blister formation or slippage issues. The general aims of this study are as follows;

- ❖ To find/ develop simple mathematical models for thermal resistance prediction in the wet state
- ❖ To investigate the effect of different moisture content [%] on the socks porosity, thermal resistance [ $\text{m}^2\text{KW}^{-1}$ ], thermal absorptivity [ $\text{Ws}^{1/2}\text{m}^{-2}\text{K}^{-1}$ ] and relative water vapour permeability RWVP [%].
- ❖ Effect of extension on porosity, thermal resistance, thermal absorptivity & RWVP

- ❖ Thermal resistance (predicted/ experimental) in the extended state (controlled moisture content %) for simulating a real extension and minimizing the effect of the dimensional changes.
- ❖ To compare the thermal resistance (dry state) measured by thermal foot model (TFM), Permetest and Alambeta.
- ❖ Yarn porosity (theoretical and experimental)
- ❖ Volume porosity of socks with and without extension by model
- ❖ Volume porosity and pore size distribution of socks by X-ray micro tomography scanning without extension
- ❖ Effect of moisture content on sock-material (insole) coefficient of friction
- ❖ Validation of models for other kind of fabrics (appendix 3)
- ❖ Coding of the developed thermal resistance models in FreeMat/ Matlab (appendix 5)

## ***2.1 Overview of the current state of problem***

### **2.1.1 Thermal resistance**

The characterization of insulation under wet conditions is very critical. There are numerous general thermal resistance prediction models to be found within the textile engineering and heat transfer literature to fulfil this need. The option of selection is depending on the required precision and nature of the question. Heat transfer through conduction is the easiest means to explain mathematically and is often the individual major way of heat transfer within a shoe from the skin to shoes having socks in between. Although methodical solutions for conduction equations through uniform shapes are available [69]. But, most textiles do not have uniform structures and the logical solution for rough figures can be intricate or not viable.

Thermal resistance in the wet state may be illustrated by a common exponential curve despite the structure of the sample. This scrutiny has permitted a product to be modelled by a methodical solution for smoothly formed items with pragmatically resultant structure and gap factors. Nevertheless, such methodologies are not appropriate for complicated thermal processes where fibre composition and discontinuity in physical properties within the socks are involved. There are many studies for thermal resistance prediction though empirical models available in the literature and these models are specifically volume fractions and their respective thermal conductivities based. These empirical models can measure thermal resistance only in the dry state.

Numerical approaches can deal with uneven profiles, solid/liquid/gas phases, different forms of heat transfer, number of boundary conditions, and uneven material properties. Numerical methods also have the potential to attain the utmost precision [70]. There are many soft wares available in the market that allows the user to describe the numerical problem and their solution. However these methods are intrinsically more complex and awkward, and in some conditions, plain methods demonstrated to be more precise for much less stab [71].

Some researchers employed ANN (artificial neural networks) models for thermal resistance [72][73] and thermal conductivity [74] predictions. In most of the studies, thermal resistance is predicted by statistical models [40][75]. Some researchers have predicted the thermal resistance of wet fabrics with mathematical approaches. Dias and Delkumburewatte [58]

suggested a three parameters series model (Eq.1) that predicts the thermal conductivity ( $\lambda$ ) of knitted fabric in terms of porosity ( $p$ ), thickness and moisture content in pores ( $w$ ). They have found that by increasing moisture content the porosity of fabric decreases causes to increase the thermal conductivity.

$$\lambda = \frac{\lambda_m \lambda_a \lambda_w}{(1-p)\lambda_w \lambda_a + (p-p_w)\lambda_m \lambda_w + p_w \lambda_w \lambda_a} \quad (1)$$

$\lambda_m$ ,  $\lambda_a$  and  $\lambda_w$  are thermal conductivity of material, air, and water respectively

Das et al. [76] assumed fabric assemblies as cuboids filled with randomly oriented infinite cylinders (fibres) and heat transfer by conduction can be calculated with the analogy to electrical resistance and Fricke's law (Eq.2).

$$\lambda_{\text{eff}} = \left[ 1 - \left\{ \frac{1 - \frac{\lambda_a}{\lambda_f}}{1 + \frac{2 \times \left( \frac{\lambda_a}{\lambda_f} \right) \left( \frac{v_f}{v_a} \right)}{1 + \frac{\lambda_a}{\lambda_f}}} \right\} \right] \times \lambda_f \quad (2)$$

Wie et al. have divided the fabric fundamental unit into three components for heat transfer i.e. 1.solid fibres, 2.series porosity, and 3.parallel porosity to the heat flow direction (Fig.1). Fabric thermal resistance mainly depends on the heat transfer process through this basic unit. In their model (Eq.3), heat flow considered through the fabric in a combination of fibre & air in series plus the air in parallel [60].

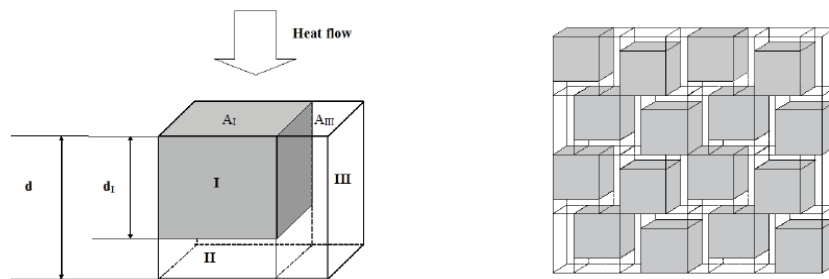


Figure 1. A Ju Wie model diagram [60]

$$R_{\text{fabric}} = \frac{d}{\lambda_{\text{air}}} \left[ \frac{\lambda_{\text{fibre}} - a(\lambda_{\text{fibre}} - \lambda_{\text{air}})}{\lambda_{\text{fibre}} - (\lambda_{\text{wet fibre}} - \lambda_{\text{air}})(a - F_{\text{fibre}})} \right] \quad (3)$$

$R_{\text{fabric}}$  = fabric thermal resistance [ $\text{m}^2\text{KW}^{-1}$ ],  $d$  = fabric thickness [meter],  $\lambda_{\text{air}}$  = air thermal conductivity [ $\text{Wm}^{-1}\text{K}^{-1}$ ],  $\lambda_{\text{wet polymer}}$  = wet fibre thermal conductivity [ $\text{Wm}^{-1}\text{K}^{-1}$ ],  
 $a$  = fabric structural parameter =  $d_{\text{compressed}}/d$ ,  $d$  = thickness [m] at 2kPa,  
while  $d_{\text{compressed}}$  = Thickness [m] at 15kPa

Schuhmeister [61] developed a relationship to calculate the thermal conductivity of the mixture of air and fibre with the following assumption:

- a) Fibres are distributed homogeneously in all directions;
- b) One-third of fibres placed parallel; and
- c) Two third were placed series or perpendicular to the heat flow.

The developed relationship (Eq.4) on the basis of the above assumptions is:

$$\lambda_{\text{eff}} = \frac{2}{3} \left( \frac{\lambda_f \times \lambda_a}{\lambda_f v_a + \lambda_a v_f} \right) + \frac{1}{3} (v_f \lambda_f + v_a \lambda_a) \quad (4)$$

Later on, many researchers followed the footprints of Schuhmeister by changing the ratio of series and parallel [62][77]. In recent times, Militky (Eq.5) considered 50% fibers placed in series and 50% in parallel to the heat flow [63][64].

$$\lambda_{\text{eff}} = \frac{1}{2} \left( \frac{\lambda_f \times \lambda_a}{\lambda_f v_a + \lambda_a v_f} \right) + \frac{1}{2} (v_f \lambda_f + v_a \lambda_a) \quad (5)$$

R. S. Hollies and Herman Bogaty have suggested a parallel combination (Eq.6) for measuring the effective thermal conductivity of moistening fabric by combining the volume fraction and thermal conductivity of water and polymer [18].

$$\lambda_{\text{eff}} = v_w \lambda_w + \lambda(1 - v_w) \quad (6)$$

Mangat presented a number of mathematical models (Eqs.7-8) for thermal resistance (wet state) in the series and in parallel combinations of air, fibre, and water resistance. His predictions are in good correlation with the experiments by model-3 (air & fibre resistance in series, water in parallel) for denim fabrics while model-5( $R_a$  and  $R_w$  in a parallel arrangement and  $R_f$  in series) and model-7( $R_f$  and  $R_w$  in a serial arrangement and  $R_a$  in parallel arrangement) for weft knitted fleece fabrics of differential fibre composition. He has suggested the following equations for model-5 & 7 respectively.

$$R_t = \frac{R_a \times R_w}{R_a + R_w} + R_f \quad (7)$$

$$R_t = \frac{R_a \times (R_w + R_f)}{R_a + R_w + R_f} \quad (8)$$

Where  $R_f = \frac{h\varepsilon}{\lambda_f}$ ,  $R_a = \frac{h \times (1-\varepsilon)}{\lambda_a \times (1-u)}$ ,  $R_w = \frac{h \times (1-\varepsilon)}{\lambda_w \times u}$ ,  $\varepsilon = \frac{\text{Fabric density}}{\text{Fibre density}}$

$$u = \frac{\text{Wet weight of fabric} - \text{oven dry weight of fabric}}{\text{Wet weight of fabric}}$$

Furthermore, he concluded that about 70% of the thermal resistance decreased up to 30% moisture content [56][19]. Another study reported a 50% reduction between 10-20% moisture content [25]. S. Naka et.al (Fig.2) suggested three parameters (air, water, and polymer) model (Eqs.9-12) for thermal conductivity prediction of wet woven fabrics with the combination of parallel and series arrangement [24].

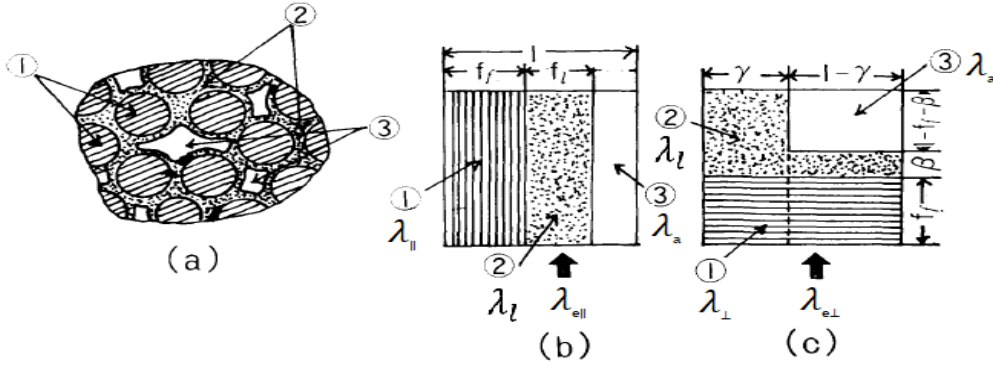


Figure 2. A model of wetted parallel fiber assemblies (1) swelled fiber, (2) Water, (3) Saturated air [24]

They have considered the effect of thermal anisotropy of fibre to calculate the thermal conductivity of fabric perpendicular ( $\lambda_v$ ) and parallel ( $\lambda_w$ ) to the surface by:

$$\lambda_v = \frac{a}{2} \lambda_{e||} + \left(1 - \frac{a}{2}\right) \lambda_{e\perp} \quad (9)$$

$$\lambda_w = d_w \{(1 - a) \lambda_{e||} + a \lambda_{e\perp}\} + d_f \left\{ \frac{a}{2} \lambda_{e||} + \left(1 - \frac{a}{2}\right) \lambda_{e\perp} \right\} \quad (10)$$

where  $\lambda_{e\parallel}$  is the thermal conductivity of fibre parallel to the fibre axis,  $\lambda_{e\perp}$  is the thermal conductivity of fibre normal to the fibre axis,  $d_w$  is the thickness of the warp layer,  $d_f$  is the thickness of weft layer and “a” is the ratio of fibre which are parallel and normal to the yarn.

$$\lambda_{e\parallel} = f_f\lambda_{\parallel} + f_l\lambda_l + (1 - f_f - f_l)\lambda_a \quad (11)$$

$$\lambda_{e\perp} = \frac{\gamma}{\frac{f_f}{\lambda_{\perp}} + \frac{1-f_f}{\lambda_l}} + \frac{1-\gamma}{\frac{f_f}{\lambda_{\perp}} + \frac{\beta}{\lambda_l} + \frac{1-f_f-\beta}{\lambda_a}} \quad (12)$$

Where

$$\beta = \frac{f_l - (1-f_f)\gamma}{1-\gamma}$$

The problem with Mangat’s models that; he assumed the filling coefficient or porosity as constant components. But they are changing by varying the moisture levels because water has a different density. Although, his second assumption that the air is replaced by water is theoretically correct but he didn’t quantify it. R. S. Hollies and Herman Bogaty have ignored the series arrangement in their suggested models. It will predict the lower thermal resistance as heat will conduct along with the thickness of the fabric.

S. Naka et al. suggested a theoretical approach for thermal conductivity prediction but they didn’t use it for calculations. They also involved the warp and weft fabric thickness in their suggested model. Dias and Delkumburewatte three parameters series model is a very simple approach but they ignored the parallel conduction part so it will predict higher thermal resistance.

As well as the thermal conductivity of fibre concerned, different values were reported in the literature. Biron reported 0.20 [Wm<sup>-1</sup>K<sup>-1</sup>] thermal conductivity for polypropylene fibre [78]. The work by Kawabata [14][79], Hearle [80] and Haghi [81] is very famous in this regard. Haghi has reported thermal conductivity values for non porous polypropylene and porous acrylic i.e. 0.518, 0.288 [Wm<sup>-1</sup>K<sup>-1</sup>] respectively. For hydrophilic fibres, he used following regression equations (Eqs.13-14) from previous studies for calculating the thermal conductivity of wool and cotton fibres are given below. R is the moisture regain [%].

$$\text{Wool } (\lambda) = 10^{-3} \times \left[ 38.49 - 0.72 \times \left( \frac{R}{100} \right) + 0.113 \times \left( \frac{R}{100} \right)^2 - 0.002 \times \left( \frac{R}{100} \right)^3 \right] \quad (13)$$

$$\text{Cotton } (\lambda) = 10^{-3} \times \left[ (44.1 + 63.0 \times \left( \frac{R}{100} \right)) \right] \quad (14)$$

As mentioned earlier, by combining the fibre and water filling coefficients approach, only three models have predicted the reasonable thermal resistance for socks that are in agreement with the experimental results. These models are as under;

### 2.1.2 Maxwell–Eucken2 (ME2)’s modified model

Maxwell introduced the two-phase concept for the determination of electrical conductivity [65]. Later on, Eucken used the same analogy for the thermal conductivity evaluation [66]. Brailsford and Major (Eq.15) have modified the Maxwell-Eucken models for thermal conductivity of a three-phase mixture assuming first phase as continuous while other two as dispersed [82].

$$\lambda = \frac{\lambda_0 v_0 + \lambda_1 v_1 \frac{3\lambda_0}{(2\lambda_0 + \lambda_1)} + \lambda_2 v_2 \frac{3\lambda_0}{(2\lambda_0 + \lambda_2)}}{v_0 + v_1 \frac{3\lambda_0}{(2\lambda_0 + \lambda_1)} + v_2 \frac{3\lambda_0}{(2\lambda_0 + \lambda_2)}} \quad (15)$$

Later on (Eq.15) was generalized by Wang et.al [83] as shown by (Eq.16).

$$\lambda = \frac{\sum_{i=1}^m \lambda_i v_i \frac{d_i \tilde{\lambda}}{(d_i - 1)\tilde{\lambda} + \lambda_i}}{\sum_{i=1}^m v_i \frac{d_i \tilde{\lambda}}{(d_i - 1)\tilde{\lambda} + \lambda_i}} \quad (16)$$

Maxwell-Eucken (Eq.17) is obtained by assuming air and wet polymer as disperse and continuous phases respectively for above (Eq.16). Maxwell–Eucken (ME) model (Eq.17) can be used to describe an effective thermal conductivity of a two-component material with simple physical structures. (Eq.17) representing a two components system for effective thermal conductivity based on volume fraction and respective. Many effective thermal conductivity models require the naming of continuous and dispersed phases. Materials with exterior porosity, individual solid particles are surrounded by a gaseous matrix, and hence the gaseous component forms the continuous phase and the solid component forms the dispersed phase [84]. For external porosity, and are considered as continuous & dispersed phases respectively.

$$\lambda_{fab} = \frac{\lambda_a F_a + \lambda_{wet\ polymer} F_{wet\ polymer} \frac{3\lambda_a}{2\lambda_a + \lambda_{wet\ polymer}}}{F_a + F_{wet\ polymer} \frac{3\lambda_a}{2\lambda_a + \lambda_{wet\ polymer}}} \quad (17)$$

$F_{wet\ polymer}$  and  $\lambda_{wet\ polymer}$  is calculated as per (Eqs.43-45).

### 2.1.3 Schuhmeister's modified model

Schuhmeister (Eq.18) summarized the relationship between the thermal conductivity of fabric and the fabric structural parameters by an empirical equation [61];

$$\lambda_{fab} = 0.67 \times \lambda_s + 0.33 \times \lambda_p \quad (18)$$

$$\text{Where } \lambda_s = \frac{\lambda_{wet\ polymer} \times \lambda_a}{\lambda_{wet\ polymer} F_a + \lambda_a F_{wet\ polymer}} \quad (19)$$

$$\text{and } \lambda_p = F_{wet\ polymer} \lambda_{wet\ polymer} + F_a \lambda_a \quad (20)$$

Where  $\lambda_{fab}$  is the thermal conductivity of fabric,  $\lambda_{wet\ polymer}$  is the conductivity of wet fibers,  $\lambda_a$  is the conductivity of air,  $F_{wet\ polymer}$  is the filling coefficient of the solid fiber,  $F_a$  is the filling coefficient of air in the insulation.

### 2.1.4 Militky's modified model

Militky (Eq.21) summarized the relationship between the thermal conductivity of fabric by an empirical equation [63][64];

$$\lambda_{fab} = \left( \frac{\lambda_s + \lambda_p}{2} \right) \quad (21)$$

Where  $\lambda_s$  and  $\lambda_p$  are calculated as per (Eqs.19-20) respectively.

Where  $\lambda_{fab}$  is the thermal conductivity of fabric,  $\lambda_{wet\ polymer}$  is the conductivity of wet fibers,  $\lambda_a$  is the conductivity of air,  $F_{wet\ polymer}$  is the filling coefficient of the solid fiber,  $F_a$  is the filling coefficient of air in the insulation.

## 2.2 Porosity

Fabric comfort properties could be significantly affected by porosity. “It is a measure of the void (i.e., empty) spaces in a fabric, and is a fraction of the voids over total volume” [85]. “Porous media refer to a solid of an unspecified form including vacuums called pores filled with liquid and gas. These vacuums can communicate with each other to exchange matter and energy” as shown in (Fig.3).

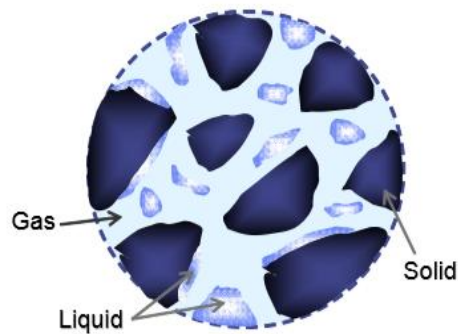


*Figure 3. The geometry of a porous medium [86]*

Porosity can be classified as inter-yarn, intra-yarn and intra-fibre; these are spaces in-between the yarns, in-between fibres in the yarn and in fibre substances respectively. The inter-yarn porosity, also known as macro porosity, is of great significance in the case of air permeability, UV rays transmission, etc. [87][88]. Inter-yarn porosity is influenced by the fabric structural parameters: yarn sett, yarn diameter, yarn twist, weave type, fabric thickness [89][90], yarn density [88], as well as the fibre characteristics [88]. For absorption and capillary phenomenon, the intra-yarn porosity, also known as micro porosity and inter-fibre porosity [88], is essential [91]. Porosity also affects the fabric heat and mass transportation. It has a significant effect on the fabric thermal conductivity [19]. Water vapour permeability of knitted fabrics increases with higher porosity and lower fabric thickness and areal density [91]. Cubric et al. reported that the evaporation resistance of fabrics has very high positive correlation with areal density, tightness factor and fabric thickness. It increases with denser fabrics as the porosity of the textile material reduces [92]. Mangat et al. considered porosity as a key parameter for the prediction of thermal absorptivity in their suggested model [34][44]. Dimitrovski et al. stated that the number of inter yarn pores; total porosity and hydraulic diameter of pores have a strong influence on air permeability prediction [91]. Ma et al. studied the relationship between fluid permeability and porosity of different knitted architectural glass fabrics. They found that permeability influenced by many factors such as pore size,

roughness, porosity, and channel lengths [88]. As the comfort parameters influenced by porosity, so the changes in porosity with extension and moisture will be studied in this work. Although different approaches were made to characterize porosity in yarns and socks, however, the aim of the work is porosity consequences on comfort parameters (under extension and wet state) not porosity characterization methods. The porosity of the woven and knitted fabrics is around 70% and can be 98% for some nonwovens [93]. Siddique et al. reported a 64-76% porosity range for different compression socks without extension [94]. Mansoor et al. investigated the effect of the pre-heat setting process on plain socks comfort. During their investigation, they have found porosity is between 83-86.5% [95]. Siddiqui and Sun have predicted the porosity of weft knitted fabrics between 86-93% by using the Karaguzel's model [96].

### 2.3 Thermal absorptivity

Thermal absorptivity is mainly a surface-related property, it could be changed by any finishing treatment, like raising, brushing coating [30][32]. Yarn spinning technology can also affect the warm-cool feeling of knits, where the ring-spun yarns provide a warmer feeling than open-end yarns [97]. Hes as a pioneer of this newly used term "thermal absorptivity", in the area of textiles has many studies on his credit [20][98][99][100].

"As the thermal contact between the textile material and the human skin is transient, the fabric was assumed to be a semi-infinite body characterized by its thermal capacity". The temperature difference between the human skin ( $t_1$ ) and the fabric ( $t_2$ ) simulates the heat flow ( $q$ ) through the textile material during a time ( $\tau$ ) [101].

$$q_{\text{dyn}} = \frac{b(t_1 - t_2)}{\sqrt{\pi\tau}} \quad (22)$$

Hes proposed to use the thermal absorptivity in the (Eq.23) as a measure the of thermal contact feeling of textile materials. Thermal absorptivity neither depends on the temperature difference between the two bodies in contact nor on the time measurement [30][32].

$$b = \sqrt{\lambda\rho c} \quad (23)$$

A thermal absorptivity prediction model proposed by Mangat and Hes for rib knitted fabrics, based on the thermal absorptivity of polyester in solid form ( $b_p$ ), fabric porosity ( $P_{\text{HW}}$ ) and the relative contact area between the human skin and fabric ( $A$ ) as shown in below (Eq.24).

$$b = b_p \times A(1 - P_{HW}) \quad (24)$$

Baczek & Hes observed 9 times higher thermal absorptivity of plaited knitted fabrics in the wet state [36]. Mangat's model for thermal absorptivity prediction is based on the contact area effect [34][44]. Oglakcioglu's contribution to thermal absorptivity covered the effect of moisture content [22], fibre composition [102] and fabric construction [40].

Up to now several researchers had analysed the effect of fabric structure, contact area [33][30], moisture content [98][20][22][99][103], extension [104][105], fibre composition, finishing (chemical/ mechanical) [95][33] on thermal absorptivity [35][36][37], but no study was found with the combined effect of moisture and extension. Faisal et al. used a special frame for extension and observed reduction in thermal absorptivity of compression socks at different extension levels [105]. Gupta also extended the compression circular knitted garments up to 60% and found a decrease in the thermal absorptivity [87]. Irrespective of other studies an embroidery hoop was used for simulation of real extension. Previous researchers have extended the fabric in one direction only. They have not considered the real situation of extension. Because elastic garments extended in both directions. So the motivation of this work is based on the following gaps;

- ❖ As the socks are extended in both directions at the same time during wearing. So the extension of socks should be simultaneous in both directions for thermal absorptivity measurement.
- ❖ No combined study found having both moisture and extension consequences on thermal absorptivity.

## 2.4 Relative water vapor permeability

“Water vapours are transmitted through the textiles by diffusion, absorption, transmission & desorption (in the fibre), adsorption & migration (along the fibre), and forced convection”. Fick's law, Darcy's law, and Kozeny equation are based on the fluid concentration gradient, hydraulic radius theory, and fluid pressure drop respectively, are generally used in evaluating the fabric permeability [106][107][108]. Fick was the first person who proposed the relation between diffusing flux and the concentration gradient as shown in (Eq.25) [109].

$$J_{AX} = -D_{AB(c)} \frac{dC_A}{dx} = -D_{AB(p)} \frac{dP_A}{dx} \quad (25)$$

Where  $J_{Ax}$  is moisture flux rate,  $dC_A/dx$  or  $dP_A/dx$  is the concentration/ pressure gradient, and  $D_{AB}$  is the mass diffusivity or diffusion coefficient. At a particular gradient, the diffusion rate along the textile material depends on the porosity and water vapour diffusivity [109].

So far researchers found that water vapor permeability could be affected by fibre type and structure, fibre composition [108][98][110][111], yarn diameter [37], fabric thickness, covering factor, porosity [112], fabric structure [40][113], chemical [114] and mechanical finishes.

The work of Hes et al. [25][15][111] for total heat flow in the wet state has opened new directions. According to their theory, total relative cooling heat flow ( $q_{tot}$ ) transferred through the boundary layer of the wet fabric surface is given by the sum of heat flow passing from the skin through the permeable fabric ' $q_{fab,w}$ ' and heat flow ' $q_{fab,surf}$ ' caused by temperature gradient between the skin and fabric surface, which is cooled by evaporating of water from the fabric surface as shown by (Eq.26) and (Fig.4).

$$q_{tot,w} = q_{fab,w} + q_{fab,surf} \quad (26)$$

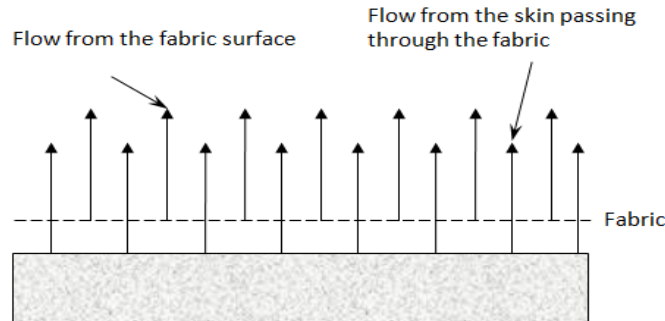


Figure 4. Cooling flow from the surface & through the fabric [25]

Rajwin & Parash observed that plasma treatment of cotton fabric for 15mins at 100kHz frequency increased the water vapor permeability [115]. Gupta extended the compression circular knitted garments up to 60% and found 47% increase in the water vapor permeability [87]. Moisture content can also significantly change the water permeability [48][100][103][111][116]. But no study was found with the combined effect of moisture and extension. Likewise thermal absorptivity an embroidery hoop also used for simulation of real extension. Previous researchers have extended the fabric in one way only. They have not considered the real situation of extension. Because elastic garments extended in both directions. So the motivation of this work is based on the following gaps;

- ❖ As the socks are extended in both directions at the same time during wearing. So the extension of socks should be simultaneous in both directions for relative water vapor permeability measurement.
- ❖ No combined study found having both moisture and extension consequences on relative water vapor permeability.

## **2.5 Coefficient of friction**

Blisters are caused by clothing friction on the skin. Their formation depends on the magnitude of the frictional forces and the number of times that an object touches across the skin [117]. The friction coefficient normally increases when epidermal moisture raises [118]. To avoid the blister occurrence, the sliding should take place either between the sock-shoe or between two layers of socks interfaces. This implies that friction between the sock-skin interface has to be higher than the other interfaces. “Activity-related blisters are mostly due to frictional shear forces” [119]. However, frictional shear forces do not appear to be adequate for a blister to arise. As per Reynolds et al., it is the combination of shear, pressure, and a moderate level of moisture [120]. Moisture accumulated within a shoe is mainly due to a high sweat rate. An athlete may have a sweat rate of nearly 3 litres per hour during a long run in a damp environment [121].

Sweat evaporation from the body into the environment is much quicker compared to the sweat accumulated within an enclosed shoe. It will increase the sock’s moisture and in return influence the friction at the plantar skin interface [122][123][124]. Furthermore, accumulated moisture in the socks has the potential to bridge air gaps between fibres which consequently increases the contact area between these two surfaces. This could lead to an increase in the available friction [125], in addition to influencing the thermal resistance and thermal conductivity of the sock fabrics [126].

Additional shear force at sock fabric - plantar skin interface could have a negative impact on the range of movement and could even potentially lead to friction blisters [125], which would increase discomfort to the wearer [127]. Blisters are caused by the rubbing pressure between the skin of the foot and adjacent sock surfaces. When a runner’s shoe strikes the ground, the shoe tends to undergo a rapid decrease in velocity whereas the foot and sock within the shoe be likely to continue forward at a fast speed until the shoe restricts the forward motion. Subsequently, there is an abrasive action occurs at the foot-sock and sock-shoe interfaces. Heat built up due to friction at these interfaces is the main cause of blisters [128].

So, both kinds are very important with respect to blisters or irritations. Many researchers have studied sock's friction at these interfaces such as sock-skin friction [129] & sock-material (shoes insole, floor covering, tile, etc.) friction [130][131][132]. Furthermore, it was well established that sock-insole friction should be lower than sock-skin to avoid friction blisters [133]. Factors recommended as changing the friction of fabrics are the fiber type [127][134][135], yarn density [136], orientation of the fabric structure [125][129], applied weight[137], and the moisture content [137][138]. The friction force is more related to the wetness of the skin than material or finishing treatment of the fabric [122][137]. Very fewer studies found on COF between sock-material (insole/shoes) interfaces in the wet state with the information of moisture content percentage.

## Chapter 3

### 3 Materials and Methods

#### 3.1 Fibre fineness

Fibre fineness is one of the important structural parameters. It has a big effect on the incoming yarn and fabric parameters. There are many methods/ instruments available to measure the fibre fineness based on the different principles and measuring technique i.e. optical microscopy, gravimetry, optical diffraction, porosity (resistance to airflow), harmonic, radiometry, photometry and image analysis etc. [139]. Single fibre fineness has been measured through vibroshop. It based on the principle of creating a natural vibration (harmonic) in the fibre by an electronic delta impulse. The titer [dtex] is derived from the fiber's vibration frequency. Fibre samples are picked from the ravelled yarn of the knitted socks. So much handling and care were required. Information about the nominal fineness of the fibres was taken from the yarn manufacturer. So pretension is selected according to the nominal fineness of the fibre. This test is just an estimation of the fibre fineness. Tiny clips that can generate pretension ranges from 30mg to 7000mg are available with the machine. One end of the fibre is clipped with the selected pretension while the other is picked with the help of tweezers. Then hanged it in the sample holder and left the tweezer's end. After 30 seconds, press the lower black button. The fineness of the fibre will be displayed on the top screen and given as under in Table 1.

*Table 1. Experimental fibre fineness results*

Fibre	Pretension [mg]	Fibre fineness [dtex]	CV [%]
Cotton	100	1.42	15.72
Viscose	100	1.43	10.24
Polyester	100	1.58	10.55
Polyamide	100	3.43	5.55
Polypropylene	200	3.40	6.91
Wool	500	8.17	15.85
Acrylic	100	3.00	7.05

#### 3.2 Yarn linear density, twist & porosity

The following are the yarns (Table 2) that have been used for socks knitting. Their nominal yarn linear density and twist per inches range has been given. These values are from raw

yarn. Dyeing makes the yarn coarser. It is rational because of some dye/ color attached to the fibre caused to increase the weight. Dyeing of spun yarns was done after soft winding on perforated springs or plastic tubes while the used filament yarn (polyamide) was dyed in muff form. So the mechanical stresses have been relaxed during wet processing. It may be another reason for the coarser yarn after dyeing.

**Table 2. Yarn specification**

Yarn description	Measured yarn count		Twist	
	[tex]	CV [%]	Twist per meter	CV [%]
20/1 Nec 100% Cotton combed spun yarn	30.407	1.35	698.82	3.85
20/1 Nec 100% Viscose Spun yarn	30.596	1.20	610.24	3.02
20/1 Nec 100% Spun Polyester yarn	30.282	1.28	551.18	2.54
100/36/2 D 100% Nylon filament yarn	24.444	7.13	94.88	3.47
84/25/2 dtex 100% polypropylene filament yarn	17.611	6.32	85.00	4.22
30/1 Nm 100% Wool spun yarn	34.603	4.53	395.00	4.46
20/1 Nm 100% Acrylic spun yarn	50.505	4.8	525.00	5.16

Porosity is more one of the most important parameters for understanding the structure and orientation of the fibres inside the yarn. It is defined as “the ratio of total empty area to the total area or the empty volume to the total volume” [140] There are many theoretical and experimental approaches are available to calculate the porosity of the yarn. A semi-empirical model by Neckar (Eq.27) has taken care of yarn linear density, yarn twist, and yarn technology factor as given below [141].

$$d_{\text{yarn}} [\mu\text{m}] = K \times N_t^q \times T^c \quad (27)$$

Where d is yarn diameter in micron, k is spinning technology coefficient and ‘q’ and ‘c’ are exponents to yarn fineness  $N_t$  [tex] and yarn twist T [twist per meter] respectively. The values of ‘q’ and ‘c’ remain constant with types of fibre. The values are based on the below Table 3;

**Table 3. Constant values for (Eq.27)**

Fibre type	K	q	c
Cotton	135	0.6416	-0.2613
Viscose	251	0.6342	-0.3763
Polyester	161	0.6650	-0.2790

Later on Ishtiaque and Das [142] have modified the above Neekar's model by separating the type of fibre and spinning technology as given in (Eq.28).

$$d_{\text{yarn}}[\mu\text{m}] = K_1 + K_2 \times N_t^q \times T^c \quad (28)$$

For ring spinning technology  $K_2 = 222$ , where as the values of the other constants for (Eq.28) have been given in below Table 4

**Table 4. Constant values for (Eq.28)**

Fibre type	K1	q	c
Cotton	86.7	0.6416	-0.403
Viscose	28.6	0.6342	-0.372
Polyester	49.5	0.665	-0.357

The equivalent fibre diameter [143] is calculated as per below (Eq.29)

$$d_{\text{fibre}}[\mu\text{m}] = \sqrt{\frac{4T_{\text{fibre}}}{10^{-6} \times \pi \times \rho_{\text{fibre}}}} \quad (29)$$

$T_{\text{fibre}}$  is the fibre fineness in tex and  $\rho_{\text{fibre}}$  is the fibre density in  $\text{kgm}^{-3}$ . (Eq.30) could be used to calculate the packing yarn density based on the theoretical fibre number (n) is as under;

$$\emptyset = \frac{n \times \frac{\pi d_{\text{fibre}}^2}{4}}{\frac{\pi d_{\text{yarn}}^2}{4}} \quad (30)$$

n is the number of fibres in the cross-section of the yarn is calculated as per (Eq.31)

$$n = \frac{\text{tex}_{\text{yarn}}}{\text{tex}_{\text{fibre}}} \times k_n \quad (31)$$

The value of  $k_n$  depends on the orientation of the fibre assemblies. For filament yarns without any twist this value will be 1 and for cotton yarn 0.95 etc [141]. After calculating the packing density the yarn porosity (Eq.32) will be;

$$\epsilon_{\text{yarn}}[\%] = (1 - \emptyset) \times 100 \quad (32)$$

For experimental yarn diameter, images of the yarns have been taken by camera (ProgRes-CT3) attached to a microscope under transmitted light. The grabbed images were analyzed by using NIS-elements software. Following are the images for all the sock samples (Fig.5);

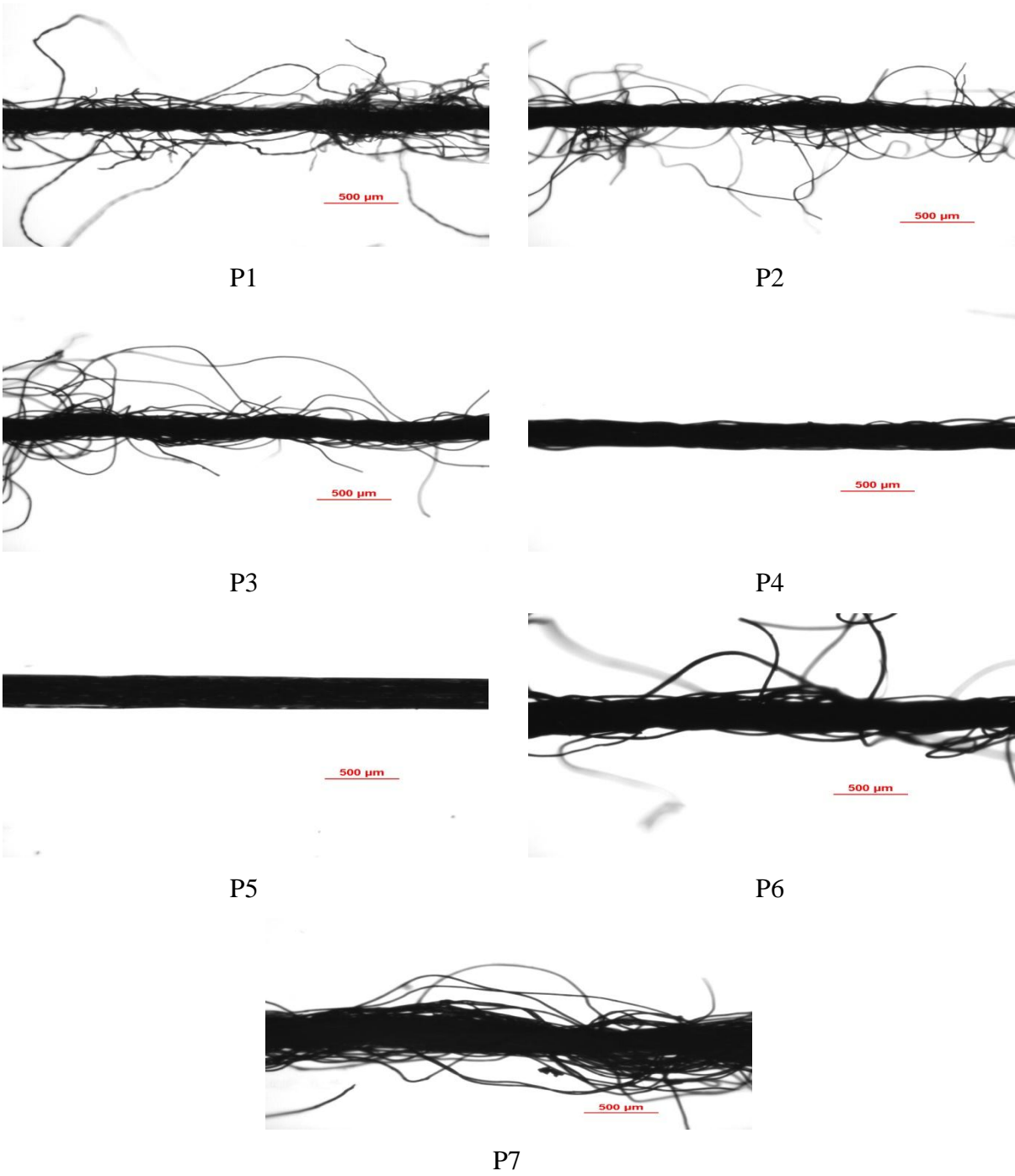


*Figure 5. Yarn images for diameter measurement*

Measured and experimental yarn diameter has been given in below Table 5

**Table 5. Yarn diameter results**

Yarn Description	Yarn diameter [ $\mu\text{m}$ ]		
	Neckar	Ishtiaque	Experimental
20/1 Nec 100% cotton carded spun yarn	218.059	228.45	239.16
20/1 Nec 100% viscose spun yarn	196.65	207.39	230.45
20/1 Nec 100% spun polyester yarn	267.29	274.76	234.86
100/36/2 D 100% nylon filament yarn			246.46
84/25/2 dtex 100% polypropylene filament yarn			236.53
30/1 Nm 100% wool spun yarn			237.83
20/1 Nm 100% acrylic spun yarn			330.21

Yarn porosity (measurement & calculated) is given in Table 6

**Table 6. Yarn porosity results**

Yarn description	Yarn count [tex]	Fibre diameter [ $\mu\text{m}$ ]	No. of fibres in yarn cross section	Yarn porosity [%]		
		(Eq.29)	(Eq.31)	Neckar	Ishtiaque	Experimental
100% cotton carded spun yarn	30.407	10.84	203.43	49.73	54.20	58.21
100% viscose spun yarn	30.596	10.88	203.26	37.78	44.06	54.69
100% Polyester spun yarn	30.282	11.43	182.08	66.70	68.49	56.87
100% nylon filament yarn	24.444	16.84	72			66.39
100% polypropylene filament yarn	17.611	16.77	50			74.87
100% wool spun yarn	34.603	26	40.24			51.91
100% acrylic spun yarn	50.505	15.75	159.93			63.62

### 3.3 Socks samples

All the plain (single jersey) socks samples as shown in (Table 7) & (Fig.7) were knitted on the same machine (Lonati Goal GL544S, 144Needles, Diameter 4'', 4Feed) settings by varying the main yarns to get the homogeneous samples with respect to specs and stretches for contrast comparison. "The yarn running at the surface of the sock is called the main yarn and the plaiting yarn (generally spandex covered polyamide or polyester filament yarn) runs inside the fabric providing stretch, elasticity, comfort and shape to the sock" [144][95]. After

knitting, all the samples were processed for washing (appendix 15) in the same machine bath followed by tumble drying and boarding.

**Table 7. Sock samples specifications**

Main yarn nominal count	Plaiting yarn	Fibre composition [%]	GSM [gm <sup>-2</sup> ]	Thickness [mm]	Sock codes
29.525/1 tex 100% Cotton spun yarn	2.22/8.33/36/1 tex Polyester air covered Elastane (91:9) %	Cotton 80%, Polyester 18.20%, Elastane 1.8%	129.88	0.95	P1
29.525/1 tex 100% Viscose Spun yarn		Viscose 81.08%, Polyester 17.22 %, Elastane 1.70%	130.44	0.90	P2
29.525/1 tex 100% Spun Polyester		Polyester 98.38%, Elastane 1.62%	125.70	0.95	P3
11.11/36/2 tex 100% Nylon filament yarn		Nylon 70.83%, Polyester 26.54%, Elastane 2.63%	115.34	0.91	P4
8.4/25/2 tex 100% polypropylene filament yarn		Polypropylene 65.22%, Polyester 31.65%, Elastane 3.13%	108.92	0.82	P5
33.33/1 tex 100% Wool spun yarn		Wool 76.19%, Polyester 21.67%, Elastane 2.14%	133.69	1.16	P6
50/1 tex 100% Acrylic spun yarn		Acrylic 81.25%, Polyester 17.06%, Elastane 1.69%	166.89	1.20	P7

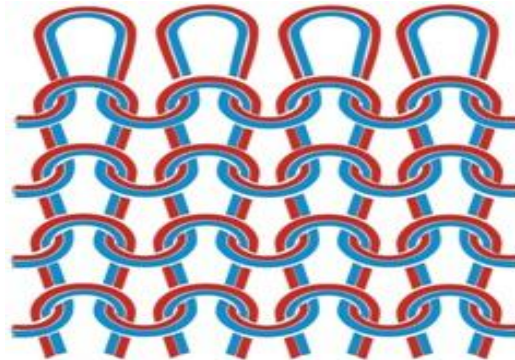
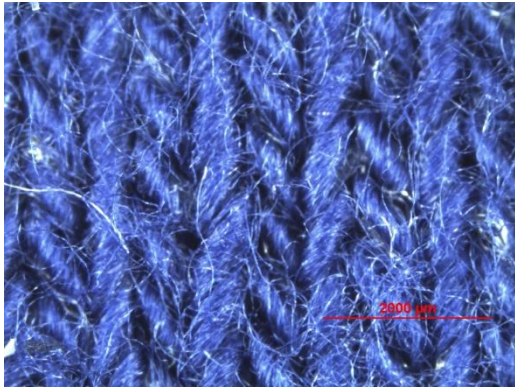
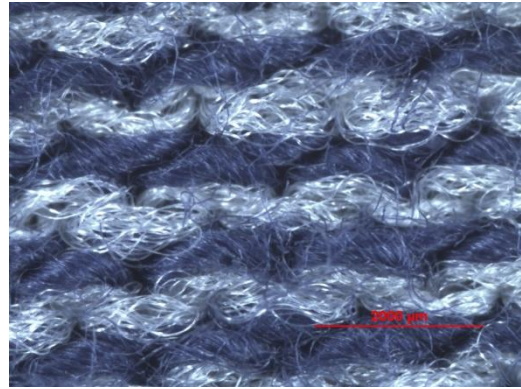


*Figure 6. Knitting style of plain (single jersey) sock construction*

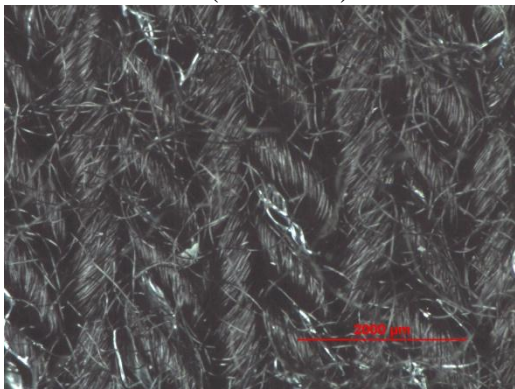
Images for all the samples have been taken through a camera (ProgRes CT3) attached to a macro scope (NAVITAR) with the lights and stand (HAISER Germany) from front and backside of the socks with (Fig.8) and without extension (Fig.7). Main and plaited yarns could easily be observed from front side and back side of the socks.



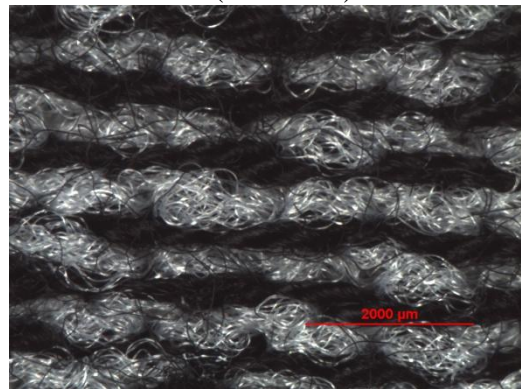
P1 (front side)



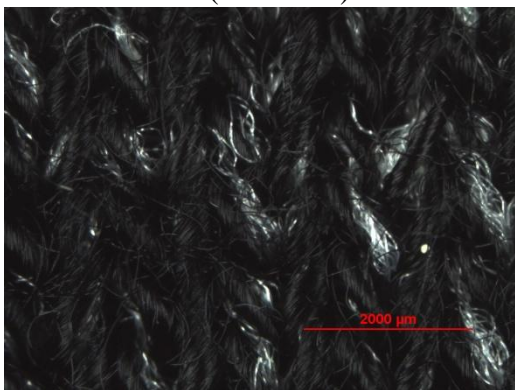
P1 (back side)



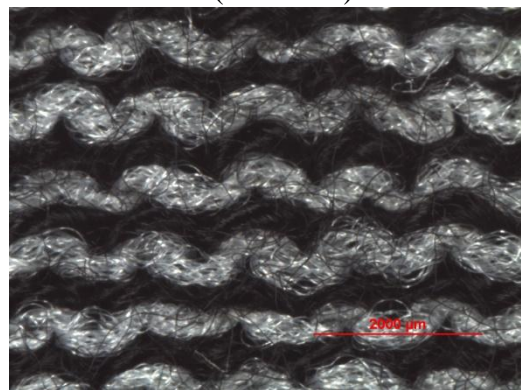
P2 (front side)



P2 (back side)



P3 (front side)



P3 (back side)



P4 (front side)

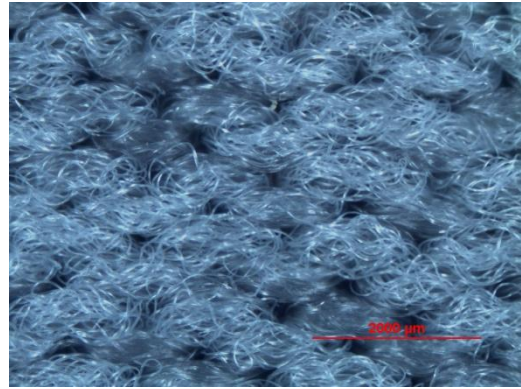


P4 (back side)

Figure 7. Sock images by macroscopic camera (without extension)



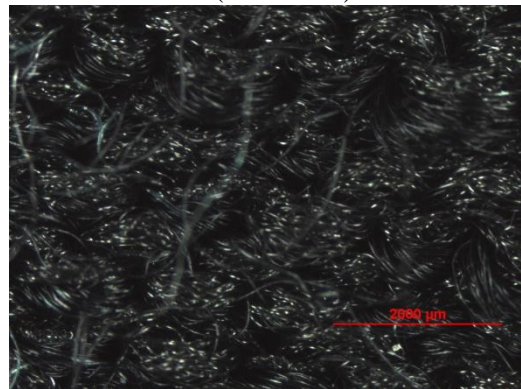
P5 (front side)



P5 (back side)



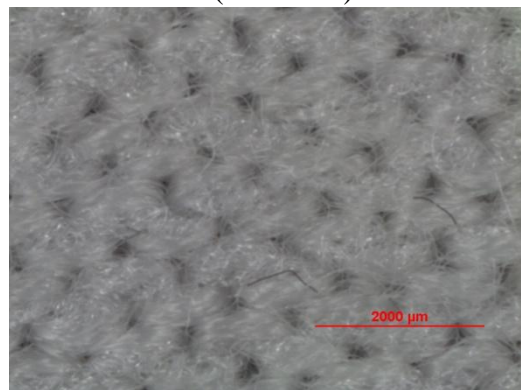
P6 (front side)



P6 (back side)



P7 (front side)



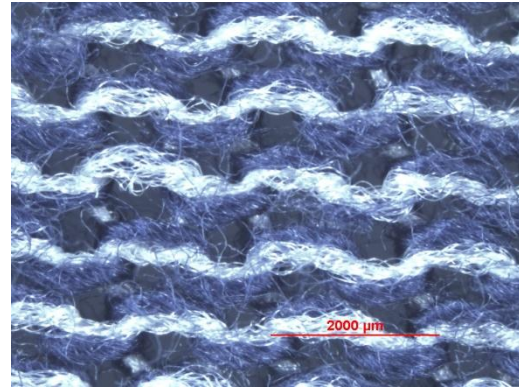
P7 (back side)

*Figure 7. Sock images by macroscopic camera (without extension)*

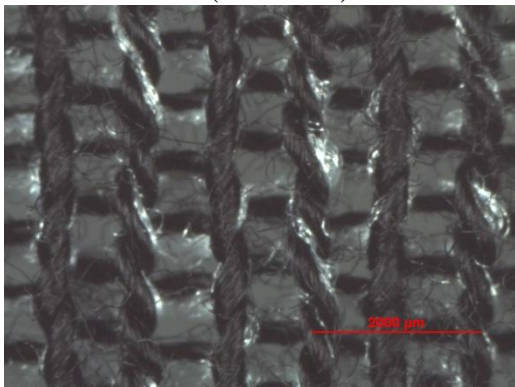
Main yarn is more prominent from side except some of the plaited yarn loops could be seen over the main yarn for samples P1, P2 & P3 due to contrast of color. Plaiting yarn along with the main yarn could be easily distinguished from the back side of these samples very easily. As well as P4, P5, P6 & P7 samples are concerned, plaited yarn could be identified with its glow difference.



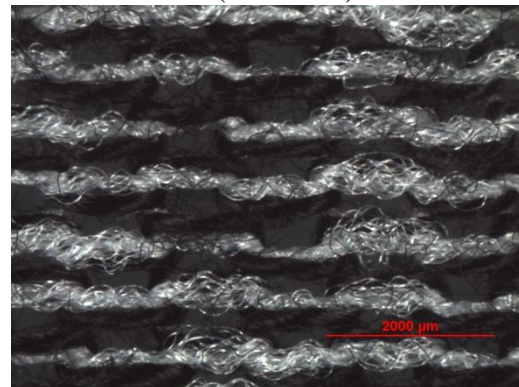
P1 (front side)



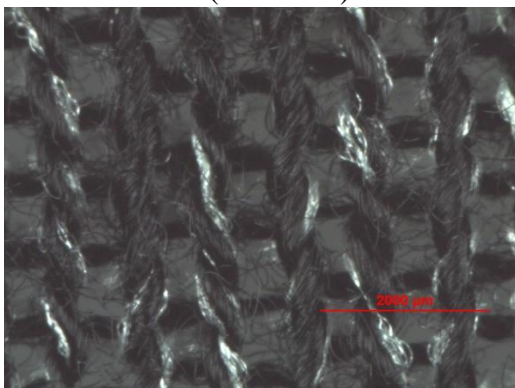
P1 (back side)



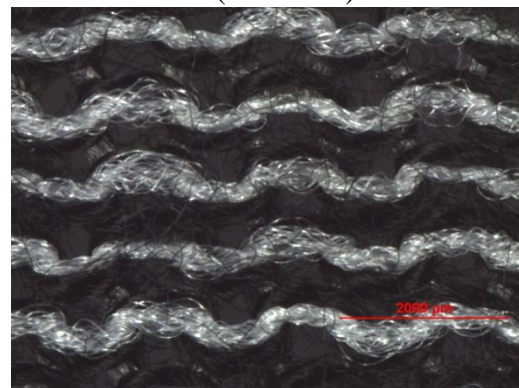
P2 (front side)



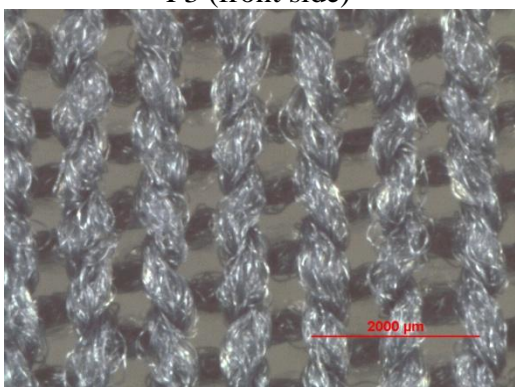
P2 (back side)



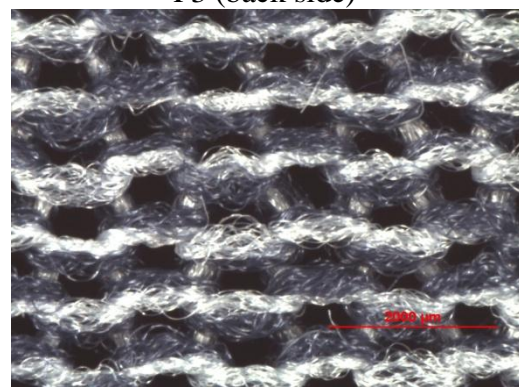
P3 (front side)



P3 (back side)

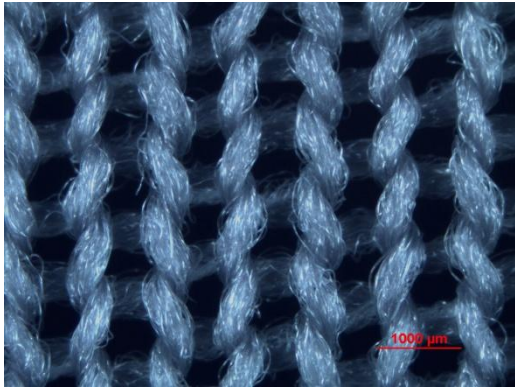


P4 (front side)

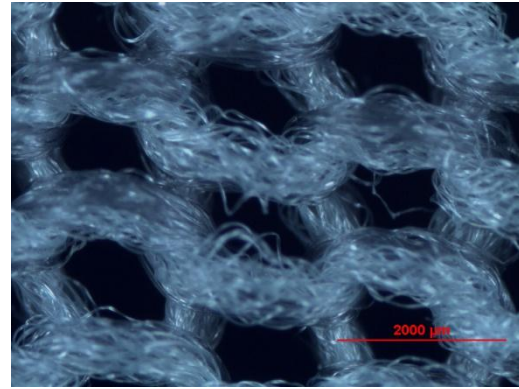


P4 (back side)

Figure 8. Sock images by macroscopic camera (with extension)



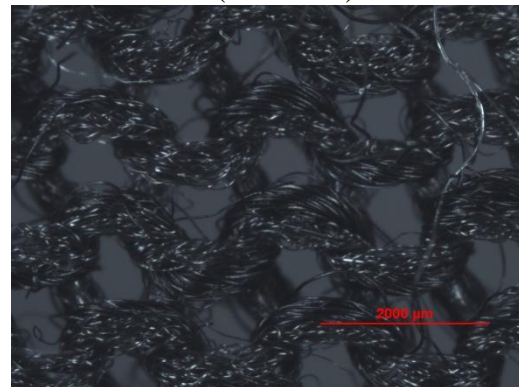
P5 (front side)



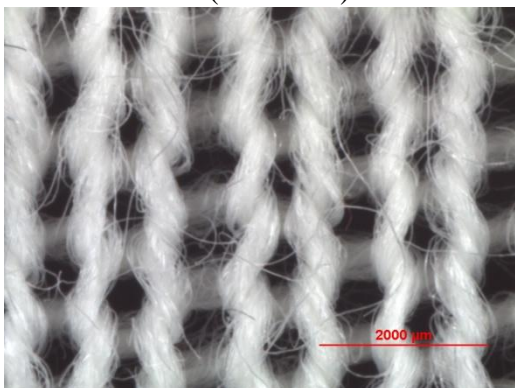
P5 (back side)



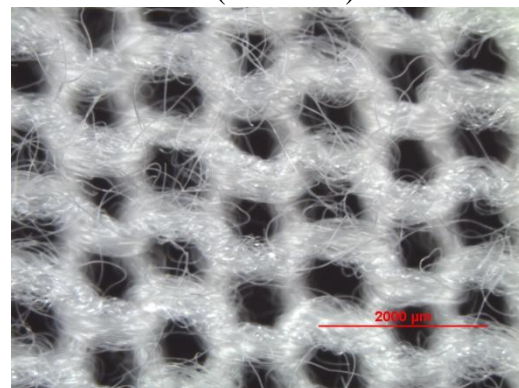
P6 (front side)



P6 (back side)



P7 (front side)



P7 (back side)

*Figure 8. Sock images by macroscopic camera (with extension)*

For friction testing, an insole (commercially available) was arranged randomly. Specifications (mentioned on the label) of the insole are as under (Table 8);

**Table 8. Insole sample specifications**

	<p>Salamander professional (melvo GmbH)  Length = 30cm  Top layer = Long terry cotton woven fabric  Middle layer = Activated carbon  Bottom layer = Latex foam</p>
---	--

### 3.4 Fibre quantitative analysis

Fibre composition of the socks was measured by the standard test method “AATCC-20A Fiber Analysis: Quantitative” [145]. A specimen of not less than 5g was taken and dried to constant weight in an oven at 105-110°C. Moisture content was calculated. After de-knit the socks, the main yarns were separated from plaiting. The weight of the main yarn recorded and converted into a percentage. Whereas, the plaiting yarns i.e. polyester covered elastane and polyamide covered elastane were chemically separated as per the instruction given in Method No.7 & Method No.6 (AATCC-20A) respectively. Record the weight of the dried residue to the nearest 0.1 mg. Fibre content was calculated as per (Eq.33).

$$X_i = \frac{G-H_i}{G} \times 100 \quad (33)$$

Where:

$X_i$  = content of fiber i, percent.

$G$  = weight of clean, dry, prepared specimen

$H_i$  = weight of dried residue after treatment

### 3.5 Volume socks porosity by model

Sock’s structure is important due to several advantages. Physically, it presents properties of comfort such as high elasticity, conformity with the shape of the body, softer hands feel, and others. In general, heat & mass transmission rate is dependent mainly on the fabric geometrical parameters, namely, thickness and porosity [146]. Porosity ( $\epsilon$ ) is the volumetric ratio of the pores accessible by total volume [147]. The porosity of the fabrics can be calculated by air permeability, image processing, and geometrical modelling approaches [148]. Volume porosity of the socks was determined according to (Eq.34) [149][150].

$$\text{Porosity } (\varepsilon)\% = \left( \frac{\rho_0 - \rho}{\rho_0} \right) \times 100 \quad (34)$$

where  $\rho_0$  is fibre density [ $\text{kgm}^{-3}$ ] and  $\rho$  is fabric density [ $\text{kgm}^{-3}$ ]

### 3.6 3D porosity of socks by micro-tomography scanning

3D porosity of the socks was investigated by using an x-ray computed micro-tomography SKYSCAN 1272 system. In this system (Fig.9), radiation is converted into an electrical signal between the x-ray source and the detector, the specimen revolves on a vertical axis. 2D images in several steps are taken during this rotary motion. Reconstruction software generates a 3D model of the actual specimen from these images [151]. Following are the common settings for all the tested samples: image pixel size – $3.0\mu\text{m}$ , lower grey threshold–33, upper grey threshold –255, rotation step –  $0.2^\circ$ , rotation degrees – $180^\circ$ , frame averaging – 3, exposure – 672 ms, voltage source – 50 kV, source current –200 uA. For more detail see (appendix 13).

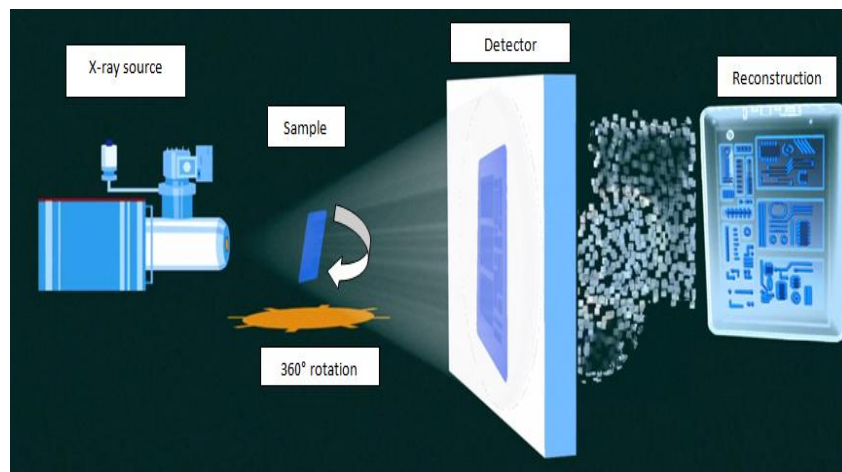


Figure 9. Working Scheme of micro-tomography [152]

### 3.7 Sample preparation for testing

For the extension simulation, the socks were loaded on a dummy leg (Salzmann MST Switzerland) [153] of medium size (24cm) as per specification of the standard method (RAL-GZ-387/1), for detail see (appendix 2 & appendix 15). Then worn socks are marked as per the testing template. After unloading, the socks were extended to the marked circle with the help of an embroidery hoop as shown in (Fig.10). Sock samples were tested for the thermal resistance & thermal absorptivity in the dry state (lab conditions moisture content). Then wet to the saturated level (100% moisture content) by BS EN ISO 105-X12 standard test method. The established technique for preparing a wet fabric of the known oven-dry fabric weight,

then thoroughly wetted in distilled water. The wet pick-up brought to  $100 \pm 0.5\%$  by putting wet testing fabric on a blotting paper. The evaporation of the moisture content below the specified level was avoided by using polyethylene bags. Furthermore, tested again for the up given tests under extension at different moisture levels.

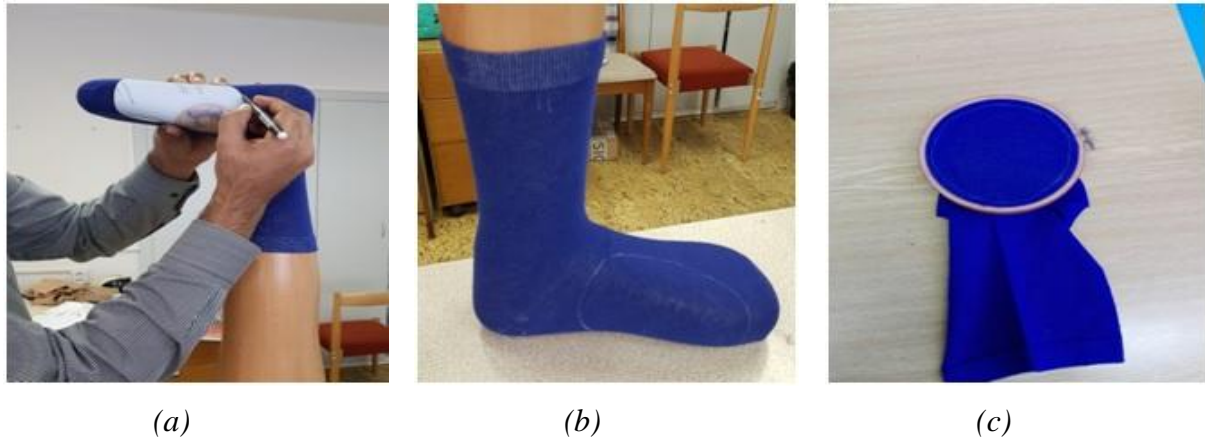


Figure 10. Schematic illustration of (a) Circle marking, (b) Socks loading on dummy foot, and (c) Embroidery hoop respectively

During adsorption and desorption of socks the hysteresis arises inherently. It is a phenomenon during which a material experiences a separate saturation level at the same relative humidity depending on its loading history as shown in (Fig.11). This phenomenon was first reported by van Bemmelen [154], but the first detailed theory of adsorption hysteresis was put forward by Zsigmondy [155]. In (Fig.11), OBT and TAO are the adsorption and desorption arms of the hysteresis loop respectively. There exist many studies on the adsorption hysteresis. But the study didn't aim to grasp it in detail.

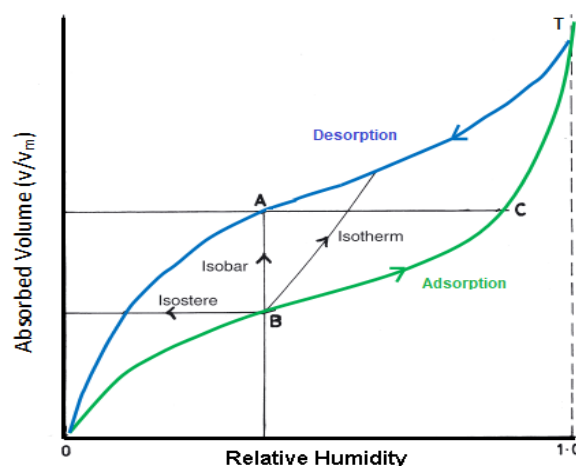


Figure 11. Schematic illustration of hysteresis loop showing the paths of the isobar, isostere and isotherm curves [156]

### 3.8 Testing equipments/ methods

Type of equipments was selected for this research as per the situation of worn socks and limitations of the manikins. Socks wore inside shoes shown 1st order boundary conditions; the constant different temperatures on both surfaces of the fabric (like Alambeta). Socks were worn (calf area) partly under 3rd order boundary conditions; conduction inside = convection outside (Thermal foot model, Permetest). The condition is more clearly illustrated in (Fig.12). Furthermore, short testing time (almost keep the specific moisture content) distinct the Alambeta and Permetest from other skin models and manikins. So Alambeta and Permetest were selected especially for wet testing.

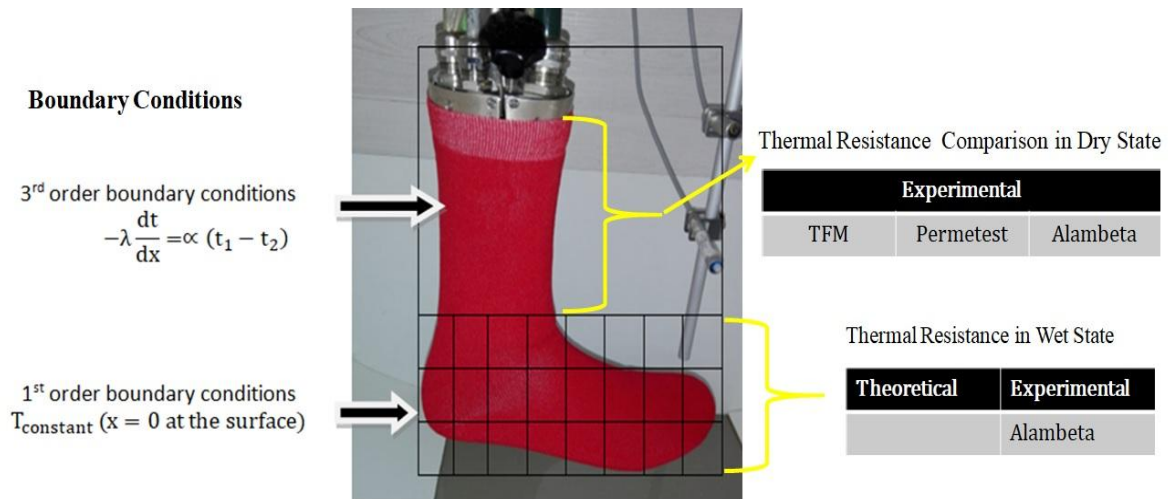


Figure 12. Worn sock situation inside the shoe

#### 3.8.1 Alambeta (equivalent to ISO 8301)

The thermal resistance (Rct) and thermal absorptivity (b) of the developed samples were measured by Alambeta tester [30], which provides a fast measurement of both steady-state and transient-state thermal properties. This instrument simulates the heat flow  $q$  [ $\text{Wm}^{-2}$ ] from the human skin to the fabric during a short initial contact in the absence of body movement and external wind flow. With the two bodies brought into ideal contact the time course of temperatures is determined by solving the known one- dimensional partial differential equation (Eq.35) according to the relation;

$$\frac{\partial T}{\partial t} = a \frac{\partial^2 T}{\partial x^2} \quad (35)$$

where  $a$  is the thermal diffusivity which can be calculated from the below (Eq.36)

$$a = \frac{\lambda}{\rho c} \quad (36)$$

The measuring head drops down, touches the fabrics, and the heat flow levels are processed and the thermo-physical properties of the measured specimen are evaluated [5]. The measurement lasts for several minutes only. Thus, reliable measurements on wet fabrics are possible, since the sample moisture during the measurement keeps almost constant. As mentioned earlier, socks are worn inside the shoes under first-order boundary conditions, and Alambeta testing corresponded well to the use of socks inside a shoe (boundary conditions of first-order). Thermal resistance ( $R_{ct}$ ) assessed using the Alambeta tester, which enables fast measurement of both steady-state and transient-state thermal properties as shown in (Fig.13). This diagram demonstrated the maximum  $q_{max}$ , dynamic (transient)  $q_{dyn}$  and  $q_{steady}$  heat flow.

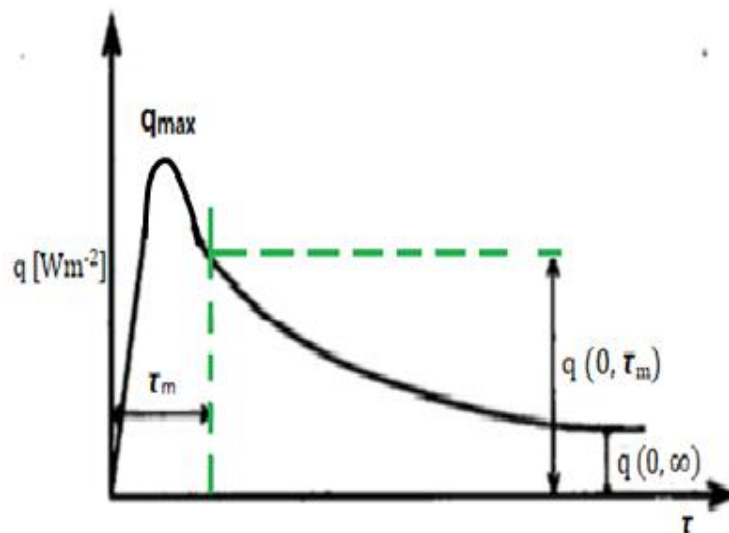


Figure 13. Time dependence heat flow after contact [30]

Steady-state heat flow has been shown by (Eq.37)

$$q_{steady} = \frac{t_1 - t_2}{R_{ct}} \quad (37)$$

Thermal resistance ( $R_{ct}$ ) [ $m^2KW^{-1}$ ] is used to express the heat insulation properties of the fabric.  $R_{ct}$  of textiles is affected by fibre conductivity, fabric porosity, and fabric structure. It is also a function of fabric thickness, as shown by the following expression (Eq.38);

$$R_{ct} = \frac{h}{\lambda} \quad (38)$$

### 3.8.2 Permetest

The relative water vapour permeability and  $R_{ct}$  [ $m^2KW^{-1}$ ] were measured by using Permetest. The Permetest [157][98][49] instrument is the so-called skin model that simulates dry and wet human skin and it serves for the determination of water vapour and thermal resistance of fabrics. Common standard measuring instruments mostly do not provide for a reliable measurement of water vapour permeability for wet fabrics due to the time-consuming measurement. Permetest is the equipment which provides a faster measurement of the water vapour permeability of fabrics, especially, in the wet state. The main contribution of the measurement is the determination of the exact ratio between the level of heat flux density of the heat flow penetrating the wet fabric having a cooling effect, and that of the heat flux density of the heat flow caused by the moisture evaporation from the fabric surface, also has a cooling effect [25]. Results of measurements are expressed in the units defined in the ISO Standard 11092. Thermal resistance  $R_{ct}$  is measured as per below (Eqs.39-41).

$$R_{ct0} = \frac{(t_s - t_a) \times A}{P} \quad (39)$$

$$R_{ctn} = \frac{(t_s - t_a) \times A}{P} \quad (40)$$

$$R_{ct} = R_{ctn} - R_{ct0} \quad (41)$$

Where,  $t_s$ ,  $t_a$  are skin and ambient temperatures respectively.  $A$  represented area [ $m^2$ ] and  $P$  is the transmitted power [ $W$ ].  $R_{ct0}$  and  $R_{ctn}$  are the thermal resistance values without and with a sample. Relative water vapour permeability (RWVP) is a non-standardized but practical parameter. It is given by the following relationship (Eq.42):

$$RWVP (\%) = 100 \left( \frac{q_s}{q_0} \right) \quad (42)$$

$q_s$ ,  $q_0$  are heat flow with and without sample respectively.

### 3.8.3 Thermal foot model

Thermal foot model (TFM) is a part of the “thermal sweating foot manikin system”. It consists of 13 silver alloy surface segments, stainless steel supporting structure, shock absorbers, heating subsystem, and sweating subsystem. TFM is intended to test the thermal resistance and evaporation resistance of footwear. Geometrically it resembles a human foot with several geometrical modifications. The size of the TFM was tuned to fit into the footwear of standard 42 EU size. The heating subsystem was connected by highly flexible cables to thermal manikin controller (TMC). The sweating subsystem was connected to the water dispensing unit (DU). For more detail see (appendix 1). At the moment water dispensing was functional as per the gravimetric method. Both TMC and DU were controlled programmatically by means of MANICON computer program on a standard PC. (Fig.14a) depicts an assembled FM, attached to Gait Simulator. (Fig.14b) is a general layout of individually controlled surface segments. The thermal resistance of the sock is measured as per the above (Eqs.39-42).

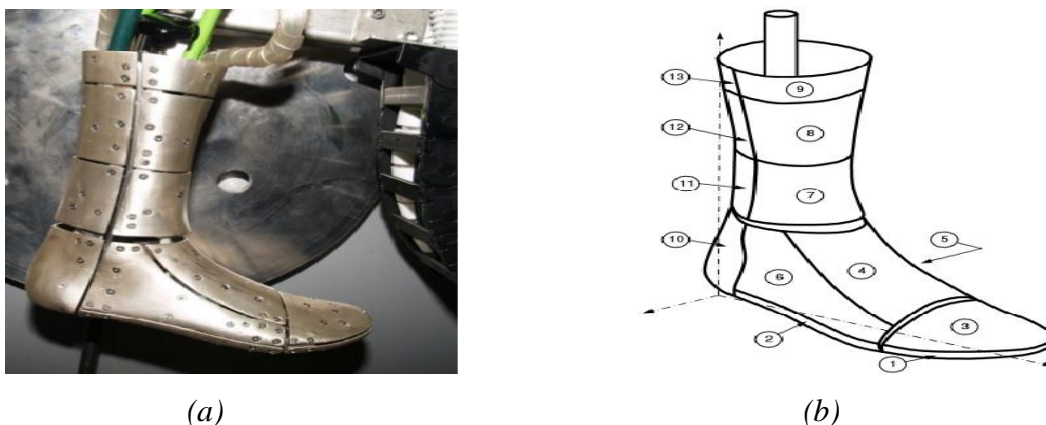


Figure 14.(a) Assembled foot manikin (b) The layout of surface segments [158]

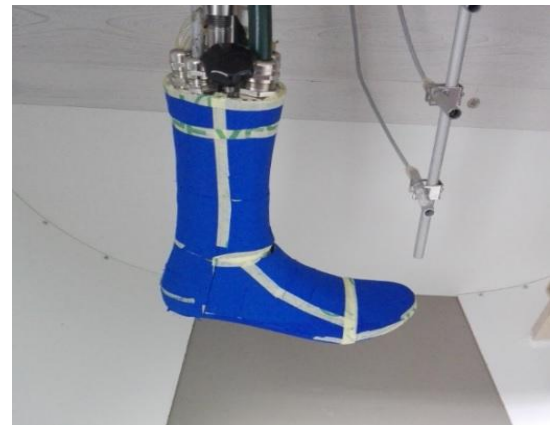
Before discussing the comparison of  $R_{ct}$  between Alambeta, thermal foot model (TFM), and Permetest, it is very important to understand the difference of measuring conditions as given in Table 9. The thermal resistance comparison was performed based on the similarity of testing conditions. There is no free convection existing on Alambeta. So ( $0.1\sim 0.25\text{ ms}^{-1}$ ) air velocity is selected when comparing Alambeta with TFM. In the case of Permetest and TFM comparison, both have  $1\text{ms}^{-1}$  air velocity.

**Table 9. Thermal skin models comparison**

Parameter	Thermal foot model	Permetest	Alambeta
Convection	0.1~0.25 ms <sup>-1</sup> , 1ms <sup>-1</sup>	1ms <sup>-1</sup>	0.1~0.25 ms <sup>-1</sup>
Relative humidity	65 ± 5 %	65 ± 5 %	65 ± 5 %
Ambient temperature	21±1 °C	21±1 °C	21±1 °C
Foot /skin model temperature	35°C	Ambient temperature +10°C	Ambient temperature +10°C
Chamber door	Open	Not Applicable	Not Applicable
Permeable membrane	TFM glued with a semi-permeable membrane as shown in (Fig.15a and Fig.15b)	Permetest already has a GORE-TEX membrane.	Not Applicable



(a)



(b)

*Figure 15. (a) A semi-permeable membrane of 2.9 m<sup>2</sup>paW<sup>-1</sup> glued (b) Open spaces between segments are covered with paper tape*

### 3.8.4 Averaging thermal conductivity & filling coefficient calculations

By assuming that the fabric density is changing by wetting, then wetting causes the change of filling coefficient, porosity and thermal conductivity of fabrics. On the basis of these assumptions following three equations are developed that will be applied to find the fabric density, filling coefficient and thermal conductivity for different moisture levels. An average thermal conductivity for different fibres (within socks) at different moisture levels will be calculated as per (Eq.43).

$$\text{Average Thermal Conductivity } (\lambda_{\text{wet Polymer}}) = \left( \frac{F_w \lambda_w + F_{\text{fib1}} \lambda_{\text{fib1}} + F_{\text{fib2}} \lambda_{\text{fib2}} + \dots}{F_w + F_{\text{fib1}} + F_{\text{fib2}} + \dots} \right) \quad (43)$$

$F_w$  = Water filling coefficient,  $F_{\text{fib1}}$  = 1<sup>st</sup> fibre filling coefficient,

$F_{\text{fib2}}$  = 2<sup>nd</sup> fibre filling coefficient,  $\lambda_w$  = Water thermal conductivity,

$\lambda_{\text{fib1}}$  = 1<sup>st</sup> fibre thermal conductivity,  $\lambda_{\text{fib2}}$  = 2<sup>nd</sup> fibre thermal conductivity

Filling coefficients for water, fibre, wet polymer, and the air is calculated as per below steps given in Table 10;

**Table 10. Filling coefficients**

Measurement	$F_w$ = Water filling coefficient	$F_{\text{fib}}$ = Fibre filling coefficient
Moisture content	%	%
Mass	gram	gram
Area	m <sup>2</sup>	m <sup>2</sup>
Areal density	$\frac{\text{gram}}{\text{m}^2}$	$\frac{\text{gram}}{\text{m}^2}$
Volumetric density	$\frac{\text{Areal density}}{\text{Fabric thickness}} [\text{kgm}^{-3}]$	$\frac{\text{Areal density}}{\text{Thickness}} [\text{kgm}^{-3}]$
Filling coefficient	$\frac{\text{Volumetric density}}{\text{Water density}}$	$\frac{\text{Volumetric density}}{\text{Fibre density}}$

Air filling coefficient ( $F_a$ ) is calculated as per below (Eq.44);

$$\text{Air filling coefficient } (F_a) = 1 - (F_w + F_{\text{fib}}) \quad (44)$$

Filling coefficient for wet polymer will be calculated as per (Eq.45). This value will be used as input in all above models for measurement of thermal resistance in wet states.

$$\text{Wet Polymer filling coefficient } (F_{\text{wet polymer}}) = F_w + F_{\text{fib}} \quad (45)$$

The output of (Eqs.43-45) is used as input in the above models. The thermal conductivity of water and air is taken as 0.60, 0.026 [Wm<sup>-1</sup>K<sup>-1</sup>] while the density of water is 1000 [Kgm<sup>-3</sup>].

Different values were found for the thermal conductivity of textile fibres. However, the following values of density [159] and thermal conductivity have been taken for different fibres in this study are given below in the below Table 11.

**Table 11. Different fibres properties**

Fibre name	Density [Kgm <sup>-3</sup> ]	Thermal conductivity [Wm <sup>-1</sup> K <sup>-1</sup> ]
Cotton	1540	0.50 [160]
Viscose	1530	0.50 [62] [159] [160]
Polyester	1360	0.40 [159]
Polyamide	1140	0.30 [159] [160] [161]
Polypropylene	900	0.20 [159] [160]
Wool	1310	0.50 [62]
Acrylic	1150	0.29 [81]

### 3.8.5 Validation of the models

Validation of the theoretical models is done by comparison of results (x) with results obtained by experiments (y) for a set of parallel determinations. If both methods (theoretical & experimental) lead to same results, the dependence of y on x is linear ( $y = \beta_1x + \beta_2$ ) with zero intercept  $\beta_2 = 0$  and unit slope  $\beta_1 = 1$ . This validation is done by the joint confidence region for intercept and slope because estimators are correlated. Assumptions for this composite inference will be as under i.e.

1. Null hypothesis  $H_0: \beta_2 = 0$  and  $\beta_1 = 1$
2. Alternative hypothesis  $H_1: \beta_2 \neq 0$  and  $\beta_1 \neq 1$
3. Level of significance:  $\alpha = 0.05$
4. Test statistics:

$$F_1 = \frac{(RSC_1 - RSC)(n-m)}{RSCq} \quad (46)$$

5. Critical region:

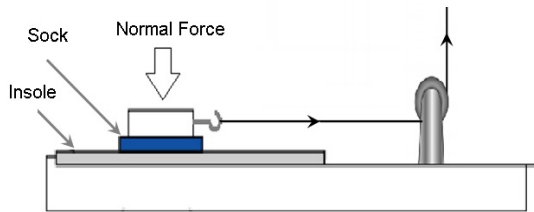
Check the value from table for Fisher-Snedecor F-distribution  $F_{0.95}(m, n-m)$

6. Conclusion:

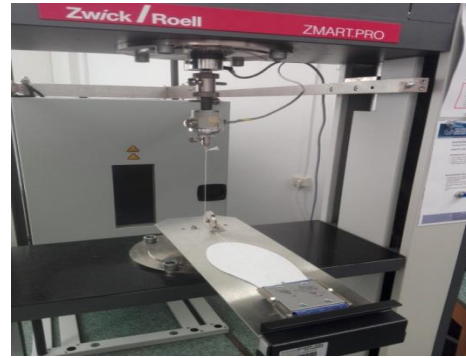
If the calculated value (Eq.46) is less than the critical value then accept the null hypothesis  $H_0: \beta_2 = 0$  and  $\beta_1 = 1$ . It means both intercept and slope isn't significantly different from 0 and 1 respectively at a 95% confidence level. A simultaneous test of the composite hypothesis confirmed that a new laboratory method (by theoretical model) is in agreement with the results of a standard one (experimental). And if the calculated value is higher than the critical then alternative hypothesis  $H_1: \beta_2 \neq 0$  and  $\beta_1 \neq 1$  will be accepted with the conclusion that theoretical model results aren't in agreement with the experimental results [162][163].

### **3.8.6 Frictional characteristics of socks in wet conditions**

Clothing comfort is an intricate theory affected by different causes i.e. thermophysiological, sensorial, and ergonomic. Thermo-physiological relates to heat and mass transfer, sensorial is a tactile property related to skin feel and ergonomic comfort links to the garment fit and an affinity to stick the skin [164]. Various researchers investigated the effect of humidity on the coefficient of friction between skin-socks & socks-textile interfaces. They all reported an increase in the coefficient of friction with higher humidity [127] [131][165][166]. Friction between another interface (sock-insole) is also very critical to design (socks/ shoes), blister formation, postural balance and friction ratio (between sock-skin & sock-insole interfaces). The purpose of the current study was to assess the effect of different levels of moisture content, influencing the sock-insole frictional performance on the plain knitted socks. All the plain knitted socks (Table 7) have been used for the characterization of friction properties at different moisture levels. The frictional property of the sock-insole interface was determined by using a horizontal plate method (ASTM D1894) where a sled of known weight (200g) connected with a tensile testing machine (Zwick/ Roell ZMART.PRO). This apparatus (Fig.16) is based on the sliding type of movement and can characterize both static and dynamic friction contacts under a variety of test conditions [167][168][169].



(a)



(b)

Figure 16. Horizontal plate friction analyzer (a) Drawing (b) Real situation

The contact area of the sock sample with the insole is  $(6.4 \times 6.4) \text{ cm}^2$ . The load cell of 5N was selected with a pretension of 0.25N and 100mm/min speed to pretension. During the friction test, the insole remained stationary, while the sock (clamped inside the sled) was submitted to a horizontal movement. The friction force between the sock-insole interface was measured by a force sensor and coefficients of friction ( $\mu$ ) were calculated according to (Eq.47).

$$\mu = \frac{F}{N} \quad (47)$$

Although, friction should be characterized under an extension to simulate the real condition, along with the load that produces equivalent normal force to the average human body weight. But it was not feasible on the above-mentioned machine until unless some modification was done through mechanical work. The bodyweight factor could be compensated by the frictional force conversion into the coefficient of friction (COF). Secondly, the aim of the study is the effect of the moisture content on the sock's frictional properties.

## Chapter 4

### 4 Results and discussions

#### 4.1 Socks porosity

##### 4.1.1 Volume porosity of socks by model & micro-tomography (MCT)

Volume porosity (with and without extension) was determined by a semi-empirical approach as per (Eq.34). As fabric areal density and thickness need to be determined experimentally. Socks are extended as per section (3.7 Sample preparation for testing). (Fig.17) shows the final (from the top, wales, and course views) images of all the tested socks scanned by micro-tomography scanner (SkyScan 1272) as 2D and converted into 3D by using NRecon. A sample size of 5x5 mm has been used for scanning these images.

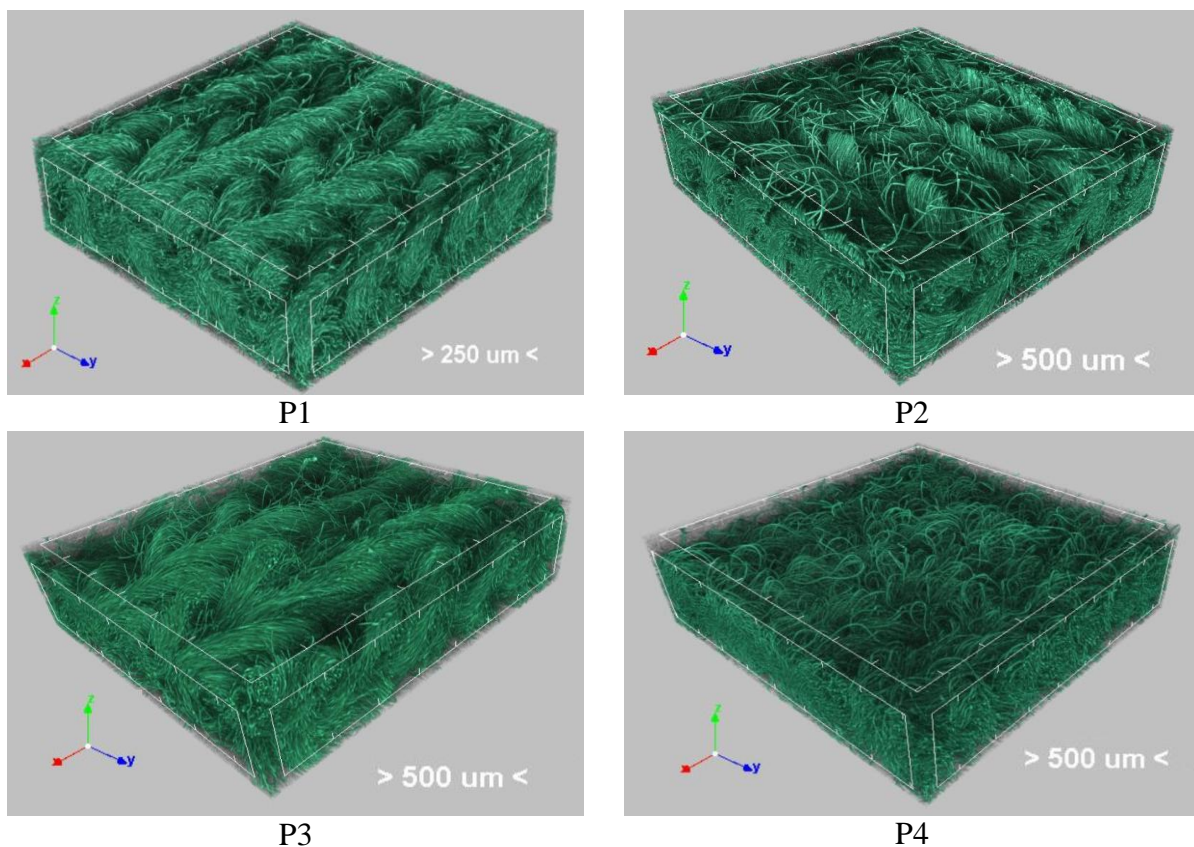


Figure 17. 2D scanned images conversion into 3D images by using NRecon

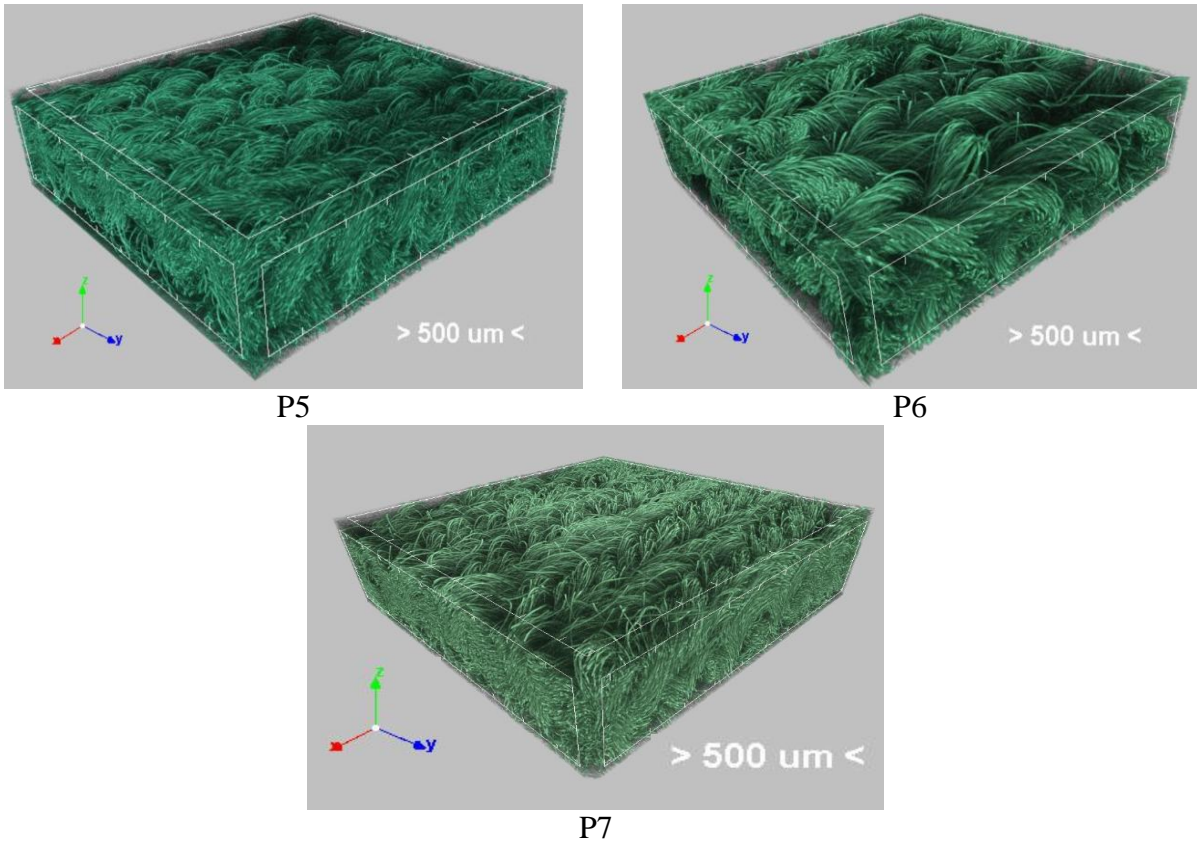


Figure 17. 2D scanned images conversion into 3D images by using NRecon

For porosity quantification, distribution of the pores, and pore thickness, above images were analyzed by using another software recommended by the manufacturer (BRUKER) is CTAn. The analysis data generated by CTAn has been given at the end (see appendices 2-8). The color coded images (Fig.18) were generated by CTVox by using the data provided by CTAn. The measurement of the 3D pore thickness referred to as “sphere-fitting” and this thickness considered as the diameter of the largest enclosed sphere [170].

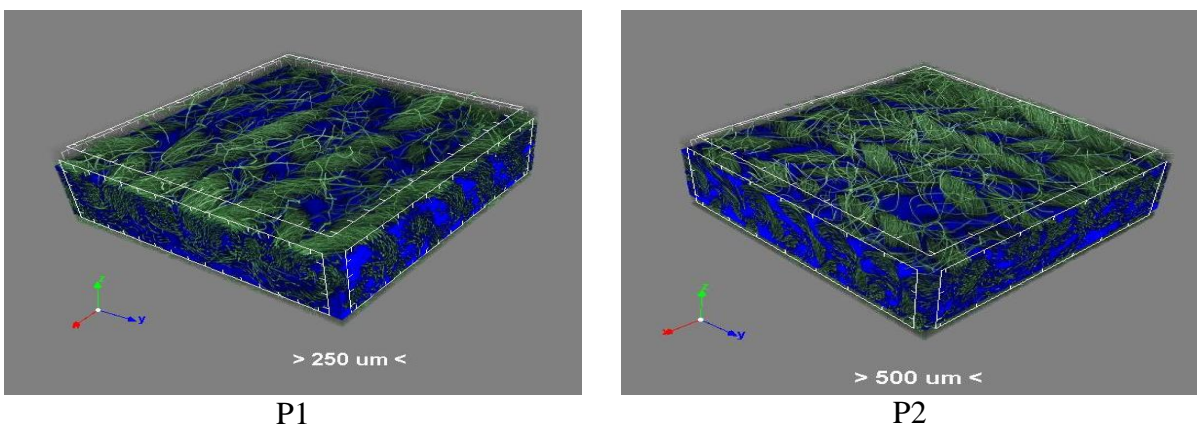


Figure 18. Color coded images by CTVox

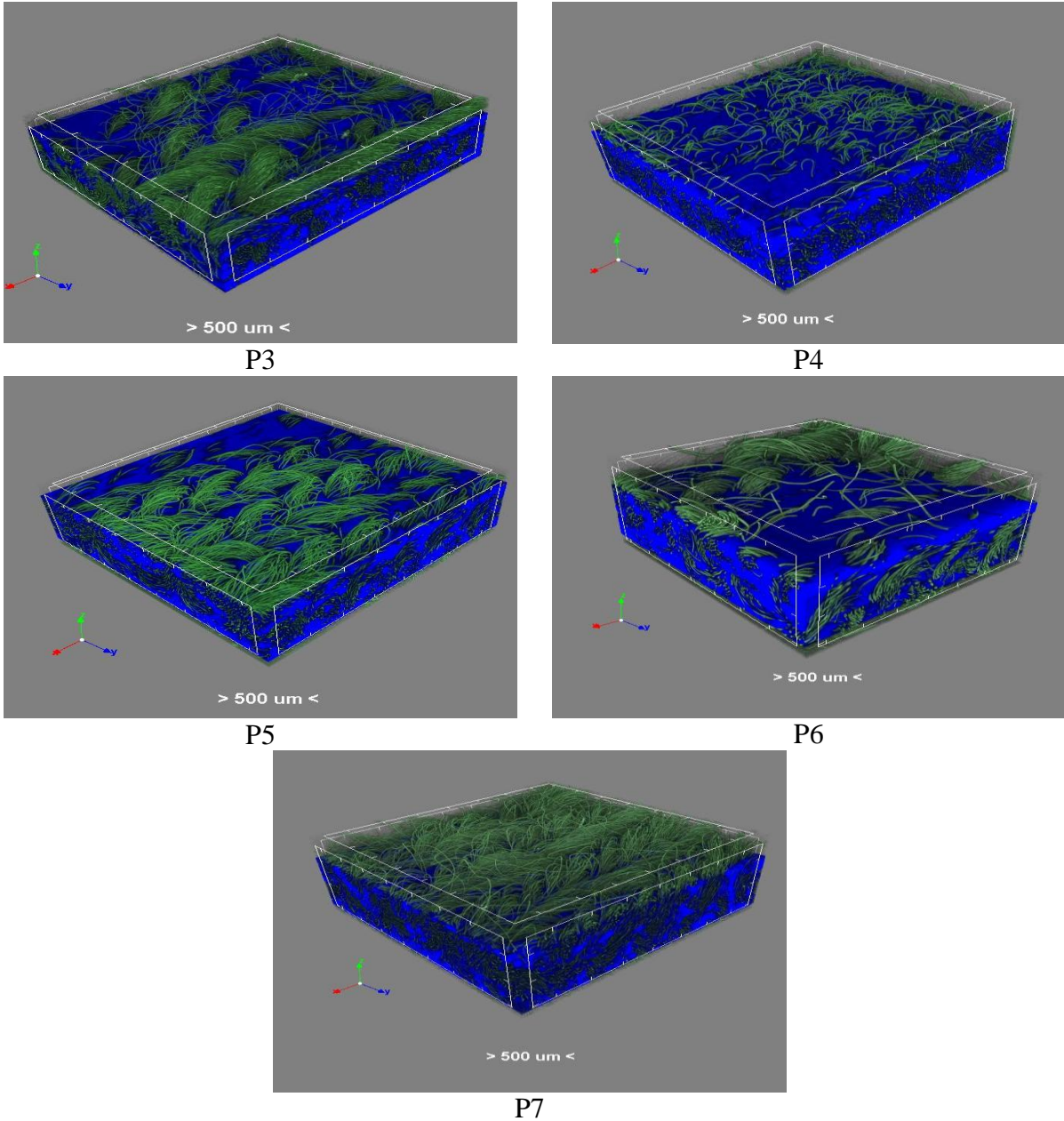


Figure 18. Color coded images by CTVox

Final plots for pore distribution presented in (Figs.19-25) are constructed on the basis of data that has been generated during micro-tomography analysis by CTAn. For more detail, see (appendixes 6 - 12). Pore distributions are colored similar to their representation in the color coded images (Fig.18) where pores are represented by light blue to blue color for large, medium and small pores respectively. Three ranges were selected for distributing the pores into three sizes randomly i.e. small pores range (0.003-0.021mm), medium range (0.021-0.075) and large range (0.075- 0.0309). Although the socks were developed with the same knitting machine on the same parameters, still variation observed in the distribution of pores. Pores distribution depends may upon many factors i.e. fibre type, fibre fineness, yarn

fineness, yarn twist, yarn manufacturing technology etc. (Fig.19) shows the pore distribution thickness for sample P1. Likewise the color coded images (Fig.19), light to dark blue color is divided in three sections for small, medium and large pores. As per the assumed ranges for pores, 22.3775%, 61.5542% and 16.0685 volume is fall in small, medium and large pores range respectively.

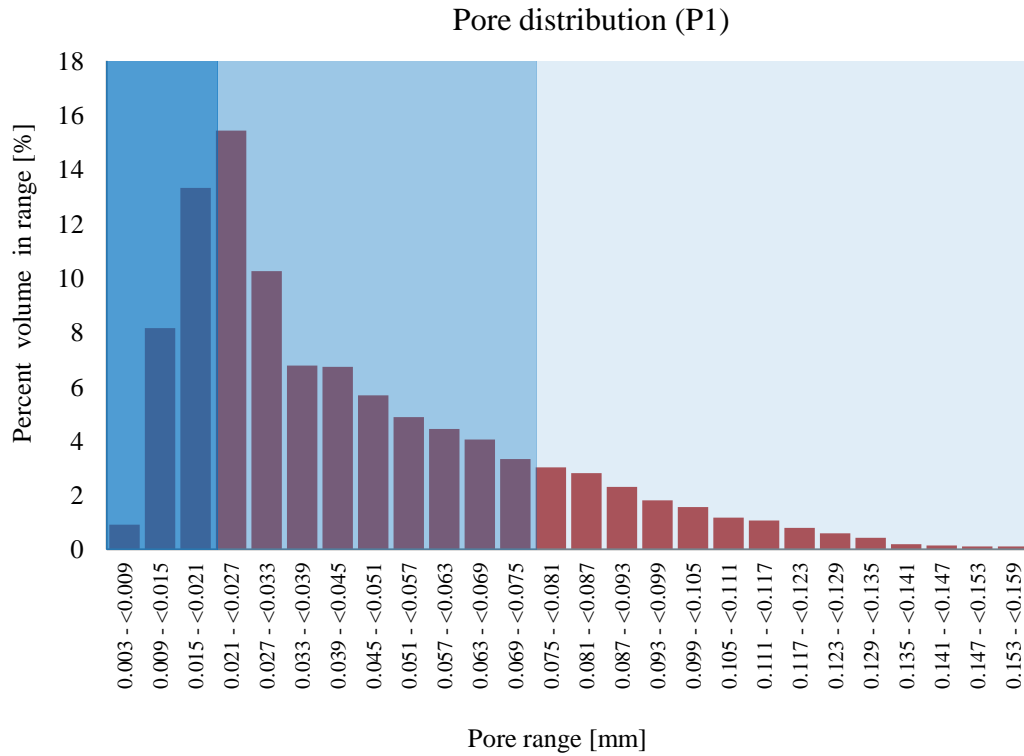


Figure 19. Pore size ranges distribution (P1)

(Fig.20) shows the pore distribution thickness for sample P2. 23.31661% volume is covered by the small pores highlighted with dark blue color. 55.6958% volume is designated for medium size pores and 20.989881% volume is for large pores. As per (Fig.21), medium pores range consist of 42.2126% volume followed by large pore size range 41.39371% and 16.2636% covered by the small pores for P3 sample. The higher percent volume of the large pores is also evident physically (plaited yarn could be seen along with main yarn) and from the macroscopic images (Fig.7). Although the plaited yarn is the same for all the samples, probably the preheat setting of the polyester yarn during dyeing at 130°C causes to reduce its shrinkage. P4 sample has 6.4242%, 58.3583%, and 35.215% volume in range for small, medium, and large pores respectively (Fig.22). Like P4, 8.0138%, 60.3677%, and 31.6184% volume is covered by small, medium, and large pores for P5 (Fig.23). P6 sample has 6.5378%, 41.2942%, and 52.1681% volume for small, medium, and bigger (large) pores

(Fig.24). Likewise to P1 and P2, P7 has 20.4087%, 57.0487%, and 22.5428% volume for small, medium, and large pores (Fig.25).

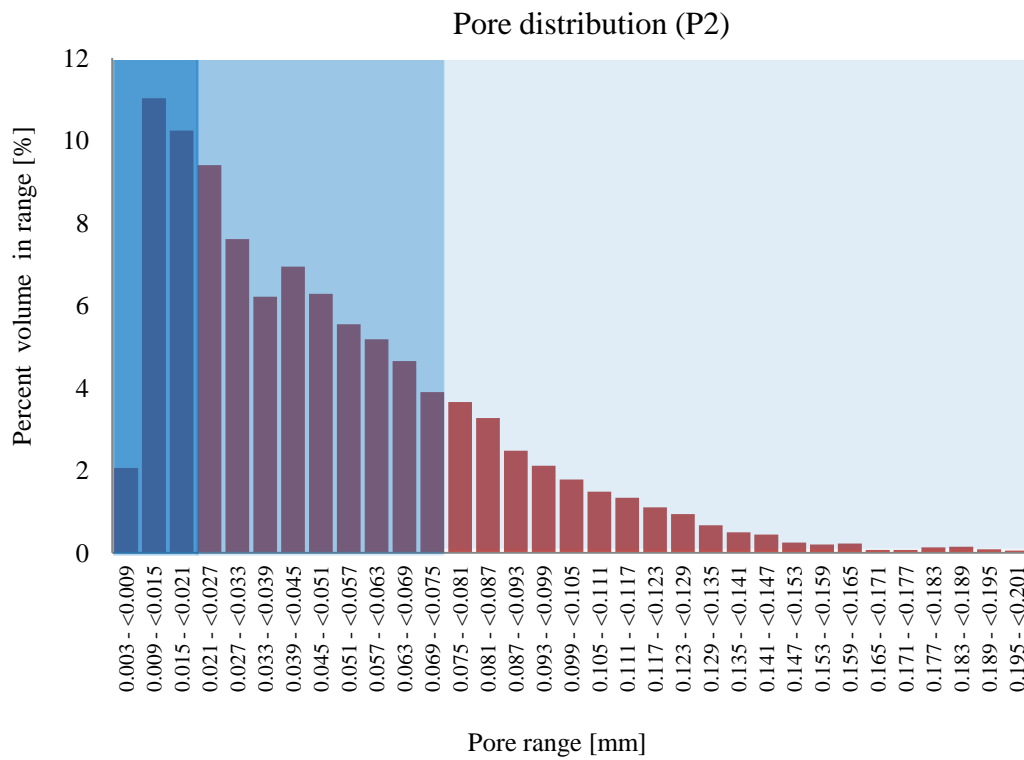


Figure 20. Pore size ranges distribution (P2)

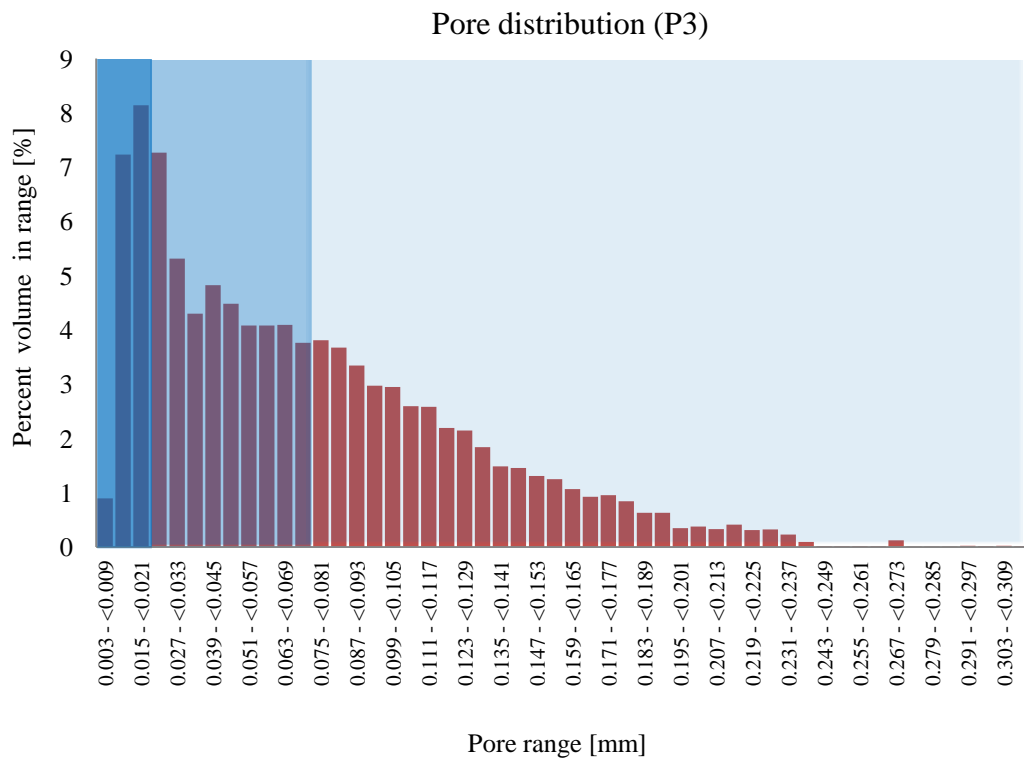


Figure 21. Pore size ranges distribution (P3)

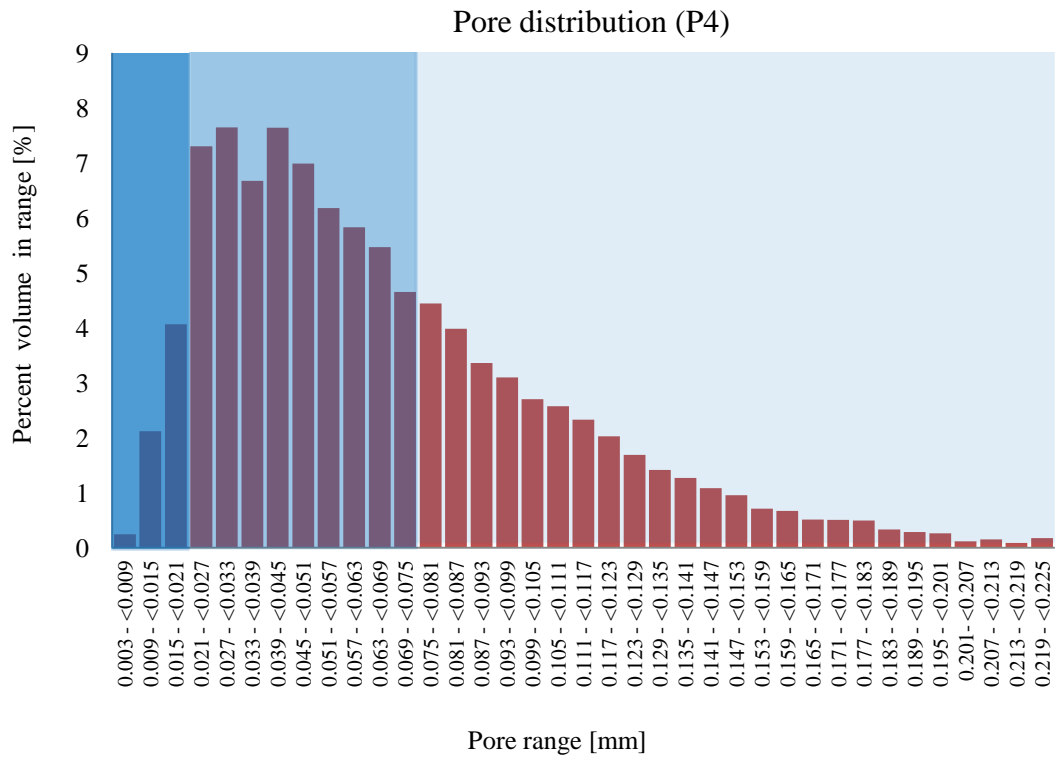


Figure 22. Pore size ranges distribution (P4)

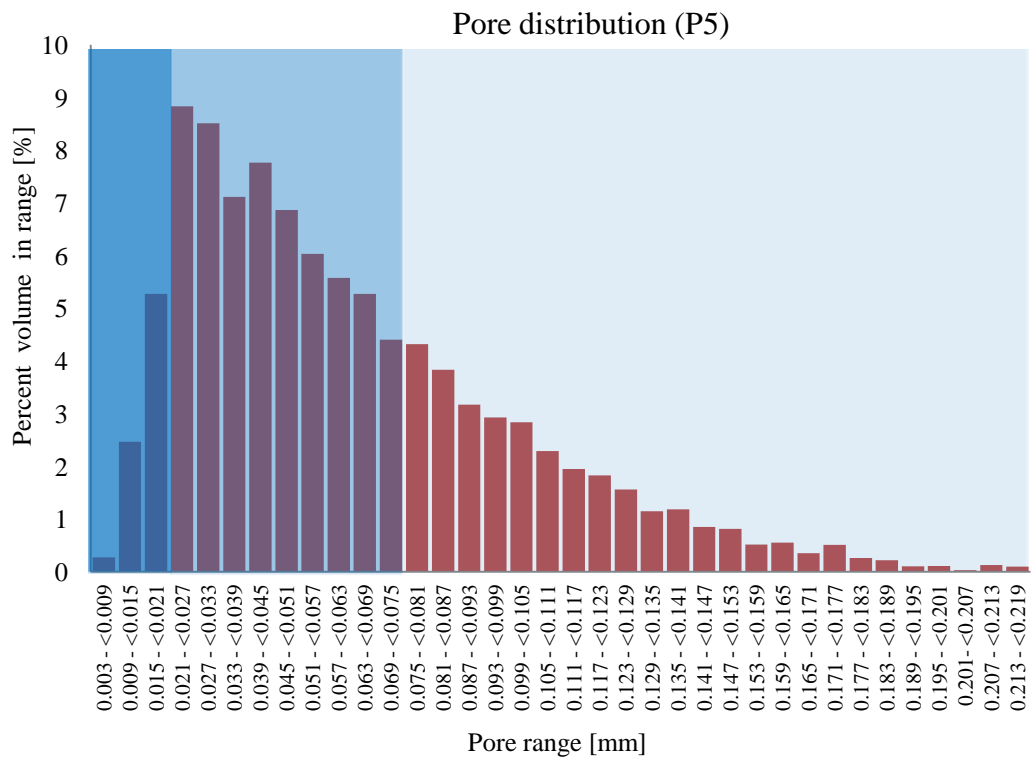


Figure 23. Pore size ranges distribution (P5)

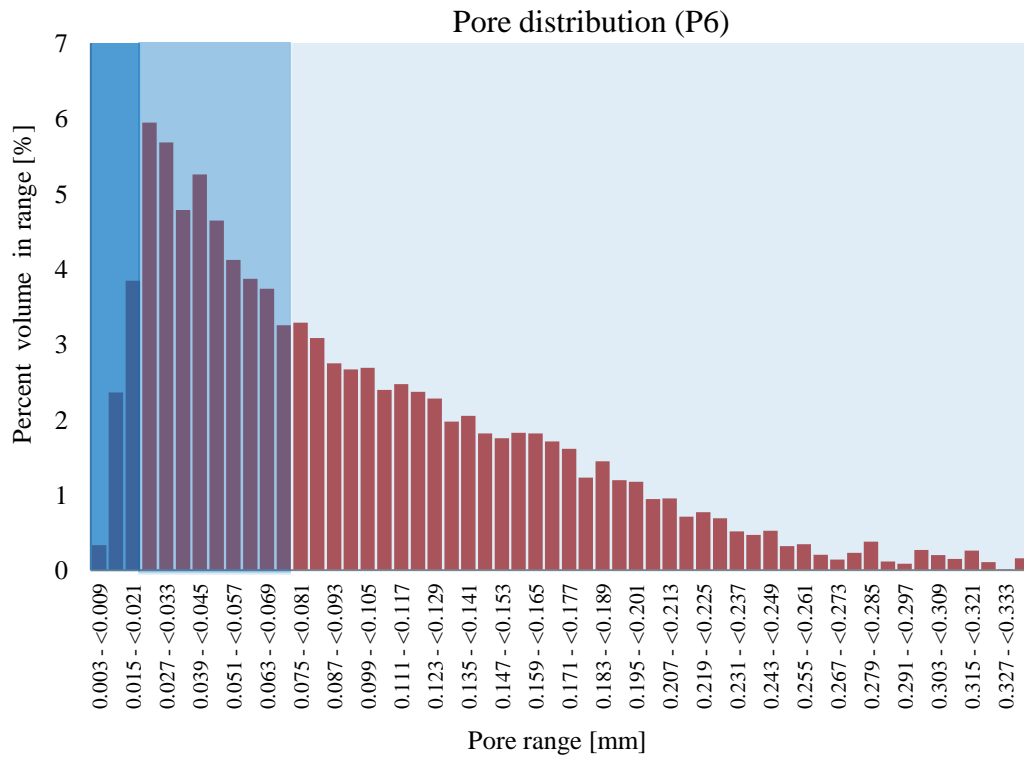


Figure 24. Pore size ranges distribution (P6)

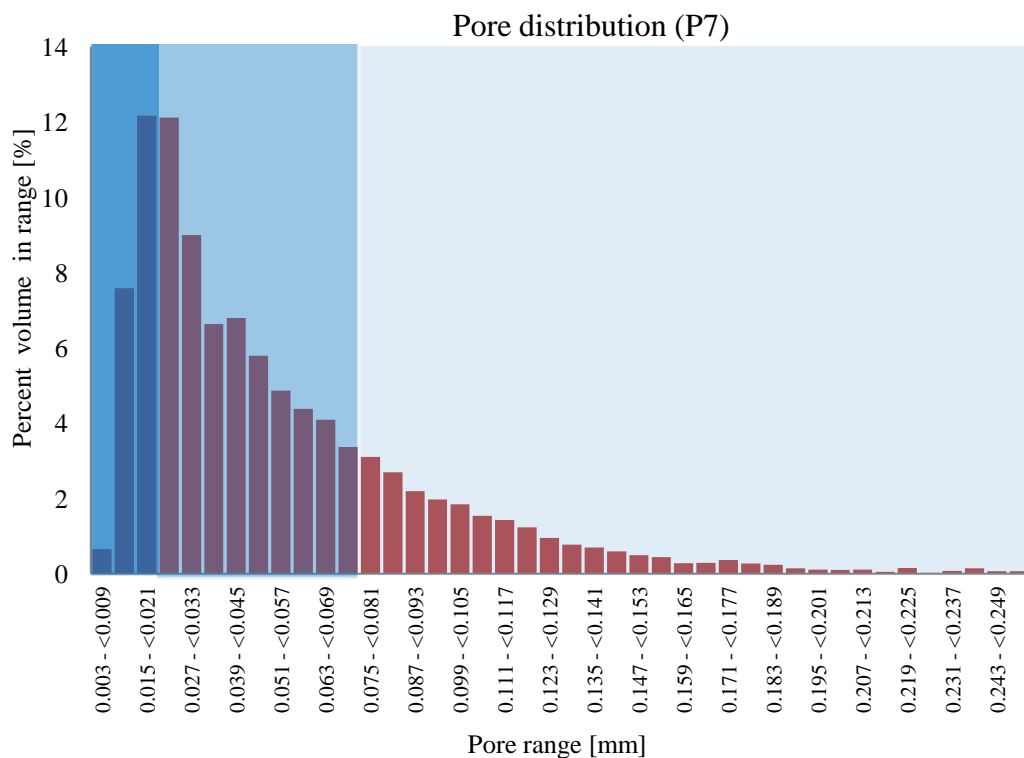


Figure 25. Pore size ranges distribution (P7)

For the measurement of volume theoretical porosity without extension, areal density and thickness are given in (appendix 4). The results of the volume porosity demonstrated that extended socks have higher porosity (Fig.26). This increase in the porosity also reported by

Abdolmaleki et al. at different extension levels for loose knitted fabrics [171]. Porosity falls between 78% to 90% range without and with extension respectively. Guidoin et al. stated that knitted fabrics porosity lies between 67%-84% and even 90% is not uncommon [149]. Extension causes to increase the pore size (space between loops) of the fabric and decrease the fabric thickness. It leads to a decrease in the volume of the fibre (solid part) and increases the volume of air corresponds to porosity. Porosity measured by micro-tomography (Fig.26) is in agreement with theoretical porosity (without extension) at a 95% confidence level for all the socks. As the thermal resistance model's prediction in the next sections is based on this porosity model. This comparison is logical and it further validated that the used model for the calculation of porosity is correct. The difference is between (0.14 - 4.3715%) for all the socks except P1. 7.4256% lower porosity is measured by micro-tomography with respect to the predicted value. That is close to the difference observed by Doczyova et al. i.e. 6% during porosity comparison of knitted structures [172].

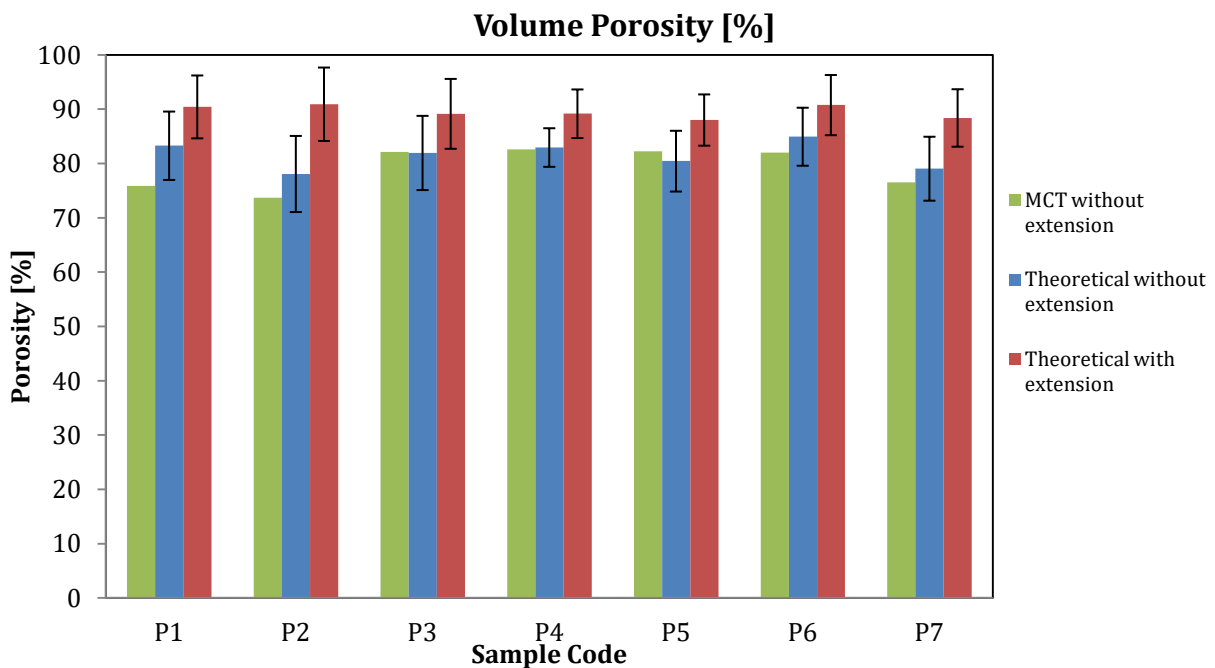


Figure 26. Volume porosity (micro-tomography vs theoretical)

## 4.2 Effect of moisture content on thermal resistance

Figures 28, 30, 32, 34, 36, 38 and 40 clearly demonstrate that as the moisture (%) increases, the thermal resistance decreases irrespective of sock fibre composition. That is in compliance with the previous researchers [22][56][19][18][57][173]. For all the models the input thermal conductivity and filling coefficients were measured in wet polymer at different moisture

levels. The correlation between experimental and predicted models was checked by coefficient of determination ( $R^2$ ). The values of coefficient of determination (Figures 29, 31, 33, 35, 37, 39 and 41) for all the three modified models (ME-2, Schuhmeister and Militky) showed that these models could make reasonable predictions of thermal resistance in the dry, as well as the wet condition also at different moisture levels for all the major fibre blends being used for socks. Coefficient of determination ( $R^2$ ) is fall between 0.7691-0.9535 for all the samples.

### 4.3 Assumptions for theoretical models

All the theoretical models for thermal resistance prediction are used by feeding the thermal conductivity ( $\lambda_{\text{wet polymer}}$ ) and the filling coefficient ( $F_{\text{wet polymer}}$ ) of wet polymer instead dry.  $F_{\text{wet polymer}}$  and  $\lambda_{\text{wet polymer}}$  is calculated as per (Eqs.43-45). After this amendment, these models can also predict thermal resistance for wet fabrics. (Fig.27) demonstrated the volume fraction of air, water, and fibre.

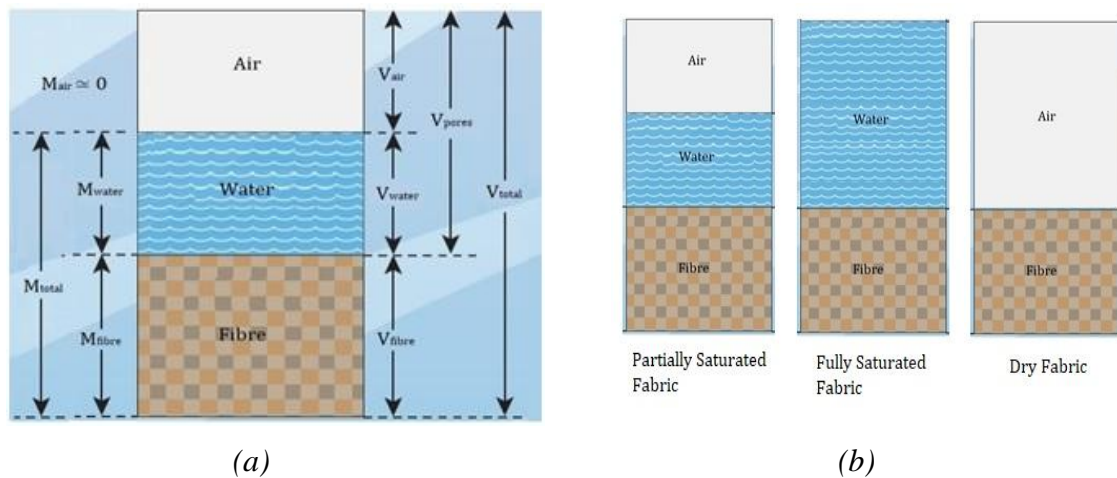


Figure 27. Schematic presentation of (a) Segmental mass & volume, and (b) Volumetric change during wetting

Following are the assumption assumed for the development of theoretical models for the prediction of thermal resistance in the wet state;

- Fabric thickness assumed as constant
- No Free convection (as Rayleigh Number  $< 1000$ )
- The constant different temperature on both surfaces of the fabric **1<sup>st</sup> order boundary conditions**

- To simplify the model, fibre filling coefficient is assumed as **constant**
- Air and water filling coefficients are **variable**
- Fibre (polymer) and water filling coefficients are **combined as wet polymer** filling coefficient
- Thermal conductivity of wet polymer (water and fibres) are combined as per their **volume**
- **No dimensional changes** occurred at different moisture levels as tested in **extended state**
- Fabric areal density and thickness measured in the extended state
- Alambeta's thickness is considered

#### **4.3.1 Effect of moisture content on cotton socks (P1)**

The predicted and experimental thermal resistance of P1 (cotton 80%, polyester 18.20%, elastane 1.8%) at various moisture levels is given in (Fig.28). All three Maxwell modified Militky modified and Schuhmeister modified models have the best prediction at different moisture levels for the P1 sample. ME-2 modified, Militky modified, and Schuhmeister modified have  $R^2$  values, i.e. 0.8911, 0.8851, and 0.8754 respectively as shown in (Fig.29). The thermal resistance is decreasing with the increase of moisture level (Fig.28). About 50% reduction in the thermal resistance is observed at 30% moisture content. This reduction is in accord with Naka and Kamata's study and close to the value reported by Mangat i.e. 70% [57][19]. Kanat et. al also observed a 50% reduction between 25-30% moisture content for single jersey cotton knitted fabrics in loose as well as tight state [173]. This decrease is uniform till 20% moisture content, a rapid decline is observed between 20% and 30% moisture content. This trend is evident in (Fig.28) with green square legends. Overall Schuhmeister has the highest prediction due to 67% consideration of thermal resistance in series followed by the Militky modified model. It means as the portion of series consideration decreases thermal resistance decreases. In line with previous investigations of fibre alignment in series having 2-3 times higher thermal resistance than parallel [77][174].The findings are in accordance with Wang et. al [83] work. They have predicted the thermal conductivity with respect to porosity by using different combinations and models i.e. ME-1, ME-2, series, parallel, EMT, series+ parallel, ME-1+ME-2, etc. According to their findings, the series

model has the lowest thermal conductivity followed by ME-2 while the parallel model has the highest prediction. Conversely, higher thermal conductivity means lower thermal resistance and vice versa. Reddy and Karthikeyan [175] also have the same findings during their study for predicting the thermal conductivity of frozen and unfrozen food materials. Carson’s work further validated these results through the thermal conductivity prediction of wheat flour.

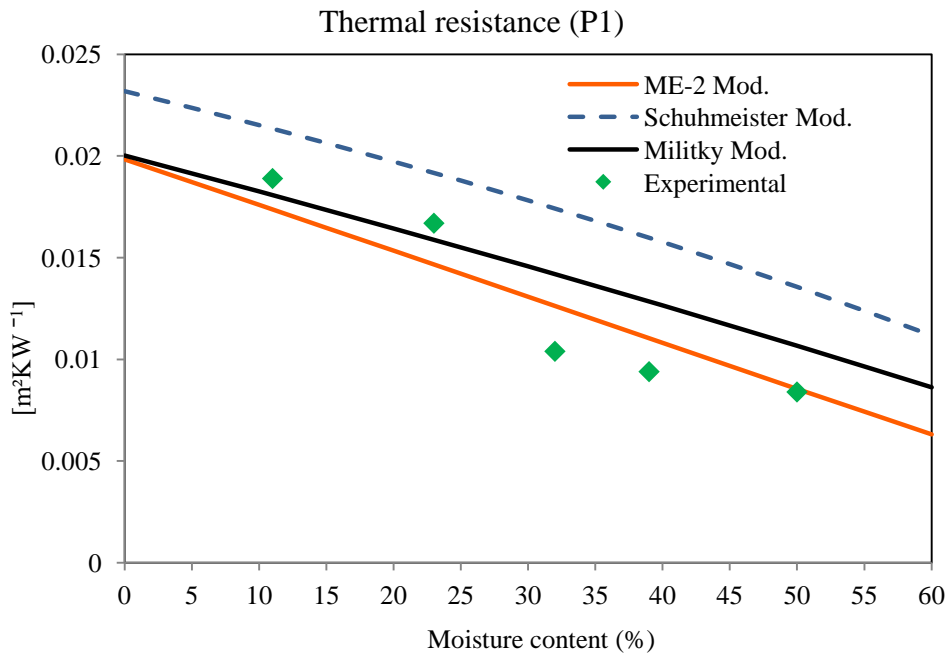


Figure 28. Predicted & experimental thermal resistance: P1 (cotton 80%, polyester 18.20%, elastane 1.8%)

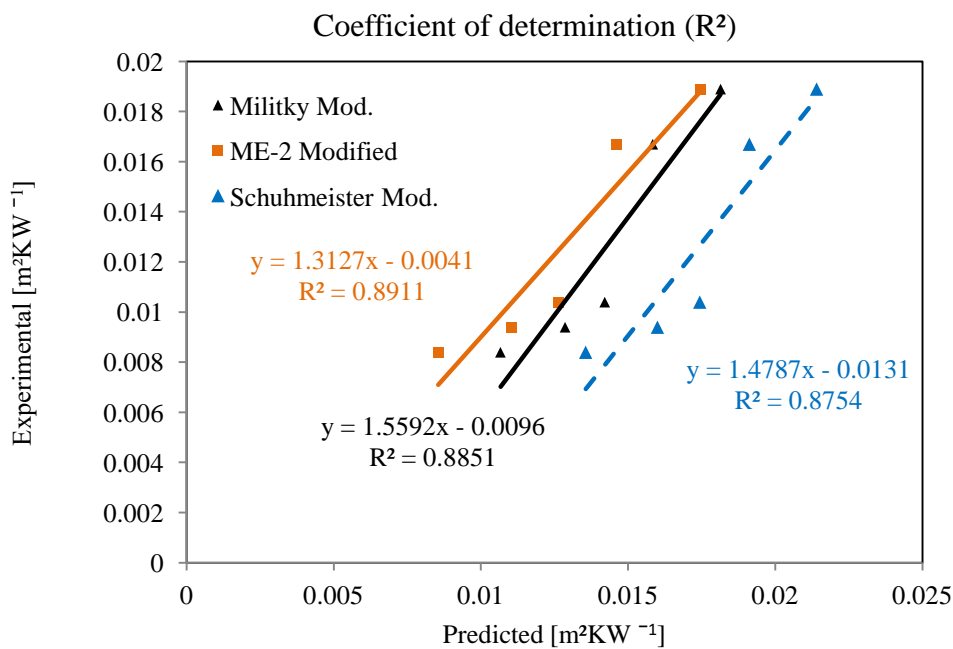


Figure 29. Coefficient of determination predicted & experimental thermal resistance: P1 (cotton 80%, polyester 18.20%, elastane 1.8%)

Validation of the theoretical models is done by comparison of results (x) with results obtained by experiments (y) for a set of parallel determinations. This validation is done by joint confidence region as shown in Table 12.

**Table 12. Summary output P1 (ME-2 Mod. Vs Experimental)**

Predicted (x)	Experimental (y)	$\hat{y}_1 = b(1) + 0$	$(y - \hat{y}_1)^2$	$\hat{y} = 1.3127x - 0.0041$	$(y - \hat{y})^2$
0.01745962	0.0189	0.01745962	0.00000207	0.01881924	0.00000001
0.01460966	0.0167	0.01460966	0.00000437	0.01507811	0.00000263
0.01264591	0.0104	0.01264591	0.00000504	0.01250028	0.00000441
0.01106021	0.0094	0.01106021	0.00000276	0.01041874	0.00000104
0.00855142	0.0084	0.00855142	0.00000002	0.00712545	0.00000162
			RSC <sub>1</sub> = 0.00001427		RSC = 0.00000971

On substitution in to (Eq.46)

$$F_1 = \frac{(0.0001427 - 0.0000971)(5-2)}{(0.0000971)(2)} = 0.7039$$

In the case of ME-2 modified model, ( $F_1 = 0.7039$ ) is lesser than the quantile of the Fisher-Snedecor F-distribution  $F_{0.95}(2, 3) = 9.5521$ , so the null hypothesis  $H_0$  cannot be rejected. It means the predicted thermal resistance with the ME-2 modified model isn't significantly different than the experimental results. Similarly, Table 13 shows the calculations for Militky modified model.

**Table 13. Summary output P1 (Militky Mod. Vs Experimental)**

Predicted (x)	Experimental (y)	$\hat{y}_1 = b(1) + 0$	$(y - \hat{y}_1)^2$	$\hat{y} = 1.5592x - 0.0096$	$(y - \hat{y})^2$
0.01814618	0.0189	0.01814618	0.00000057	0.01869353	0.00000004
0.01584099	0.0167	0.01584099	0.00000074	0.01509927	0.00000256
0.01420975	0.0104	0.01420975	0.00001451	0.01255584	0.00000465
0.01286227	0.0094	0.01286227	0.00001199	0.01045485	0.00000111
0.01066660	0.0084	0.01066660	0.00000514	0.00703136	0.00000187
			RSC <sub>1</sub> = 0.00003295		RSC = 0.00001024

On substitution in to (Eq.46)

$$F_1 = \frac{(0.00003295 - 0.00001024)(5-2)}{(0.00001024)(2)} = 3.3266$$

In Militky modified model, ( $F_1 = 3.3266$ ) is lesser than the quantile of the Fisher-Snedecor F-distribution  $F_{0.95}(2, 3) = 9.5521$ , so the null hypothesis  $H_0$  cannot be rejected. Again it verified that the predicted thermal resistance with the Militky modified model isn't

significantly different than the experimental results. Table 14 shows the summary out for calculation of composite confidence region validation with Schuhmeister modified model.

**Table 14. Summary output P1 (Schuhmeister Mod. Vs Experimental)**

Predicted (x)	Experimental (y)	$\hat{y}_1 = b(1) + 0$	$(y - \hat{y}_1)^2$	$\hat{y} = 1.4787x - 0.0131$	$(y - \hat{y})^2$
0.0214083	0.0189	0.0214083	0.0000063	0.0185565	0.0000001
0.0191248	0.0167	0.0191248	0.0000059	0.0151798	0.0000023
0.0174395	0.0104	0.0174395	0.0000496	0.0126878	0.0000052
0.0160012	0.0094	0.0160012	0.0000436	0.0105610	0.0000013
0.0135620	0.0084	0.0135620	0.0000266	0.0069541	0.0000021
			RSC <sub>1</sub> = 0.0001319		RSC = 0.0000111

On substitution in to (Eq.46)

$$F_1 = \frac{(0.0001319 - 0.0000111)(5-2)}{(0.0000111)(2)} = 16.3287$$

Schuhmeister modified model, ( $F_1 = 16.3287$ ) is greater than the quantile of the Fisher-Snedecor F-distribution  $F_{0.95}(2, 3) = 9.5521$ , so the null hypothesis  $H_0$  cannot be accepted. It means that the predicted thermal resistance with the Schuhmeister modified model is significantly different than the experimental results.

### 4.3.2 Effect of moisture content on viscose socks (P2)

In the case of P2 sock (viscose 81.08%, polyester 17.22% & elastane 1.77%), Militky modified model has the best prediction at 11.45%, and 19.50% moisture levels as shown in (Fig.30). ME-2 modified has a better thermal resistance prediction at 30.30, 40.17% and 49.80% moisture levels. All three models have a reasonable prediction of thermal resistance with  $R^2 > 0.94$  as shown in (Fig.31). Similar to the P1 sample a rapid decline in the thermal resistance with the increased moisture content is also observed, between 20% to 30% moisture content. This reduction is in agreement with Naka and Kamata's study and close to the value reported by Mangat i.e. 70% [57][19]. Schuhmeister modified model has the highest prediction followed by Militky modified and ME-2 modified at all the moisture levels. Over again lowest to the highest prediction of thermal resistance order by different models has verified the findings of Finck[174], Bogaty et. al [77], Wang et. al [83] & Reddy [175]. From these studies, it has been established that series alignment has predicted the highest thermal resistance followed by ME-2, combinations of (ME-2, ME-1, EMT, series, and parallel), EMT, ME-1, and parallel.

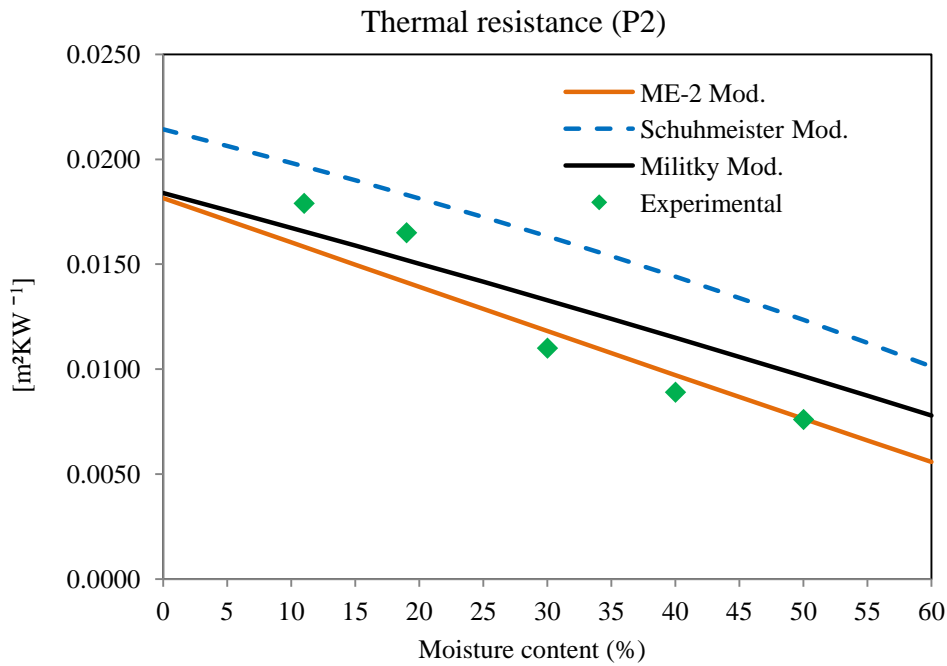


Figure 30. Predicted & experimental thermal resistance: P2 (viscose 81.08%, polyester 17.22% & elastane 1.77%)

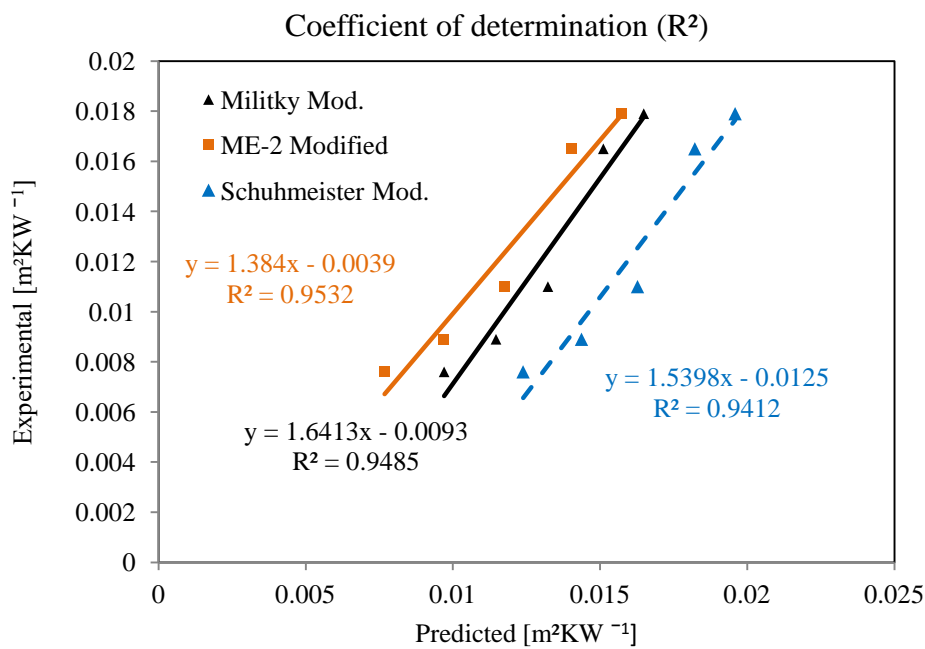


Figure 31. Coefficient of determination predicted & experimental thermal resistance: P2 (viscose 81.08%, polyester 17.22% & elastane 1.77%)

Tables (15-17) show that the value of composite confidence region for slope and intercept at 95% confidence level validated all the theoretical models except Schuhmeister modified model as the calculated value  $F_1=24.6719$  is higher than the critical value  $F_{0.95}(2, 3) =$

9.5521. It means the thermal resistance prediction with Schuhmeister modified model is not significantly correct with respect to experimental results. As per Table 15 and acceptance of the null hypothesis  $H_0$ , ME-2 modified model is validated as having lower  $F_1$  i.e. 3.0476 than the critical value 9.5521. In case of Militky modified model, ( $F_1 = 3.0476$ ) is lower than the quantile of the Fisher-Snedecor F-distribution  $F_{0.95}(2, 3) = 9.5521$ , so the null hypothesis  $H_0$  cannot be rejected.

**Table 15. Summary output P2 (ME-2 Mod. Vs Experimental)**

Predicted (x)	Experimental (y)	$\hat{y}_1 = b(1) + 0$	$(y - \hat{y}_1)^2$	$\hat{y} = 1.384x - 0.0039$	$(y - \hat{y})^2$
0.015732933	0.0179	0.015732933	0.000004696	0.017874379	0.000000001
0.014030435	0.0165	0.014030435	0.000006099	0.015518121	0.000000964
0.011750911	0.0110	0.011750911	0.000000564	0.012363261	0.000001858
0.009679554	0.0089	0.009679554	0.000000608	0.009496502	0.000000356
0.007675258	0.0076	0.007675258	0.000000006	0.006722557	0.000000770
			RSC <sub>1</sub> = 0.000011972		RSC = 0.000003949

On substitution in to (Eq.46)

$$F_1 = \frac{(0.000011972 - 0.000003949)(5-2)}{(0.000003949)(2)} = 3.0476$$

**Table 16. Summary output P2 (Militky Mod. Vs Experimental)**

Predicted (x)	Experimental (y)	$\hat{y}_1 = b(1) + 0$	$(y - \hat{y}_1)^2$	$\hat{y} = 1.641x - 0.0093$	$(y - \hat{y})^2$
0.01648714	0.0179	0.01648714	0.00000200	0.01776035	0.00000002
0.01511428	0.0165	0.01511428	0.00000192	0.01550706	0.00000099
0.01323149	0.0110	0.01323149	0.00000498	0.01241684	0.00000201
0.01146789	0.0089	0.01146789	0.00000659	0.00952225	0.00000039
0.00970520	0.0076	0.00970520	0.00000443	0.00662915	0.00000094
		0.06600600	RSC <sub>1</sub> = 0.00001992		RSC = 0.00000434

On substitution in to (Eq.46)

$$F_1 = \frac{(0.00001992 - 0.00000434)(5-2)}{(0.00000434)(2)} = 3.0476$$

**Table 17. Summary output P2 (Schuhmeister Mod. Vs Experimental)**

Predicted (x)	Experimental (y)	$\hat{y}_i = b(1) + 0$	$(y - \hat{y}_i)^2$	$\hat{y} = 1.641x - 0.0093$	$(y - \hat{y})^2$
0.01959151	0.0179	0.01959151	0.00000286	0.01766701	0.00000005
0.01822300	0.0165	0.01822300	0.00000297	0.01555978	0.00000088
0.01627555	0.0110	0.01627555	0.00002783	0.01256109	0.00000244
0.01437243	0.0089	0.01437243	0.00002995	0.00963067	0.00000053
0.01238805	0.0076	0.01238805	0.00002293	0.00657512	0.00000105
			RSC <sub>1</sub> = 0.00008653		RSC = 0.00000496

On substitution in to (Eq.46)

$$F_1 = \frac{(0.00008653 - 0.00000496)(5-2)}{(0.00000496)(2)} = 24.6719$$

### 4.3.3 Effect of moisture content on polyester socks (P3)

(Fig.32) depicts theoretical and experimental thermal resistances of P3 socks (polyester 98.38% & elastane 1.62%) at various moisture levels. ME-2 modified, Militky modified and Schuhmeister modified models have R<sup>2</sup> values 0.7999, 0.7876, and 0.7671 respectively (Fig.33). The drop off in the thermal resistance is slower and uniform between 5 % to 10% and 20% to 50% moisture content levels. But this decline (42% reduction) is fast between 10% to 20% moisture content as evident from experimental green square legends (Fig.32). This is in concurrence to Bogusławska and Hes work who reported a 50% reduction in the thermal resistance between 10 to 20% moisture content in different fabrics [25]. Kanat et. al have reported a 30-35% reduction at 25% moisture level for single jersey polyester knitted fabrics [173]. Unlike P1 and P2, 50% of the thermal resistance reduction in P3 is observed at 50% moisture content due to the hydrophobic nature of polyester. Once more Schuhmeister modified model has a higher prediction at all the moisture levels except 5% and 10% moisture content. It has predicted 0.5 to 2 times higher thermal resistance. It is in accord with Mao and Russel's study [176]. They have observed 0.5 to 3 times lower thermal conductivity prediction for 100% polyester spacer fabric with Schuhmeister's model. They haven't incorporated moisture content. Even then their predictions are very high with respect to experiments. Lowest to the highest prediction of thermal resistance sequence with these models are in line with the findings of previous researchers [174][77][83][175].

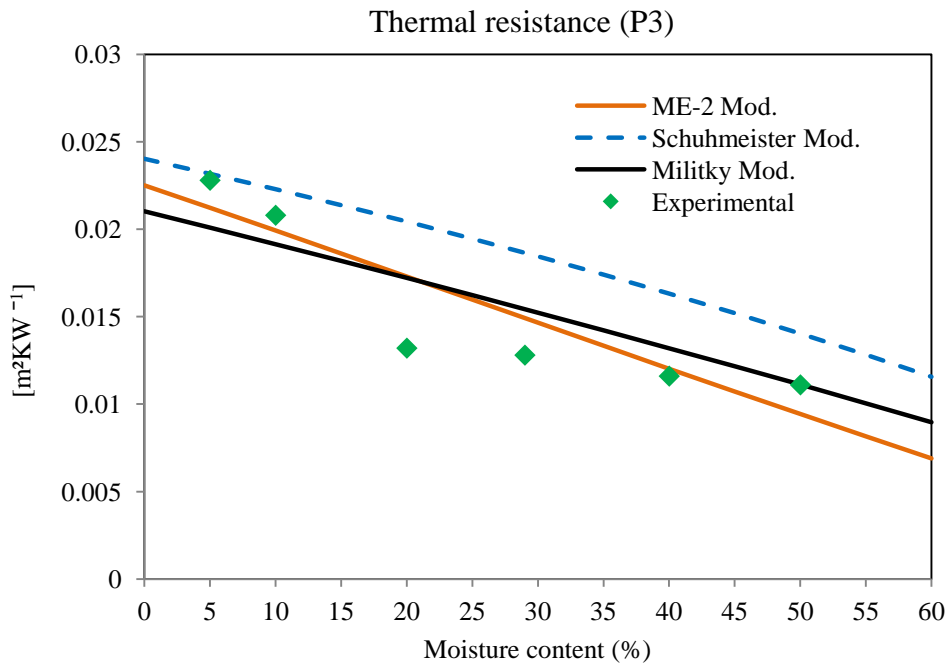


Figure 32. Predicted & experimental thermal resistance: P3 (polyester 98.38% & elastane 1.62%)

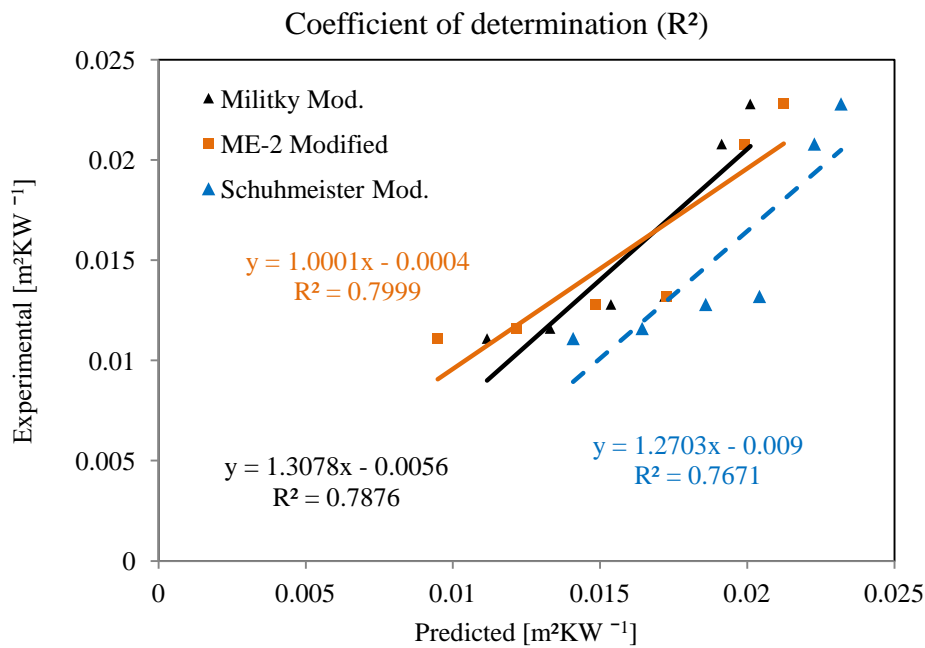


Figure 33. Coefficient of determination predicted & experimental thermal resistance: P3 (polyester 98.38% & elastane 1.62%)

As per Tables (18-20) and the values of the constructed confidence region for slope and intercept at 95% confidence level validated all the theoretical models. All the models have lower  $F_1$  values than the tabulated values (critical region). So the null hypothesis couldn't be rejected for these models. It means the intercepts ( $\beta_2$ ) and slopes ( $\beta_1$ ) aren't significantly different from zero and one respectively. So the thermal resistance prediction with all three

modified models is not significantly different with respect to experimental results for sample P3. Calculated values of  $F_1$  also justify the ME-2 modified model has top prediction among all others followed by Militky modified and Schuhmeister modified. On the nutshell ME-2 modified model has the better forecast for sample P3 than both other models i.e. Militky modified and Schuhmeister modified.

Test statistics (calculated  $F_1$ ) values are 0.2369, 1.1055 and 6.8867 for ME-2, Militky & Schuhmeister modified models respectively against the critical value of the Fisher-Snedecor F-distribution  $F_{0.95}(2, 4) = 6.9443$ . So the null hypothesis  $H_0$  cannot be rejected. It means the predicted thermal resistance with these models isn't significantly different than the experimental results. Similarly, Table 19 shows the calculations for Militky modified model.

**Table 18. Summary output P3 (ME-2 Mod. Vs Experimental)**

Predicted (x)	Experimental (y)	$\hat{y}_1 = b(1) + 0$	$(y - \hat{y}_1)^2$	$\hat{y} = 1.0001x - 0.0004$	$(y - \hat{y})^2$
0.021242	0.0228	0.021242	0.000002	0.020844	0.000004
0.019911	0.0208	0.019911	0.000001	0.019513	0.000002
0.017272	0.0132	0.017272	0.000017	0.016873	0.000013
0.014835	0.0128	0.014835	0.000004	0.014437	0.000003
0.012155	0.0116	0.012155	0.000000	0.011756	0.000000
0.009490	0.0111	0.009490	0.000003	0.009091	0.000004
			RSC <sub>1</sub> = 0.000024		RSC = 0.000022

On substitution in to (Eq.46)

$$F_1 = \frac{(0.000024 - 0.000022)(6-2)}{(0.000022)(2)} = 0.2369$$

**Table 19. Summary output P3 (Militky Mod. Vs Experimental)**

Predicted (x)	Experimental (y)	$\hat{y}_1 = b(1) + 0$	$(y - \hat{y}_1)^2$	$\hat{y} = 1.3078x - 0.0056$	$(y - \hat{y})^2$
0.020105	0.0228	0.020105	0.000007	0.020694	0.000004
0.019135	0.0208	0.019135	0.000003	0.019424	0.000002
0.017196	0.0132	0.017196	0.000016	0.016889	0.000014
0.015372	0.0128	0.015372	0.000007	0.014503	0.000003
0.013305	0.0116	0.013305	0.000003	0.011800	0.000000
0.011164	0.0111	0.011164	0.000000	0.009000	0.000004
			RSC <sub>1</sub> = 0.000036		RSC = 0.000023

On substitution in to (Eq.46)

$$F_1 = \frac{(0.000036 - 0.000023)(6-2)}{(0.000023)(2)} = 1.1055$$

**Table 20. Summary output P3 (Schuhmeister Mod. Vs Experimental)**

Predicted (x)	Experimental (y)	$\hat{y}_i = b(1) + 0$	$(y - \hat{y}_i)^2$	$\hat{y} = 1.2703x - 0.009$	$(y - \hat{y})^2$
0.023190	0.0228	0.023190	0.000000	0.020458	0.000005
0.022284	0.0208	0.022284	0.000002	0.019308	0.000002
0.020419	0.0132	0.020419	0.000052	0.016938	0.000014
0.018592	0.0128	0.018592	0.000034	0.014618	0.000003
0.016433	0.0116	0.016433	0.000023	0.011875	0.000000
0.014089	0.0111	0.014089	0.000009	0.008897	0.000005
			RSC <sub>1</sub> = 0.000111		RSC <sub>1</sub> = 0.000025

On substitution in to (Eq.46)

$$F_1 = \frac{(0.000111 - 0.000025)(6-2)}{(0.000025)(2)} = 6.8867$$

#### 4.3.4 Effect of moisture content on polyamide socks (P4)

ME-2 modified has the overall top thermal resistance prediction in general and at 5.17%, 10.01%, 20.51%, 40.06% and 49.93% moisture levels specifically for P4 (nylon 70%, polyester 26.54% & elastane 2.63%) as shown in (Fig.34). This is also evident by the highest  $R^2 = 0.9446$  (Fig.35). Militky modified prediction is on second number with ( $R^2 = 0.9416$ ) as shown in (Fig.35). A rapid decline in the thermal resistance similar to P1, P2, and P3 between 20-30% moisture content is detected for the P4 sample as well. In the case of P4, a 50% reduction in the thermal resistance is observed at a 40% moisture level. Schuhmeister modified has better prediction till 20% moisture content. However, it didn't follow the experimental footprints as Militky modified and ME-2 modified models.

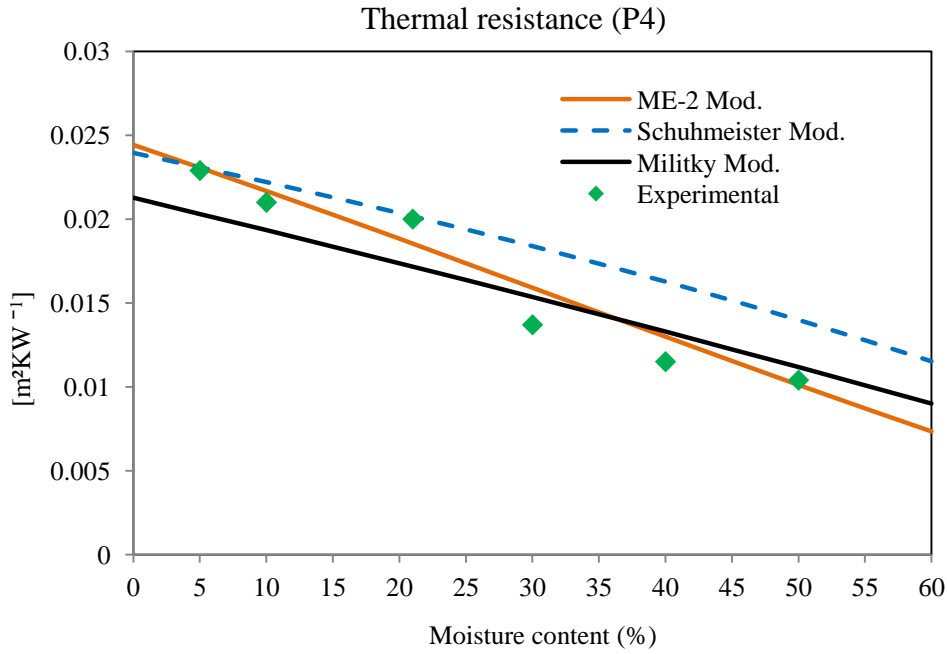


Figure 34. Predicted & experimental thermal resistance: P4 (polyamide nylon 70%, polyester 26.54% & elastane 2.63%)

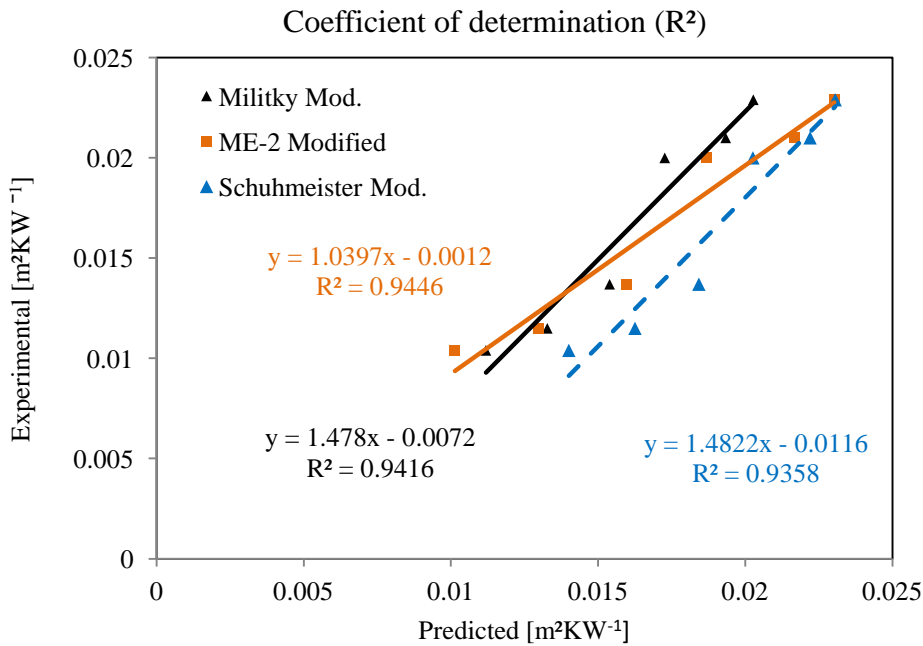


Figure 35. Coefficient of determination predicted & experimental thermal resistance: P4 (polyamide nylon 70%, polyester 26.54% & elastane 2.63%)

Null hypothesis acceptance ( $F_1$  calculated values i.e. 0.7963, 4.3633 and 5.4464 are lesser than the critical value of the Fisher-Snedecor F-distribution  $F_{0.95}(2, 4) = 6.9443$ ) further provide strong evidence for the validity of the ME-2 Militky and Schuhmeister modified models against the assumptions i.e.  $H_0: \beta_2 = 0$  and  $\beta_1 = 1$  at 95% confidence level. It means

their structured confidence region isn't significantly different from "0" and "1" for intercept & slope respectively. It means the modified model's prediction isn't significantly different from experimental results. Tables (21-23) show the calculation for  $F_1$ .

**Table 21. Summary output P4 (ME-2 Mod. Vs Experimental)**

Predicted (x)	Experimental (y)	$\hat{y}_1 = b(1) + 0$	$(y - \hat{y}_1)^2$	$\hat{y} = 1.0397x - 0.0012$	$(y - \hat{y})^2$
0.02302799	0.0229	0.02302799	0.00000002	0.02274220	0.00000002
0.02168373	0.0210	0.02168373	0.00000047	0.02134458	0.00000012
0.01868030	0.0200	0.01868030	0.00000174	0.01822190	0.00000316
0.01596953	0.0137	0.01596953	0.00000515	0.01540352	0.00000290
0.01297455	0.0115	0.01297455	0.00000217	0.01228964	0.00000062
0.01014068	0.0104	0.01014068	0.00000007	0.00934327	0.00000112
			RSC <sub>1</sub> = 0.00000955		RSC = 0.00000683

On substitution in to (Eq.46)

$$F_1 = \frac{(0.00000955 - 0.00000683)(6-2)}{(0.00000683)(2)} = 0.7963$$

**Table 22. Summary output P4 (Militky Mod. Vs Experimental)**

Predicted (x)	Experimental (y)	$\hat{y}_1 = b(1) + 0$	$(y - \hat{y}_1)^2$	$\hat{y} = 1.478x - 0.0072$	$(y - \hat{y})^2$
0.02027761	0.0229	0.02027761	0.00000688	0.02277030	0.00000002
0.01933921	0.0210	0.01933921	0.00000276	0.02138336	0.00000015
0.01726859	0.0200	0.01726859	0.00000746	0.01832297	0.00000281
0.01539516	0.0137	0.01539516	0.00000287	0.01555404	0.00000344
0.01327859	0.0115	0.01327859	0.00000316	0.01242576	0.00000086
0.01119267	0.0104	0.01119267	0.00000063	0.00934276	0.00000112
		0.08555915	RSC <sub>1</sub> = 0.00002313		RSC <sub>1</sub> = 0.00000727

On substitution in to (Eq.46)

$$F_1 = \frac{(0.00002313 - 0.00000727)(6-2)}{(0.00000727)(2)} = 4.3633$$

**Table 23. Summary output P4 (Schuhmeister Mod. Vs Experimental)**

Predicted (x)	Experimental (y)	$\hat{y}_1 = b(1) + 0$	$(y - \hat{y}_1)^2$	$\hat{y} = 1.4822x - 0.0116$	$(y - \hat{y})^2$
0.0230595	0.0229	0.0230595	0.00000000	0.0211953	0.00000029
0.0222070	0.0210	0.0222070	0.00000015	0.0199828	0.00000010
0.0202639	0.0200	0.0202639	0.00000001	0.0172193	0.00000077
0.0184277	0.0137	0.0184277	0.00000224	0.0146078	0.00000008
0.0162570	0.0115	0.0162570	0.00000226	0.0115207	0.00000000
0.0140097	0.0104	0.0140097	0.00000130	0.0083246	0.00000043
			RSC <sub>1</sub> = 0.0000465		RSC = 0.0000125

On substitution in to (Eq.46)

$$F_1 = \frac{(0.0000465 - 0.0000125)(6-2)}{(0.0000125)(2)} = 5.4464$$

### 4.3.5 Effect of moisture content on polypropylene socks (P5)

In (Fig.36) for P5 (polypropylene 65.22%, polyester 31.65% & elastane 3.13%) socks Militky modified prediction is the best with respect to ME-2 modified model with lower SSE (standard error) at 10.21%, 19.13%, 29.99%, 38.50 and 50.22%. ME-2 modified has the best forecast at 5.05%, 38.50% and 50.22% moisture contents. SSE values with respect to the experimental thermal resistance are shown in Tables (24-26). Militky-2 modified, ME-2 modified and Schuhmeister modified have 0.001799, 0.001817 and 0.001928 SSE values in that order. The coefficient of determination values ( $R^2$ ) 0.867, 0.8643, and 0.8472 also have the same sequence as shown in (Fig.37). P5 curve is like P3, i.e. after the sudden decline, there is some stability in the drop. Similar to P3 it has 50% thermal resistance fall at 50% moisture content.

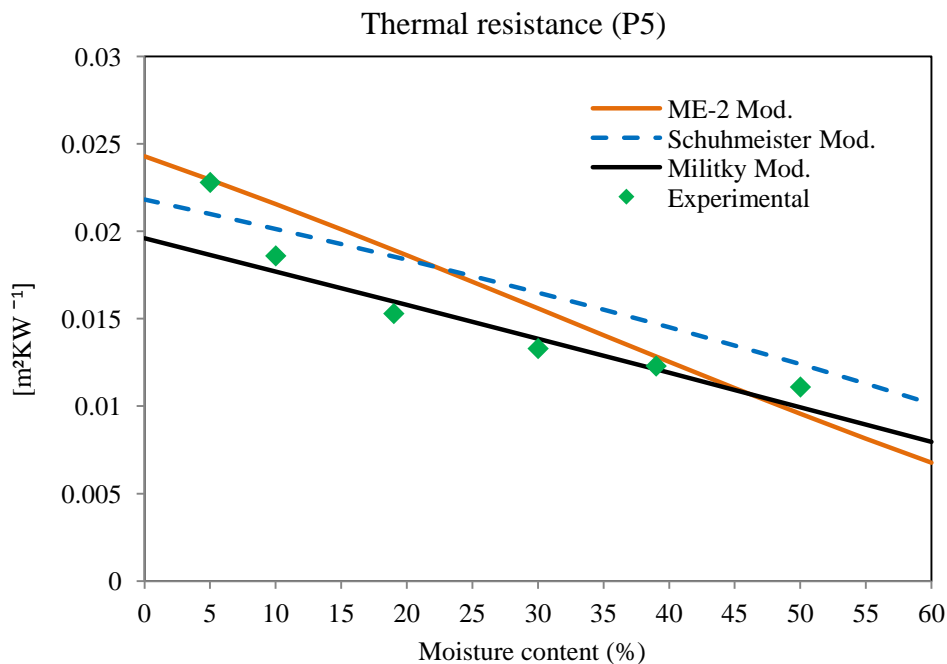


Figure 36. Predicted & experimental thermal resistance: P5 (polypropylene 65.22%, polyester 31.65% & elastane 3.13%)

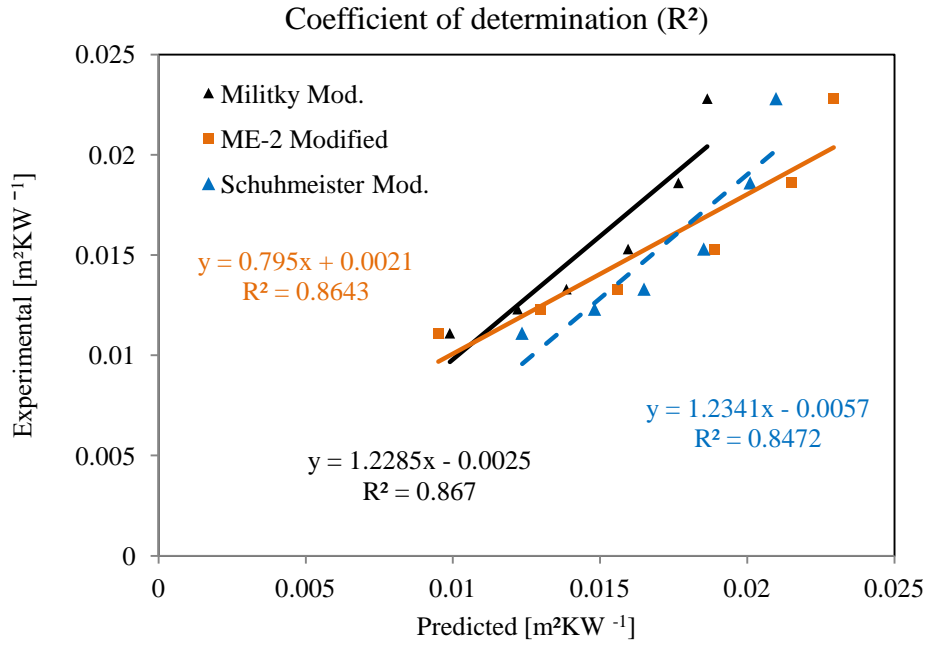


Figure 37. Coefficient of determination predicted & experimental thermal resistance: P5 (polypropylene 65.22%, polyester 31.65% & elastane 3.13%)

Tables (24-26) are the calculation behind the  $F_1$  values. These values i.e. 2.8625, 1.4727 and 3.2226 (for ME-2, Militky and Schuhmeister models respectively) are smaller than the critical value i.e.  $F_{0.95}(2, 4) = 6.9443$ . So the null hypothesis i.e.  $H_0: \beta_2 = 0$  and  $\beta_1 = 1$  for all these models couldn't be rejected. It validates that ME-2 modified, Militky modified and Schuhmeister modified models prediction isn't significantly different from experimental results.

Table 24. Summary output P5 (ME-2 Mod. Vs Experimental)

Predicted (x)	Experimental (y)	$\hat{y}_1 = b(1) + 0$	$(y - \hat{y}_1)^2$	$\hat{y} = 0.795x + 0.0021$	$(y - \hat{y})^2$
0.0229367	0.0228	0.0229367	0.0000000	0.0202200	0.0000067
0.0214947	0.0186	0.0214947	0.0000084	0.0190809	0.0000002
0.0188827	0.0153	0.0188827	0.0000128	0.0170173	0.0000029
0.0155861	0.0133	0.0155861	0.0000052	0.0144130	0.0000012
0.0129903	0.0123	0.0129903	0.0000005	0.0123624	0.0000000
0.0095082	0.0111	0.0095082	0.0000025	0.0096115	0.0000022
			RSC <sub>1</sub> = 0.0000269		RSC = 0.0000111

On substitution in to (Eq.46)

$$F_1 = \frac{(0.0000269 - 0.0000111)(6-2)}{(0.0000111)(2)} = 2.8625$$

**Table 25. Summary output P5 (Militky Mod. Vs Experimental)**

Predicted (x)	Experimental (y)	$\hat{y}_1 = b(1) + 0$	$(y - \hat{y}_1)^2$	$\hat{y} = 1.2285x - 0.0025$	$(y - \hat{y})^2$
0.0186460	0.0228	0.0186460	0.0000173	0.0204066	0.0000057
0.0176635	0.0186	0.0176635	0.0000009	0.0191996	0.0000004
0.0159560	0.0153	0.0159560	0.0000004	0.0171019	0.0000032
0.0138599	0.0133	0.0138599	0.0000003	0.0145269	0.0000015
0.0122030	0.0123	0.0122030	0.0000000	0.0124914	0.0000000
0.0098982	0.0111	0.0098982	0.0000014	0.0096599	0.0000021
			RSC <sub>1</sub> = 0.0000189		RSC = 0.0000109

On substitution in to (Eq.46)

$$F_1 = \frac{(0.0000189 - 0.0000109)(6-2)}{(0.0000109)(2)} = 1.4727$$

**Table 26. Summary output P5 (Schuhmeister Mod. Vs Experimental)**

Predicted (x)	Experimental (y)	$\hat{y}_1 = b(1) + 0$	$(y - \hat{y}_1)^2$	$\hat{y} = 1.2341x - 0.0057$	$(y - \hat{y})^2$
0.0209804	0.0228	0.0209804	0.0000033	0.0201919	0.0000068
0.0201015	0.0186	0.0201015	0.0000023	0.0191073	0.0000003
0.0185246	0.0153	0.0185246	0.0000104	0.0171612	0.0000035
0.0164966	0.0133	0.0164966	0.0000102	0.0146584	0.0000018
0.0148154	0.0123	0.0148154	0.0000063	0.0125837	0.0000001
0.0123511	0.0111	0.0123511	0.0000016	0.0095424	0.0000024
			RSC <sub>1</sub> = 0.0000325		RSC = 0.0000124

On substitution in to (Eq.46)

$$F_1 = \frac{(0.0000325 - 0.0000124)(6-2)}{(0.0000124)(2)} = 3.2226$$

#### 4.3.6 Effect of moisture content on wool socks (P6)

(Fig.38) shows the effect of moisture content (%) on the thermal resistance of P6 socks (wool 76.19%, 21.67% polyester & elastane 2.14%). All the models have an appropriate prediction of thermal resistance as evident in (Fig.39). Both ME-2 and Militky models have a better prediction at 21.30%, 28.90%, 40.38% and 49.90% moisture levels. But this forecast is not so close at 10% moisture level. This trend is also manifested in (Fig.38). As well as the coefficient of determination is concerned, ME-2 modified, Militky modified and Schuhmeister modified models have 0.882, 0.8723 and 0.8566 in that order as shown in

(Fig.39). Similar to the above samples P6 has also half a thermal resistance with 30% moisture content.

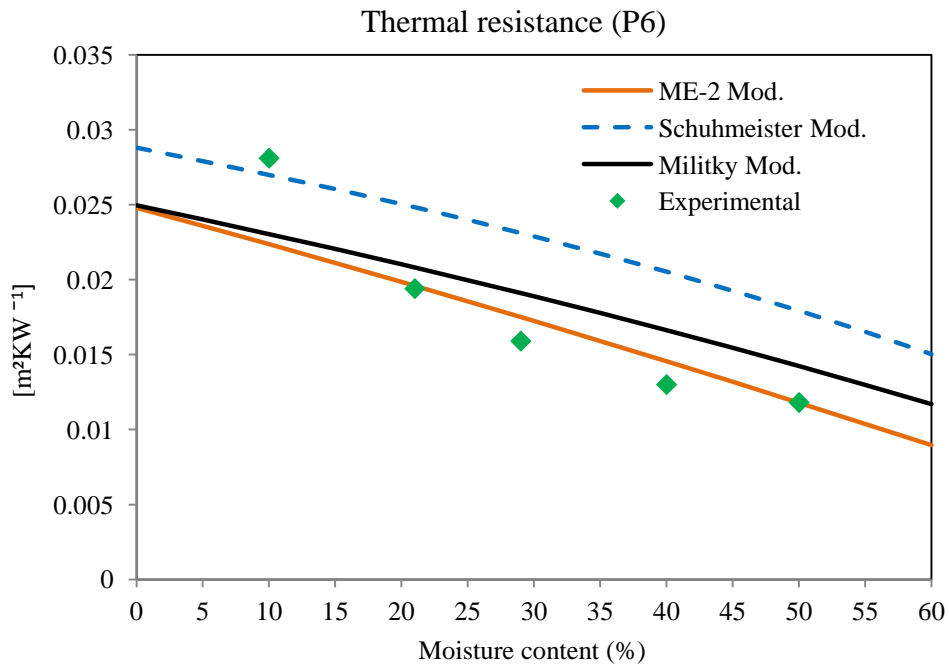


Figure 38. Predicted & experimental thermal resistance: P6 (wool 76.19%, 21.67% polyester & elastane 2.14%)

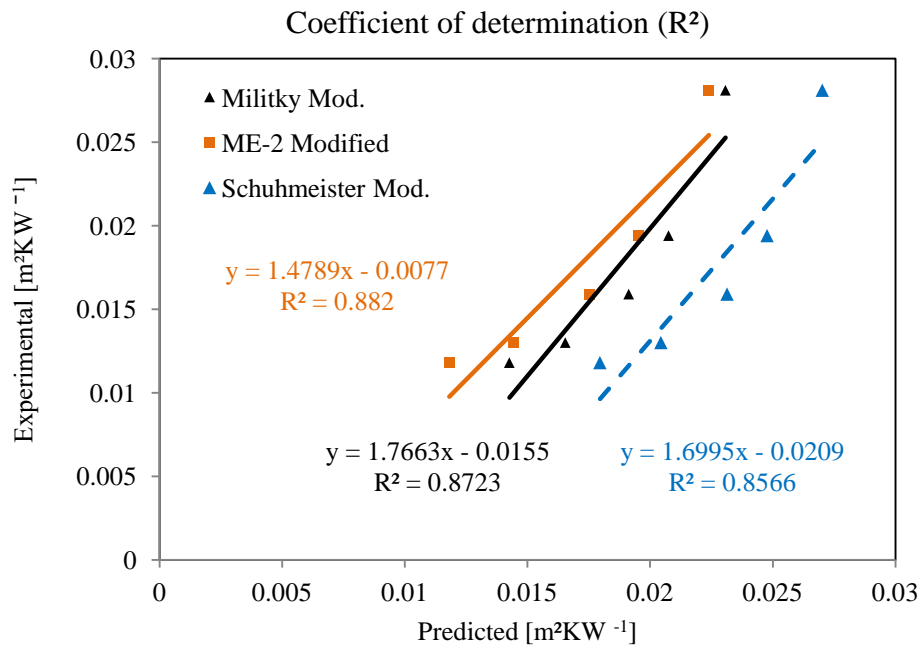


Figure 39. Coefficient of determination predicted & experimental thermal resistance: P6 (wool 76.19%, 21.67% polyester & elastane 2.14%)

Hypothesized results for intercept and slope assuming them as equal to zero and one also validated that the suggested models have not significantly different results at a 95% confidence level. Because the F1 values i.e. 1.2677, 2.3522 and 9.2379 for ME-2, Militky and Schuhmeister modified models are smaller than the critical value i.e. 9.5521 for  $F_{0.95}(2, 3)$ . So the null hypothesis couldn't be rejected. It concluded that predicted (theoretical) results are in agreement with the experimental results. Tables (27-29) show the computation behind the calculated values of  $F_1$ .

**Table 27. Summary output P6 (ME-2 Mod. Vs Experimental)**

Predicted (x)	Experimental (y)	$\hat{y}_1 = b(1) + 0$	$(y - \hat{y}_1)^2$	$\hat{y} = 1.4789x - 0.0077$	$(y - \hat{y})^2$
0.0224008	0.0281	0.0224008	0.0000325	0.0254285	0.0000071
0.0195146	0.0194	0.0195146	0.0000000	0.0211602	0.0000031
0.0175331	0.0159	0.0175331	0.0000027	0.0182298	0.0000054
0.0144509	0.0130	0.0144509	0.0000021	0.0136715	0.0000005
0.0118179	0.0118	0.0118179	0.0000000	0.0097774	0.0000041
			RSC <sub>1</sub> = 0.0000373		RSC = 0.0000202

On substitution in to (Eq.46)

$$F_1 = \frac{(0.0000373 - 0.0000202)(5-2)}{(0.0000202)(2)} = 1.2667$$

**Table 28. Summary output P6 (Militky Mod. Vs Experimental)**

Predicted (x)	Experimental (y)	$\hat{y}_1 = b(1) + 0$	$(y - \hat{y}_1)^2$	$\hat{y} = 1.7663x - 0.0155$	$(y - \hat{y})^2$
0.023073	0.0281	0.023073	0.000025	0.025254	0.000008
0.020754	0.0194	0.020754	0.000002	0.021158	0.000003
0.019131	0.0159	0.019131	0.000010	0.018290	0.000006
0.016543	0.0130	0.016543	0.000013	0.013720	0.000001
0.014263	0.0118	0.014263	0.000006	0.009692	0.000004
			RSC <sub>1</sub> = 0.000056		RSC = 0.000022

On substitution in to (Eq.46)

$$F_1 = \frac{(0.000056 - 0.000022)(5-2)}{(0.000022)(2)} = 2.3522$$

**Table 29. Summary output P6 (Schuhmeister Mod. Vs Experimental)**

Predicted (x)	Experimental (y)	$\hat{y}_1 = b(1) + 0$	$(y - \hat{y}_1)^2$	$\hat{y} = 1.6995x - 0.0209$	$(y - \hat{y})^2$
0.027023	0.0281	0.027023	0.000001	0.025025	0.000009
0.024771	0.0194	0.024771	0.000029	0.021198	0.000003
0.023140	0.0159	0.023140	0.000052	0.018426	0.000006
0.020441	0.0130	0.020441	0.000055	0.013840	0.000001
0.017956	0.0118	0.017956	0.000038	0.009616	0.000005
			RSC <sub>1</sub> = 0.000176		RSC = 0.000025

On substitution in to (Eq.46)

$$F_1 = \frac{(0.000176 - 0.000025)(5-2)}{(0.000025)(2)} = 9.2379$$

### 4.3.7 Effect of moisture content on acrylic socks (P7)

(Fig.40) shows the effect of moisture content (%) on the thermal resistance of P7 sock (acrylic 81.25%, 17.06% polyester & elastane 1.69%). All the models have the apposite prediction of thermal resistance as evident in (Fig.40 and Fig.41). (Fig.40) shows the coefficient of the determination between the theoretical (predicted) and experimental thermal resistance. All the models have good conformity with the experimental thermal resistance, i.e. 0.9051 and 0.8988 for ME-2 modified and Militky modified models, respectively.

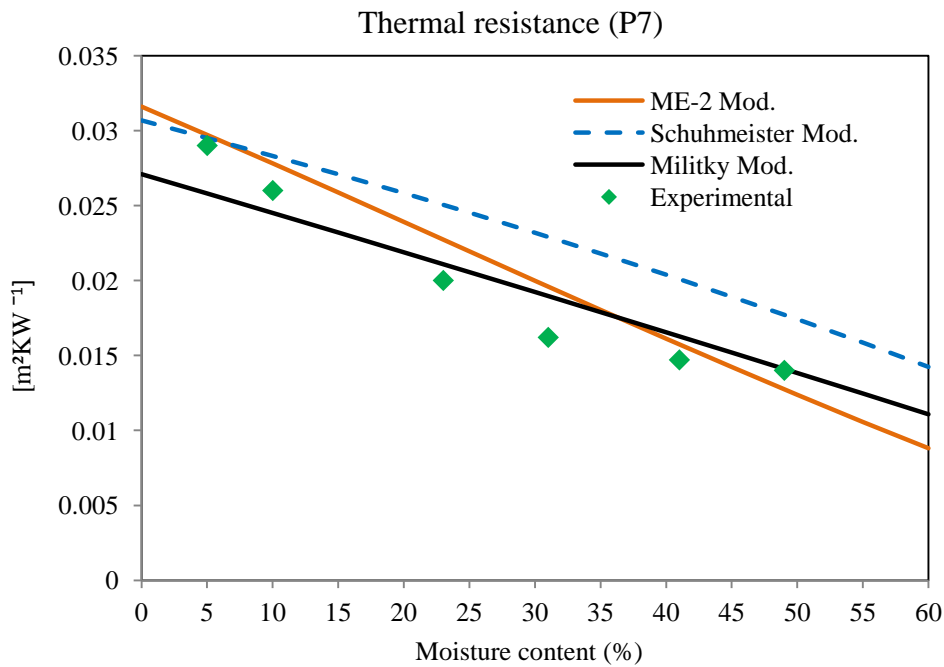


*Figure 40. Predicted & experimental thermal resistance: P7 (acrylic 81.25%, 17.06% polyester & elastane 1.69%)*

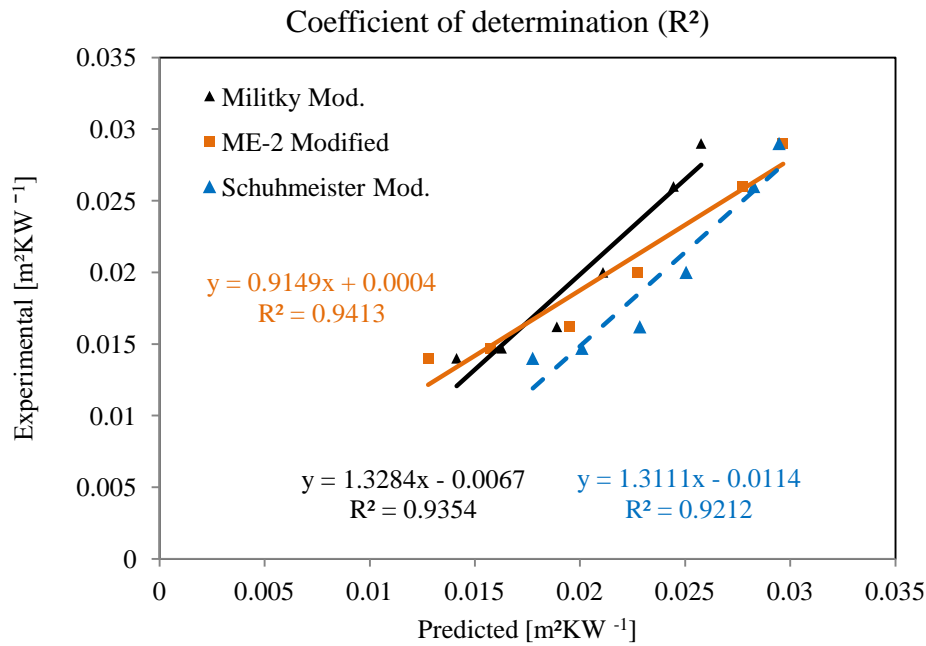


Figure 41. Coefficient of determination predicted & experimental thermal resistance: P7 (acrylic 81.25%, 17.06% polyester & elastane 1.69%)

F1 values for ME-2 and Militky modified models i.e. 3.8301, 3.3563 respectively are lesser than the quantile of the Fisher-Snedecor F-distribution  $F_{0.95}(2, 4) = 6.9443$ , so the null hypothesis  $H_0$  cannot be rejected. It means the predicted thermal resistance with the ME-2 and Militky modified models isn't significantly different than the experimental results. However this value ( $F_1 = 17.0908$ ) is greater than the critical value (6.9443). It concluded that the thermal resistance predicted by Schuhmeister modified model isn't in agreement with the experimental values for P7 sample. The computations for the values of  $F_1$  have been given in Tables (30-32).

Table 30. Summary output P7 (ME-2 Mod. Vs Experimental)

Predicted (x)	Experimental (y)	$\hat{y}_1 = b(1) + 0$	$(y - \hat{y}_1)^2$	$\hat{y} = 0.9149x + 0.0004$	$(y - \hat{y})^2$
0.0296542	0.0290	0.0296542	0.0000004	0.0275306	0.0000022
0.0277264	0.0260	0.0277264	0.0000030	0.0257669	0.0000001
0.0227405	0.0200	0.0227405	0.0000075	0.0212053	0.0000015
0.0195054	0.0162	0.0195054	0.0000109	0.0182455	0.0000042
0.0157317	0.0147	0.0157317	0.0000011	0.0147930	0.0000000
0.0127835	0.0140	0.0127835	0.0000015	0.0120956	0.0000036
			$RSC_1 = 0.0000229$		$RSC = 0.0000079$

On substitution in to (Eq.46)

$$F_1 = \frac{(0.0000229 - 0.0000079)(6-2)}{(0.0000079)(2)} = 3.8301$$

**Table 31. Summary output P7 (Militky Mod. Vs Experimental)**

Predicted (x)	Experimental (y)	$\hat{y}_1 = b(1) + 0$	$(y - \hat{y}_1)^2$	$\hat{y} = 1.3284x - 0.0066$	$(y - \hat{y})^2$
0.02576045	0.0290	0.02576045	0.00001049	0.02752018	0.00000219
0.02444877	0.0260	0.02444877	0.00000241	0.02577775	0.00000005
0.02109527	0.0200	0.02109527	0.00000120	0.02132296	0.00000175
0.01890094	0.0162	0.01890094	0.00000730	0.01840801	0.00000488
0.01627148	0.0147	0.01627148	0.00000247	0.01491504	0.00000005
0.01413186	0.0140	0.01413186	0.00000002	0.01207276	0.00000371
			RSC <sub>1</sub> = 0.00002387		RSC = 0.00000891

On substitution in to (Eq.46)

$$F_1 = \frac{(0.00002387 - 0.00000891)(6-2)}{(0.000022)(2)} = 3.3563$$

**Table 32. Summary output P7 (Schuhmeister Mod. Vs Experimental)**

Predicted (x)	Experimental (y)	$\hat{y}_1 = b(1) + 0$	$(y - \hat{y}_1)^2$	$\hat{y} = 1.3111x - 0.0114$	$(y - \hat{y})^2$
0.0294703	0.0290	0.0294703	0.0000002	0.0272385	0.0000031
0.0282617	0.0260	0.0282617	0.0000051	0.0256539	0.0000001
0.0250497	0.0200	0.0250497	0.0000255	0.0214426	0.0000021
0.0228465	0.0162	0.0228465	0.0000442	0.0185540	0.0000055
0.0200921	0.0147	0.0200921	0.0000291	0.0149427	0.0000001
0.0177518	0.0140	0.0177518	0.0000141	0.0118744	0.0000045
			RSC <sub>1</sub> = 0.0001041		RSC = 0.0000109

On substitution in to (Eq.46)

$$F_1 = \frac{(0.0001041 - 0.0000109)(6-2)}{(0.000025)(2)} = 17.0908$$

## 4.4 Effect of moisture content on thermal absorptivity

This section explains the results for the thermal absorptivity of socks in wet state. Dry and wet socks with different moisture content were checked on the Alambeta instrument in extended state. These are simulated to real extension as described (under section 3.7 Sample preparation for testing). Mangat's model for thermal absorptivity prediction is also based on the contact area effect [34][44]. (Fig.42) clearly demonstrated that as the moisture (%) increases, the thermal absorptivity also increases irrespective of sock fibre composition. That is in compliance with the previous researchers [177][110][22][178]. Baczek & Hes observed

9 times higher thermal absorptivity of plaited knitted fabrics in the wet state [36]. P5 sock has the lowest thermal absorptivity under dry and wet conditions (at 10%, 20%, 30%, 40% & 50% moisture content) followed by P3 (composed of 100% polyester) socks. Even at 50% moisture content P5 socks have the thermal absorptivity  $<300$ . So these socks will have a higher feeling of dryness than any other socks due to the composition of hydrophobic fibres of polypropylene and polyester. At 10% moisture content all the socks P3, P4, P5, P6, and P7 have the thermal absorptivity between  $(100-110 \text{ Ws}^{1/2} \text{ m}^{-2} \text{ K}^{-1})$  apart from P1 and P2 socks. P1 & P2 socks have  $134$  and  $130 \text{ Ws}^{1/2} \text{ m}^{-2} \text{ K}^{-1}$  respectively. At 20% moisture content this range is between  $(143-171 \text{ Ws}^{1/2} \text{ m}^{-2} \text{ K}^{-1})$ . P5 has the lowest value followed by P3, P7, P4, P1, P6, and P2. At 30% humidity level the rise of thermal absorptivity is more significant, i.e. 47.95%, 52%, 61.78, 63.03 and 66.66% for P2, P4, P7, P6, and P1 socks. This increase is also observed in P5 and P3 socks, but to a lower extent, i.e. 38.46% and 34.64%, respectively.

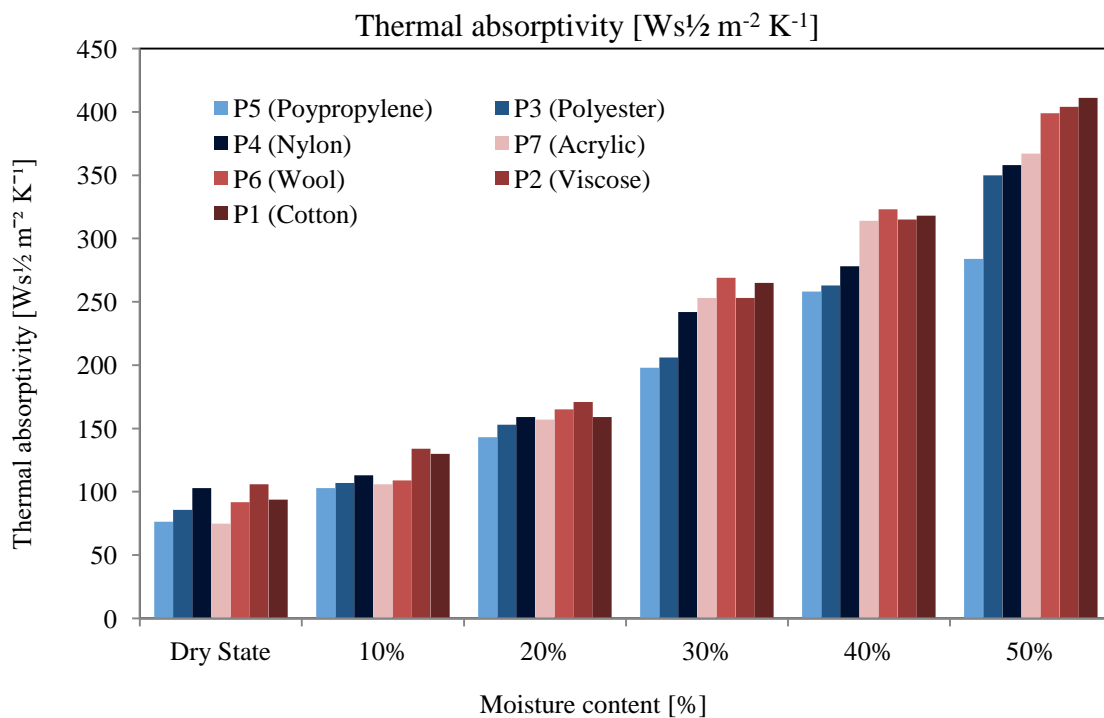


Figure 42. Effect of moisture content on thermal absorptivity

## 4.5 Effect of moisture content on RWVP

(Fig.43) shows that the increasing moisture content in fabrics leads to increasing their ability to transport water vapour. Same behaviour was also observed by Hes[25], Lenfeldova[116] and Baczek[15]. Higher RWVP (%) leads to a higher cooling effect. As moisture content and water condensation in the fabric increased, it causes to increase water vapour permeability

through the fabric [6]. P6 and P7 will be the warmest socks with a lower RWVP (%). The approach of the wet study is as follows: if liquid water in the wet fabric structure creates a partially continuous film, then the transfer of water vapour should be limited. Here are three main factors that affect significantly the water vapour permeability, i.e.  $\text{gm}^{-2}$ , fibre composition and thickness.

The presented results show that the addition of hydrophobic fibres affects the water vapor transportability of hydrophilic fabrics. The water vapour permeability through the textiles is a very complicated phenomenon. Water vapours are transmitted through the textiles by 1) Diffusion, 2) Absorption, Transmission and Desorption (in the fibre), 3) Adsorption and Migration (along the fibre), and 4) Forced Convection. As mentioned earlier, the relation between the diffusing flux and the concentration gradient was first proposed by Fick [109]. But the vapour diffusion does not obey Fick's law in the case of hydrophilic fibre assemblies. It is governed by a non-Fick's, inconsistent diffusion [47][80].

Relative water vapour permeability increases almost 100% with 50% moisture content. The study by Hes showed the same results without any air gap [49]. Most of the socks, i.e. P5 (polypropylene 65.22%, polyester 31.65%, elastane 3.13%), P4 (nylon 70.83%, polyester 26.54%, elastane 2.63%), P3 (polyester 98.38%, elastane 1.62%) are composed of synthetic fibres and have a higher relative water vapour permeability. P6 (wool 76.19%, polyester 21.67%, elastane 2.14%) has the lowest RWVP at the dry and wet state (10%, 20% & 30% moisture content) followed by P2 (viscose 81.08%, polyester 17.22 %) and P7 (acrylic 81.25%, polyester 17.06%, elastane 1.69%) in the dry state, at 10%, and 20% moisture content. At 40% and 50% moisture level P7 has the lowest RWVP among all the socks, slightly different to P6.

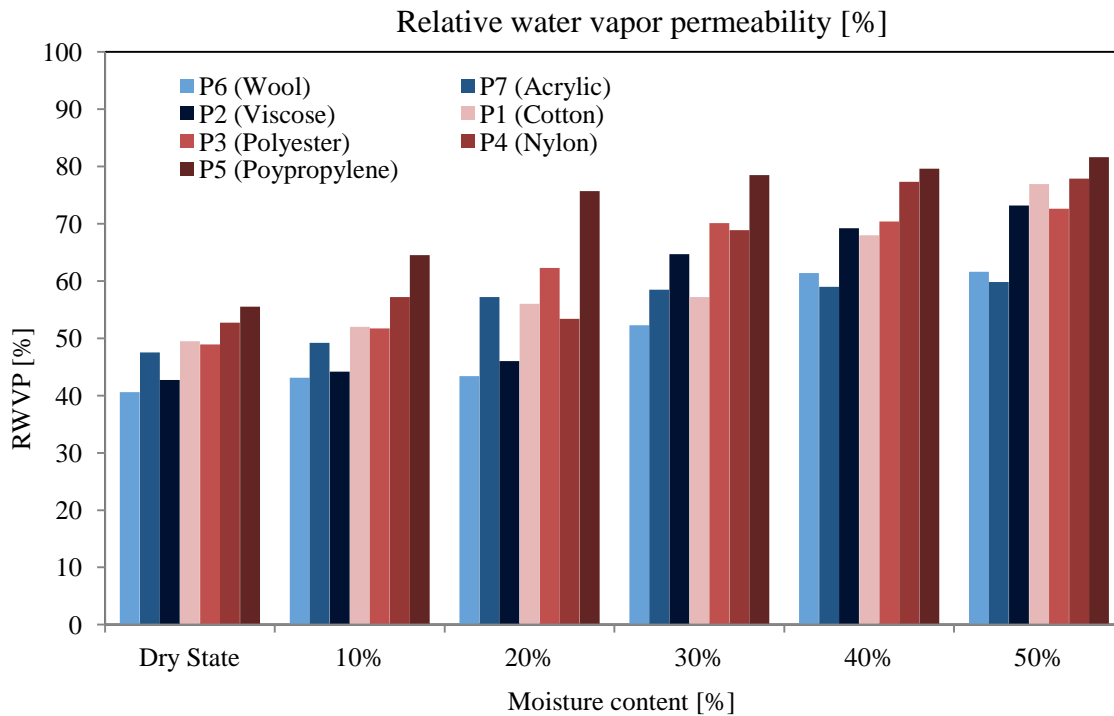


Figure 43. Effect of moisture content on RWVP

Hydrophilic fibres composed socks like wool and cotton owing to bond with water molecules. Therefore, they have poor moisture transportation. On the other hand, synthetic fibers such as polyester, polypropylene, and nylon have an advantage of liquid transport and release by capillary wicking. It is in accordance with previous studies [110][179][180][181]. Swelling can also set up internal stresses that may affect the sorption process. This could increase the adsorption hysteresis with the increase of hydrophilic fibres [182]. There is an inverse relation between the diffusion fibre volume fraction and the flatness of fibre cross section, also reported in the literature [13]. A higher fabric thickness can also decrease RWVP significantly [183]. P7 sample has the highest thickness followed by P6, P1, P3, P4, P2 and P5. RWVP is affected by the thickness at all moisture levels.

## 4.6 Effect of extension on comfort properties

This section explains the results for the effect of extension on porosity, thermal resistance, thermal absorptivity and relative water vapour permeability of socks in a wet state. Socks are extended as described (under section 3.7 Sample preparation for testing). This extension is very important for the real simulation of socks during wearing. As discussed earlier, some researchers extended the knitted fabric in the uniaxial direction [87][105][171]; but that is not in accordance with the real situation of extension. Although this kind of extension isn't

required for thermal manikins, they have some other limitations as described before (3.7 Testing Equipments/ Methods).

#### 4.6.1 Effect of extension on thermal resistance

To measure the effect of extension, all the socks were tested for thermal resistance with and without extension by Alambeta in a dry state. (Fig.44) demonstrated that extended socks have a lower thermal resistance. This is mainly due to the thickness reduction with extension. Thickness is one of the major factors that affect the thermal insulation. This fact already established by many researchers that thickness has a positive correlation with thermal insulation [184][185][186]. Gnanauthayan et al. reported that thermal resistance increased by increasing fabric thickness [187]. Abdel-Rehim et al. also observed higher insulation for nonwoven 100% polyester and 100% polypropylene fabrics by increasing thickness [188]. It could be revealed from (Fig.44) that all the socks haven't close thermal resistance even at 95% confidence level except P1, P3 & P5 socks. So this situation is the motivation for characterizing the socks in an extended state.

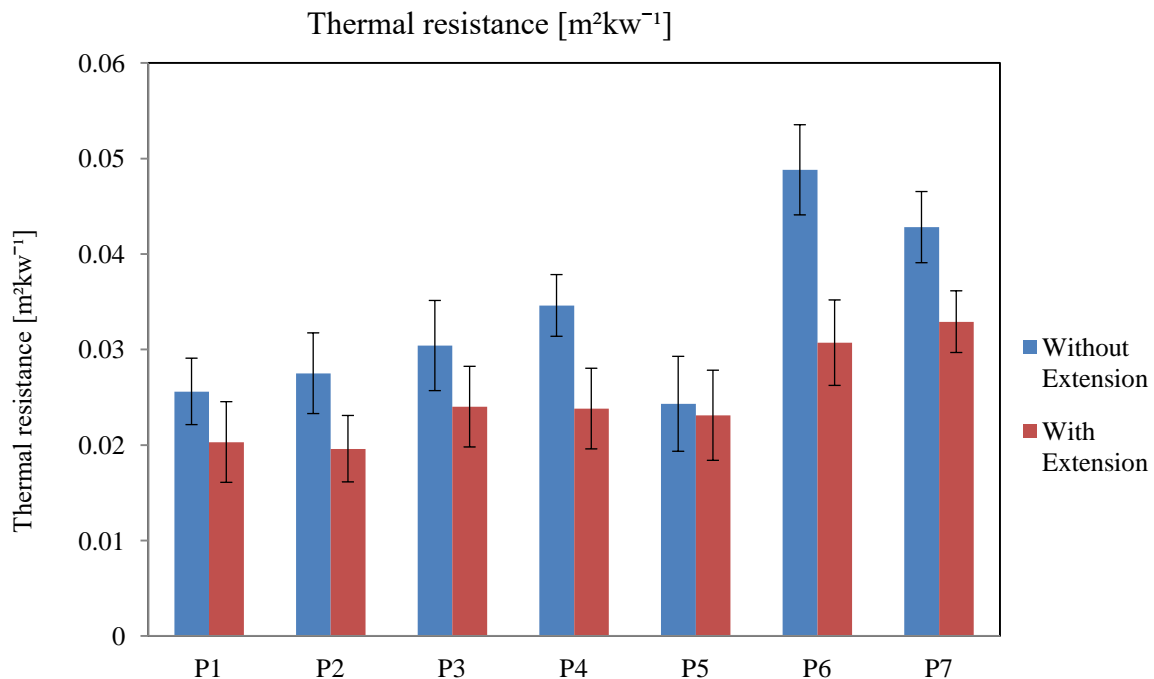


Figure 44. Effect of extension on thermal resistance

#### 4.6.2 Effect of extension on thermal absorptivity

(Fig.45) confirmed that extended socks have a lower thermal absorptivity (dry state) for all the socks. Thermal absorptivity has a positive relation with contact points (area). As socks

extended, the number of contact points decreased. It results in a lower value of thermal absorptivity. These are the expected findings. Many researchers had acknowledged the negative correlation of contact area [33][30] and extension [104][105] on thermal absorptivity. Mangat's model for thermal absorptivity prediction is also based on the contact area effect [34][44]. Faisal et al. observed a reduction in thermal absorptivity of compression socks at different extension levels [105]. Gupta also extended the compression circular knitted garments up to 60% and found a decrease in the thermal absorptivity [87]. So the characterization of the socks in the extended state is justified to their real simulation and significant difference of results.

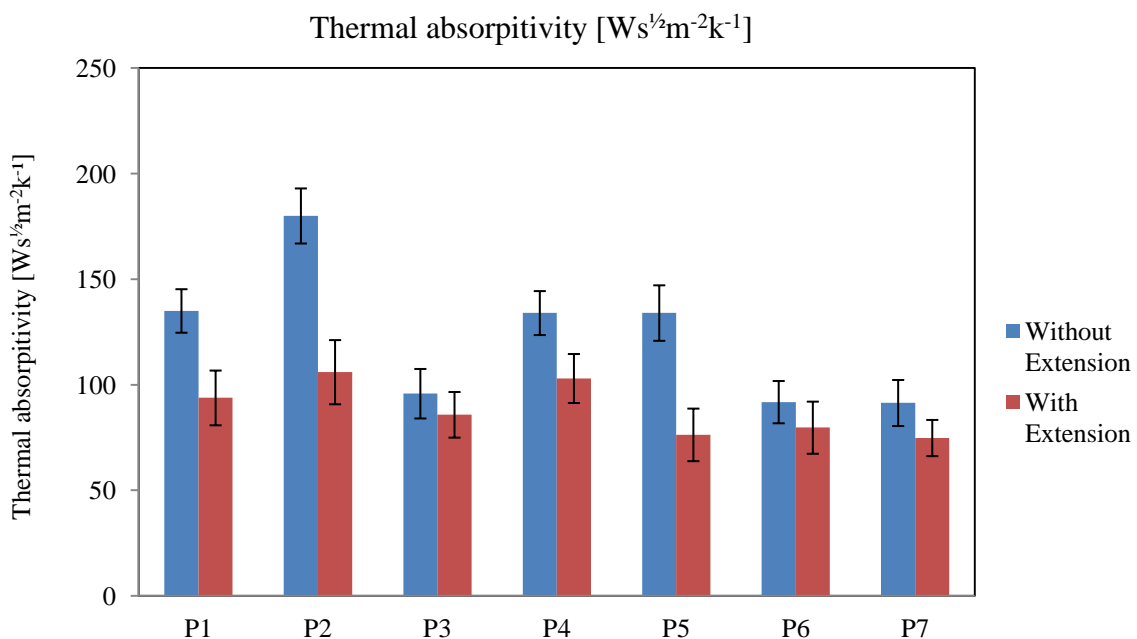


Figure 45. Effect of extension on thermal absorptivity

### 4.6.3 Effect of extension on RWVP

(Fig.46) shows that extended socks have higher relative water vapor permeability (dry state) for all the socks. RWVP has a positive relation with extension. Extension changed the structure, thickness, and porosity of the fabric. And these parameters lead to change the permeability. These findings are in line with previous studies that verified the effect of fabric structure [40][113], fibre composition [108][98][110][111], fabric thickness, covering factor and porosity on relative water vapour permeability [112]. Gupta extended the compression circular knitted garments up to 60% and found a 47% increase in the water vapor

permeability [87]. In the current situation, the difference is not significant as evident from the confidence interval at 95%, but extended socks have higher RWVP for all the socks.

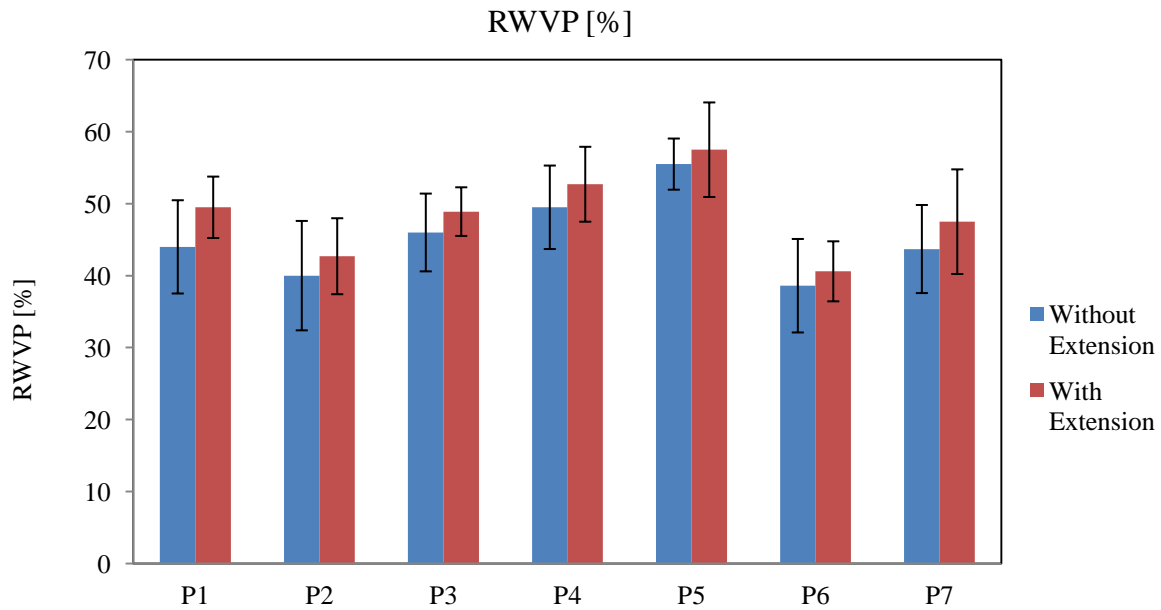


Figure 46. Effect of extension on relative water vapour permeability

#### 4.7 Effect of moisture content on coefficient of friction

Results for the sock-insole static and dynamic coefficients of friction (COF) at different water content for all the seven socks are shown in (Figures 47-53). (Fig.47) shows the graphs for frictional force (Fig.47a) & COF (Fig.47b) at different moisture levels for P1 sock. The results clearly demonstrated that as the moisture content increases, it causes to increase the coefficient of friction. That is in accord with the previous studies[127][137][165][189]. Bertaux et al. reported an 83.87% increase in sock-skin static COF from 0.31 to 0.57 (dry to wet state) by the addition of 5.58g of water having cotton/polyamide at toes and waist area [127]. There is a continuous increase in the friction with the increase of moisture content except between 20-30%. That is also evident from (Fig.47a and Fig.47b). Hes et al. observed the same increase in static and dynamic friction in a wet state for cotton elastic knitted fabrics [165]. Tasron et al. reported  $0.33 \pm 0.07$ ,  $0.67 \pm 0.08$  &  $0.74 \pm 0.08$  dynamic COF values for cotton plain knitted socks in dry, low moisture and high moisture content respectively [190].

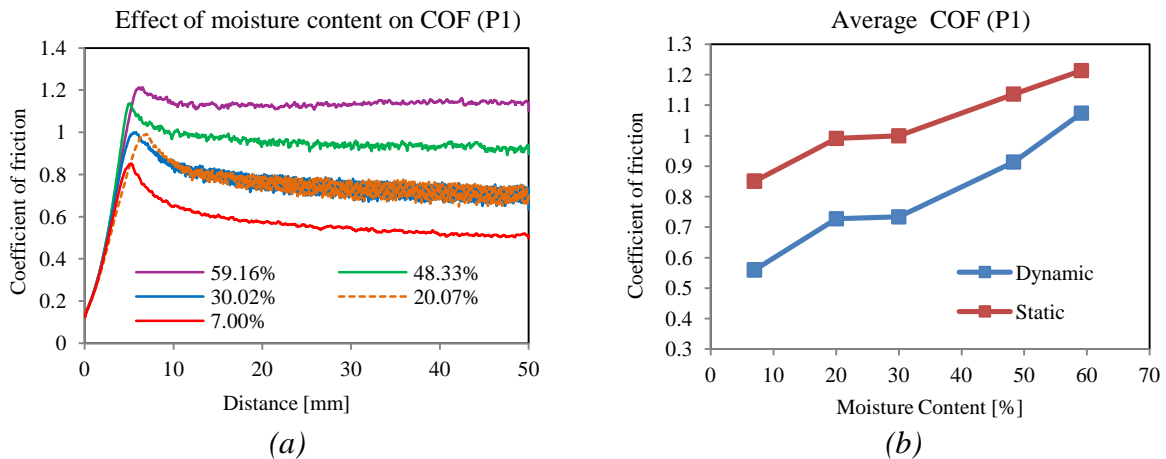


Figure 47. (a) Effect of moisture content on coefficient of friction (b) Average COF at different moisture levels (P1)

(Fig.48) shows the graphs for frictional force (a) & average COF (b) at different moisture levels for P2 sock. Similar to P1 sock, as the moisture content increases, it causes to increase the coefficient of friction. There is a continuous increase in friction with the increase of moisture content. That is also evident from (Fig.48a and 48b). Viscose has lower insole-sock frictional force or COF with respect to P1 (cotton rich sock) at the nearer moisture levels due to its smooth glossy surface [191].

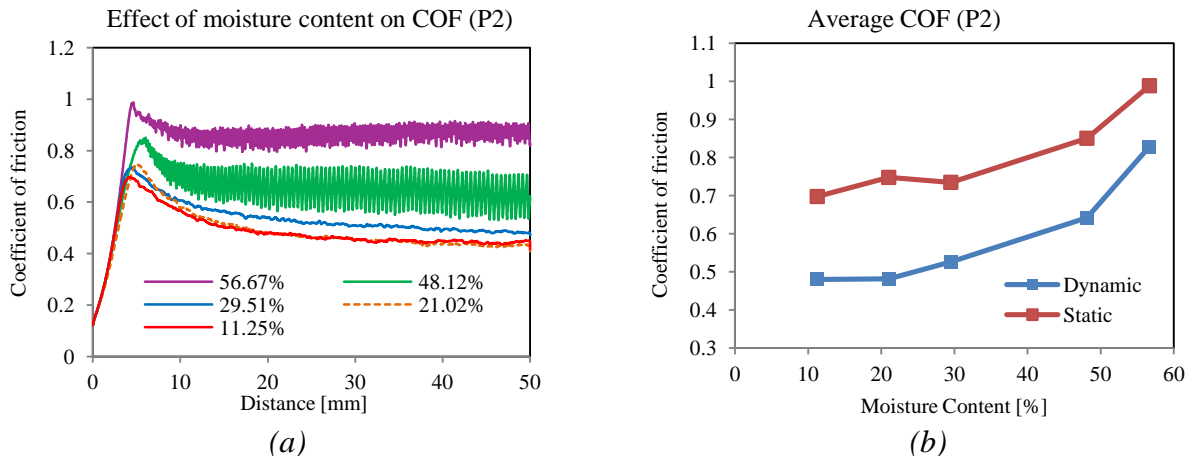


Figure 48. (a) Effect of moisture content on coefficient of friction (b) Average COF at different moisture levels (P2)

(Fig.49) shows the frictional force (a) & average COF (b) at different moisture levels for P3 sock. Even though there is a continuous increase in the friction with the increase of the moisture content. But unlike with P1 & P2 socks, the increment in the friction isn't so rapid. That is manifested especially by the blue line slope representing dynamic COF as shown by (Fig.49b). Dynamic COF almost has the same values between 36.74-56.44% moisture levels. Here a decline is observed for static COF between this range. The dynamic COF slope is more uniform than the static COF slope with respect to different moisture levels. Previously,

Rotaru et al. measured the dynamic friction between human skin and knitted bed sheets consisting of 50% cotton and 50% polyester and reported 0.50 and 0.90 in the dry, wet state respectively [192]. Both dynamic and static COF is lower than the P1 sample. Ramakrishnan and Jeganathan have also found that polyester inner layer fabric has a lower COF value than a cotton inner layer in the wet state [193].

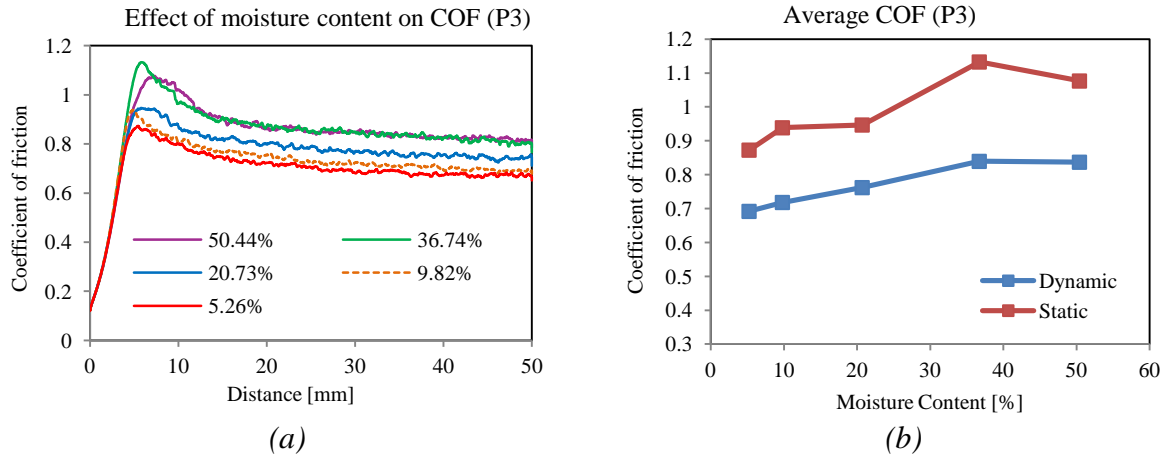


Figure 49. (a) Effect of moisture content on coefficient of friction (b) Average COF at different moisture levels (P3)

Frictional force & average COF at different moisture levels for P4 sock is illustrated by (Fig.50a and Fig.50b) respectively. Similar to P3 sock, there is a continuous increase in the friction (both static & dynamic) with the increase of the moisture content. Bertaux et al. observed dynamic COF (sock-skin interface) values are 0.495, 0.475 for two different wet socks at heel and waist consist of polyamide after 40 min of exercise [127]. The increment in the friction isn't so higher and rapid. Only 10.82 to 11.50% increase in static and dynamic COF is observed between 10.80% to 59.13% moisture content. It is the 2<sup>nd</sup> lowest increase observed after P7 sock. That is manifested by their slopes as shown by (Fig.50b). The results of dynamic COF for P4 socks are in line with Tasron et al. work. As average dynamic COF falls between 0.57 to 0.64 at 10.80% to 59.13% moisture level. Earlier, Tasron et al. reported  $0.44 \pm 0.1$ ,  $0.61 \pm 0.08$  &  $0.69 \pm 0.07$  dynamic COF values for polyamide plain knitted socks in dry, low moisture and high moisture content respectively [190]. Similar results have been observed by Ke et al. They have measured the dynamic COF between human skin and five different polyamide rich medical compression stockings in dry/ wet states and observed that the COF range is 0.31-0.60 for 1x1 jersey structures in the wet state [194]. But they haven't mentioned the moisture content value.

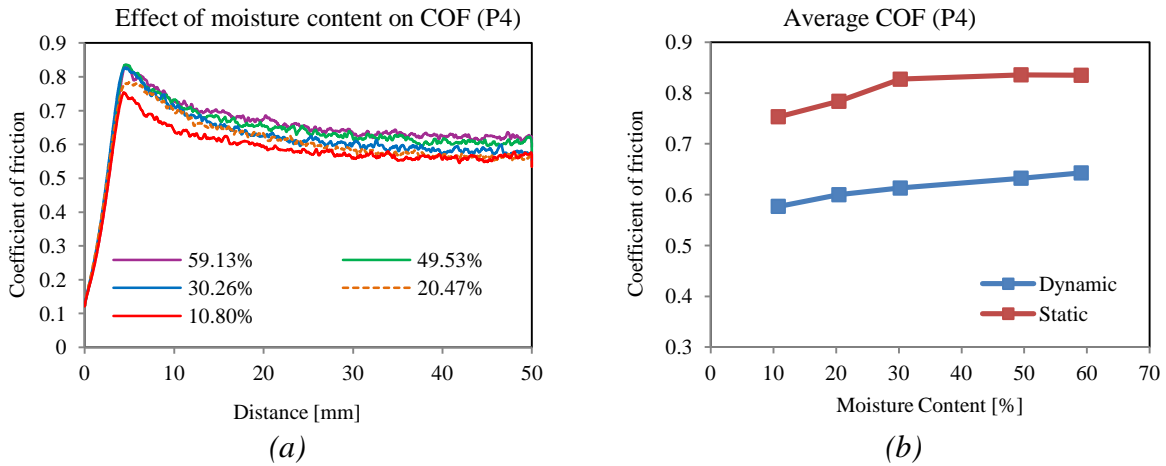


Figure 50. (a) Effect of moisture content on coefficient of friction (b) Average COF at different moisture levels (P4)

Frictional force & average COF for P5 sock is showed by (Fig.51a and Fig.51b) in that order. Similar to P3 and P4 socks, there is a continuous increase in the dynamic friction with the increase of the moisture content. The increase isn't so higher and rapid. Merely 16.97% to 17.46% increase in static and dynamic COF is observed between 5.13% to 59% moisture content. It is the 3<sup>rd</sup> lowest increase observed after P4 and P7 socks. That is manifested by their slopes as shown by (Fig.51b). Bertaux et al. observed dynamic COF (sock-skin interface) value is 0.52 for wet sock's toe consist of polypropylene after 40 min of exercise [127].

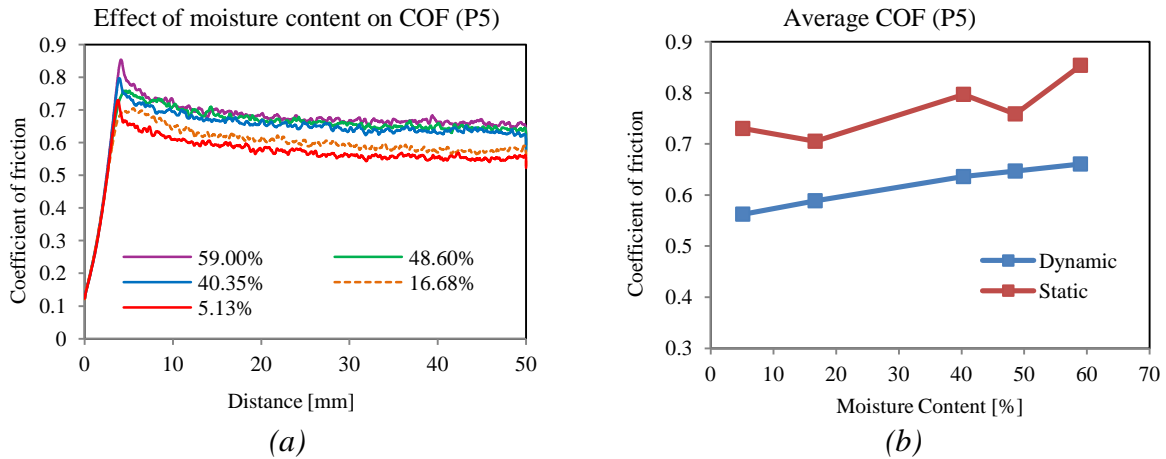


Figure 51. (a) Effect of moisture content on coefficient of friction (b) Average COF at different moisture levels (P5)

Frictional force (N) at different moisture levels for P6 sock has been shown by (Fig.52a) whereas average dynamic and static COF were shown by (Fig.52b). The results clearly demonstrated that as the moisture content increases, it causes to increase in the coefficient of friction following Amber et al. work [195]. There is a uniform increase in the friction with the increase of moisture content.

Unlike other hygroscopic fibre containing socks i.e. P1 (cotton rich) and P2 (viscose rich), P6 has not shown a rapid increase in dynamic friction with the increase of the moisture content. 20% increase in dynamic COF observed between (10.77% to 47.40%) moisture content range, whereas about dynamic COF raised to about 25% among the same moisture range. Minimum dynamic COF (0.60) is observed at 10.77% moisture content. This could be considered as a dry state for wool fibres as 16% moisture regain is known for wool fibre in standard atmospheric conditions. This value is close to the result reported by Sanders et al. They have observed dynamic COF range is 0.60 to 0.79 between wool socks and different materials (insoles) interfaces in the dry state.

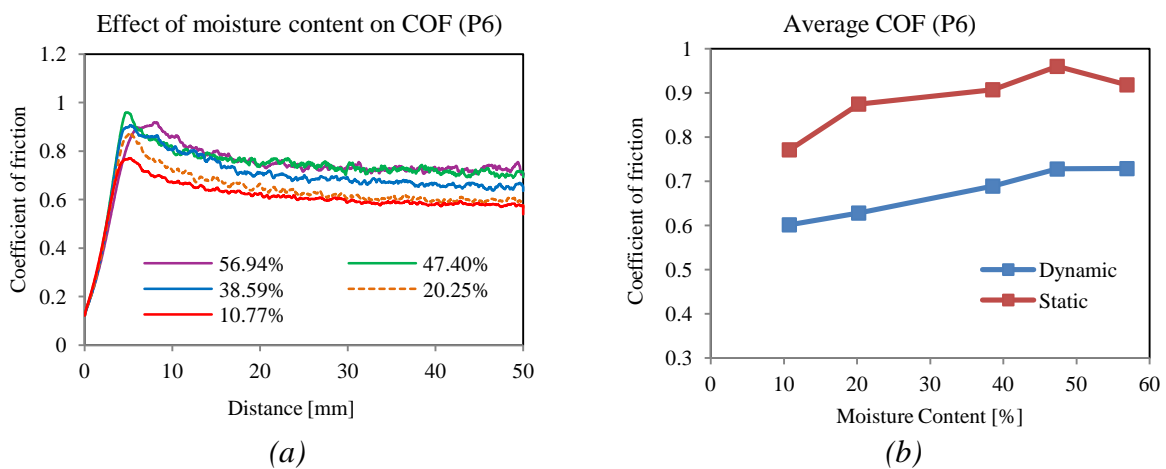


Figure 52. (a) Effect of moisture content on coefficient of friction (b) Average COF at different moisture levels (P6)

(Fig.53) shows the graphs for frictional force (Fig.53a) & COF (Fig.53b) at different moisture levels for P7 sock. Unlike with all the above socks, P7 has not shown a significant increase in static or dynamic friction with the increase of the moisture content. Arai et al. have observed the same kind of results on measuring the static COF for water-absorbing acrylic (Kanebo Lumiza) knitted fabrics at different moisture levels [189].

(Fig.53b) illustrates that there is no change in the dynamic COF till 40% moisture level and a slight rise of 5.67% at 56.38% moisture level. While static COF has shown a slight decrease trend with the increase of the moisture. But it is not significant. In an earlier study, the effect of wetting on the frictional behavior of acrylic and polypropylene multifilament yarns was examined by El-Mogahzy [196]. The results show that the coefficient of friction increased with wetting. But the change in the value of the friction is not significant. Suchatlampong et al. also reported a decline or no change in the value of the friction coefficient when tested acrylic liners against aluminium plate and silicone impression material [197].

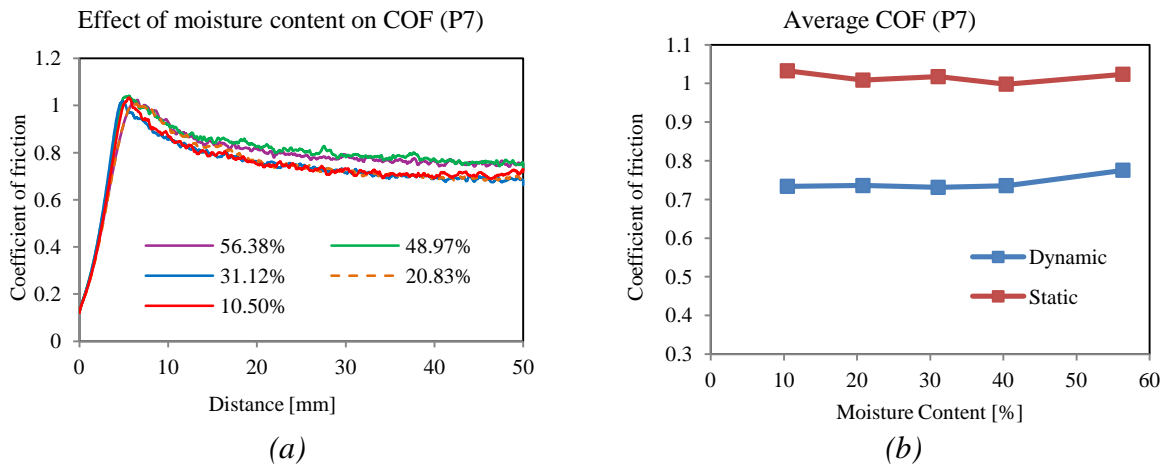


Figure 53. (a) Effect of moisture content on coefficient of friction (b) Average COF at different moisture levels (P7)

#### 4.8 Thermal resistance comparison among different skin models

Thermal resistance study in the wet state should be planned on TFM with aspect to the real simulation of extension and foot geometry. It was tried, but couldn't succeed due to the equipment limitations. The thermal foot model is closer to the real simulation of the worn sock but due to a longer period of measurement (about 1hour) and 35°C temperature of the thermal foot plus free convection of  $1\text{ms}^{-1}$  dries the sample or changes the moisture content. The second choice may be Permetest. Although Permetest has a short time of testing, free convection existence here also leads to continuous evaporation of the moisture from the fabric. Finally, Alambeta was selected for thermal resistance testing in the wet state. The comparison is done in the dry state to indirectly prove that if the results of thermal resistance on the selected skin model (Alambeta) are in good agreement in the dry state. They will have also good conformity in the wet state as well. For a real simulation of the extension like the thermal FM, socks were loaded on a dummy leg and marked with a circle of 12.2cm diameter with the help of a paper card (Fig.10). Then socks were slashed and extended on an embroidery hoop to the marked circle. Finally, these samples were tested on Alambeta and Permetest for Rct under the dry condition. (Fig.54) shows the comparisons of thermal resistance, between TFM and Alambeta. Although thermal resistance measured by TFM is higher for all the samples, however the error bars at 95% confidence interval demonstrated that these results from two different skin models are comparable between ( $0\sim 0.25\text{ms}^{-1}$ ) air velocity. These results are in line with the previous researchers. Mansoor et al. observed the coefficient of determination value is 0.55 while comparing the thermal resistance of terry knitted socks measured by Alambeta and TFM [110]. Abdelhamid et al. also reported good agreement of thermal resistance measured by Alambeta and TFM for woven compression

bandages [198]. Mansoor et al. measured thermal resistance of plain socks with TFM & Alambeta and found that the coefficient of determination 0.6228 [199].

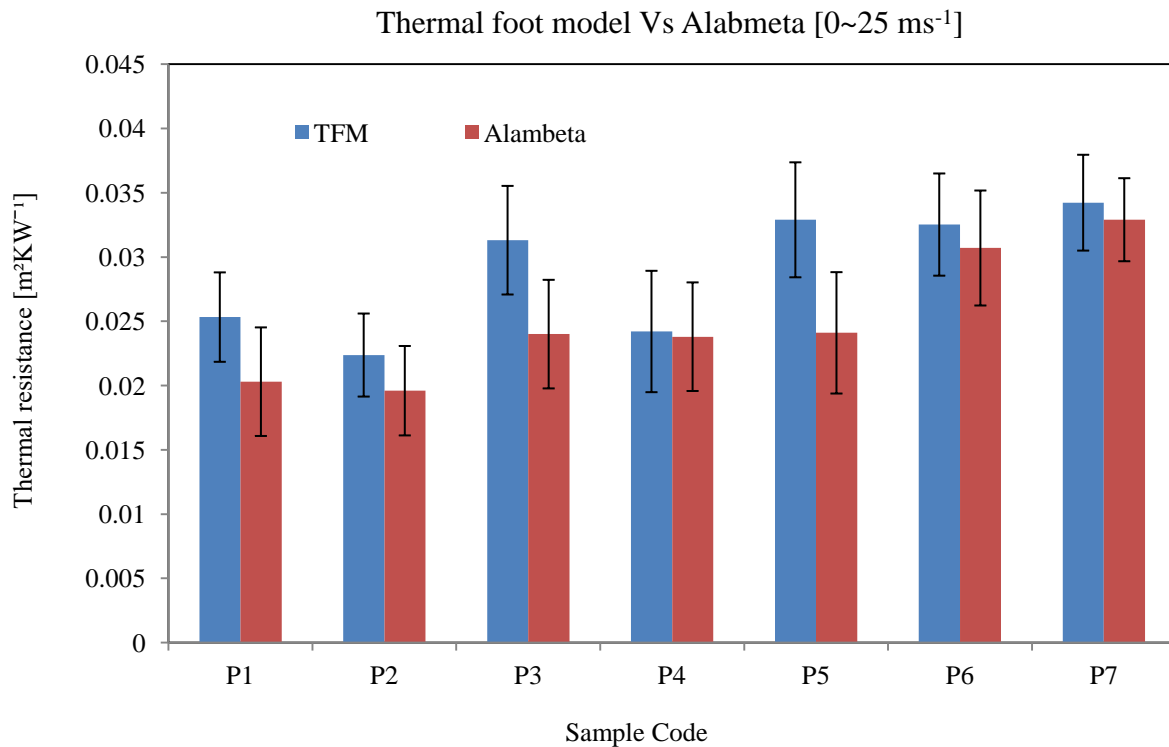


Figure 54. Thermal resistance comparison (TFM Vs Alambeta)

(Fig.55) shows the comparison of thermal resistance, between TFM and Permetest. The error bars at a 95% confidence interval verified that these results from two different skin models are comparable at  $1\text{ms}^{-1}$  air velocity. These results are aligned with the previous researchers. Mansoor et al. observed the coefficient of determination value is 0.64 while comparing the thermal resistance of terry knitted socks measured by Permetest and TFM [110]. Mansoor et al. measured thermal resistance of plain socks with TFM & Permetest and found that the coefficient of determination is 0.615 [199].

Thermal foot model Vs Permetest [1 ms<sup>-1</sup>]

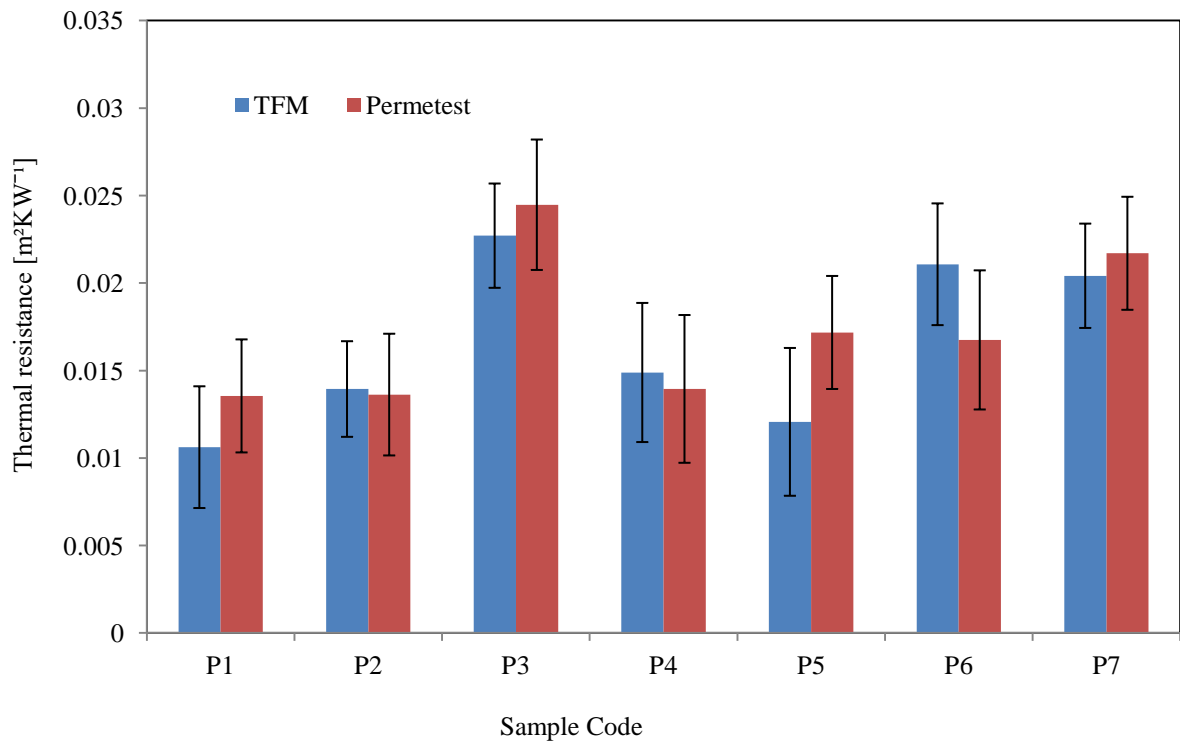


Figure 55. Thermal resistance comparison (TFM Vs Permetest)

## Chapter 5

### 5 Conclusion

A semi-empirical approach was used to model the Thermal resistance prediction of plain knitted socks in the wet state. The aim was to modify/ develop the aforementioned thermal resistance models with acceptable degrees of accuracy from simple inputs of fabric (socks) geometrical parameters such as fibre composition, areal density, and thickness. These parameters were first derived and then used as predictors for the thermal resistance prediction.

This work focuses on the thermal resistance prediction of socks in the wet state followed by some other comfort parameters such as thermal absorptivity, relative water vapour permeability and sock-insole interface friction. The effects of fibre dimensions, orientation, and yarn hairiness were not taken into account. Although both theoretical porosity (for yarn and socks) and experimental (socks) were calculated but thermal resistance prediction is based on theoretical results. Image processing and analysis were used to obtain data on the porous structure of fabrics. Validation of the models has been done through the coefficient of determination ( $R^2$ ) and inference statistics i.e. hypothesizing slope =1 & intercept = 0 at 95% confidence interval.

By adopting this new approach of feeding the wet polymer filling coefficient and the thermal conductivity instead of dry polymers different models can provide a justified prediction of thermal resistance under wet conditions as well. All the models (Militky modified, ME-2 modified & Schuhmeister modified) have a coefficient of determination, i.e.  $R^2$  range in between 0.76~0.95 for all the sock samples at different moisture levels. As well as the validation through hypothesis i.e. slope =1 & intercept =0, Schuhmeister's modified model couldn't qualify for P2 and P4 socks. The polymer filling coefficient remains constant while water and air filling coefficients are changing with the variation of moisture that leads to changing the thermal conductivity. A higher value of moisture causes to decrease the thermal resistance. 50% reduction in thermal resistance occurs at 30% moisture content in all the samples, except P3 (polyester), P4 (nylon) and P5 (polypropylene) socks.

Thermal absorptivity increases by increasing moisture content. It may provide an indication of dry to cool, cold and wet feelings. The results of this study show that the thermal

absorptivity values of dry fabrics range from 79.7 to 180 [ $\text{Ws}^{1/2}\text{m}^{-2}\text{K}^{-1}$ ]. When the fabric is getting wet, as the thermal conductivity of water is much higher than that of fibre and there is the air entrapped in the textile structure, these values increase. In the case of plain socks, only P5 sock has the thermal absorptivity  $< 300$  at 50% moisture level. P1 ( $>80\%$  cotton) and P2 ( $>80\%$  viscose) have the highest thermal absorptivity.

Relative water vapour permeability (RWVP) of the most synthetic fibres is higher, except P7 composed of ( $>80\%$  acrylic). P7 has the worsened RWVP due to its highest thickness and GSM among all the socks.

Socks theoretical porosity falls between 74% to 90% range without and with extension respectively. Extension causes to increase the pore size (space between loops) of the fabric and decrease the fabric thickness. It leads to a decrease in the volume of the fibre (solid part) and increases the volume of air corresponds to porosity. Volume porosity and pore size distribution for socks has been measured by micro-tomography also. It is in agreement with the theoretical volume porosity.

Extended socks have a lower thermal resistance. This is mainly due to the thickness reduction with extension. Thickness is one of the major factors that affect the thermal insulation. Most of the socks haven't close thermal resistance even at 95% confidence level. As socks extended, the number of contact points decreased. It results in a lower value of thermal absorptivity. So this condition is the stimulus for characterizing the socks in an extended state. The thermal resistance measured in the dry and extended state by Alambeta and Permetest is comparable with  $R_{ct}$  measured by the thermal Foot Model at a 95% confidence interval.

Modified thermal resistance models were also verified on some plain-woven and single jersey knitted fabrics (Appendix 3). The results demonstrated that these models can make reasonable prediction for other kinds of fabrics in the wet state as well. The models have been implemented in a programming language FreeMat (Appendix 5) which potentially provides a software tool for textile designers and technologists to predict the thermal resistance of fabrics in a wet state for various applications.

The results of the frictional characterization between the sock-insole interface as expected has positive correlation with the humidity levels. A comparatively higher COF observed for plain knitted socks with respect to previous studies probably due to the long terry of the insole

fabric and testing without extension. Sock-insole interface is also very critical with respect to design (socks/ shoes), blister formation, postural balance and friction ratio (between sock-skin & sock-insole interfaces). A uniform and slight increase is observed in dynamic COF except for P1 (cotton based sock) and P2 (viscose rich sock). Whereas static COF has uneven and rapid risen except P7 (acrylic rich sock).

Working on this dissertation has uncovered many worthy avenues for future investigations. The inquisitive readers will no doubt have ideas of their own, but there are some suggestions for research of possible interest:

- ❖ This study was conducted by assuming thickness and GSM as constant. A separate study could be planned to identify the effect of swelling on the thickness, especially in hydrophilic fabrics.
- ❖ Future studies could be planned for examining other types of fabrics and mathematical models by adopting this approach.
- ❖ Shoes could be added with the addition of more boundary conditions
- ❖ COF between the sock-skin interface for the same samples

## 6 References

- [1] Fogarty AL, Barlett R, Ventenat V, et al. Regional foot sweat rates during a 65-minute uphill. 2006; 2006–2007.
- [2] Taylor NAS, Caldwell JN, Mekjavic IB. The sweating foot: local differences in sweat secretion during exercise-induced hyperthermia. *Aviat Space Environ Med* 2006; 77: 1020–1027.
- [3] Kùklane K. Footwear for cold weather conditions. *Handb Footwear Des Manuf* 2013; 283–317.
- [4] Kuklane K, Gavhed D, Fredriksson K. A field study in dairy farms: thermal condition of feet. *Int J Ind Ergon* 2001; 27: 367–373.
- [5] Slater K. Discussion paper the assessment of comfort. *J Text Inst* 1986; 77: 157–171.
- [6] Adler MM, Walsh WK. Mechanisms of transient moisture transport between fabrics. *Text Res J* 1984; 54: 334–343.
- [7] Woodcock AH. Moisture transfer in textile systems, Part I. *Text Res J* 1962; 32: 628–633.
- [8] Gagge AP, Gonzalez RR. Physiological and physical factors associated with warm discomfort in sedentary man. *Environ Res* 1974; 7: 230–242.
- [9] Plante AM, Holcombe B V, Stephens LG. Fiber hygroscopicity and perceptions of dampness part I: subjective trials. *Text Res J* 1995; 65: 293–298.
- [10] Havenith G, Holmér I, Meinander H, et al. Assessment of thermal properties of protective clothing and their use. *EU Final Rep*.
- [11] Lotens W. Heat transfer from humans wearing clothing. 1993; 1–213.
- [12] Endrusick TL. Effects of prolonged water contact on the thermal insulation of cold weather footwear. In: *Proceedings of the Fifth International Conference on Environmental Ergonomics, Lotens WA and Havenith G (Eds.)*. 1992, pp. 188–189.
- [13] Woo SS, Shalev I, Barker RL. Heat and moisture transfer through nonwoven fabrics: Part I: Heat transfer. *Text Res J* 1994; 64: 149–162.
- [14] Kawabata S. Measurement of anisotropic thermal conductivity of single fiber. *Sen'i Kikai Gakkaishi (Journal Text Mach Soc Japan)* 1986; 39: T184–T186.
- [15] Baczek MB, Hes L. The effect of moisture on thermal resistance and water vapour permeability of Nomex fabrics. *J Mater Sci Eng A* 2011; 1: 358.
- [16] Wong ASW, Li Y. Psychological requirement of professional athlete on active

- sportswear. In: *The 5th Asian Textile Conference, Kyoto, Japan*. 1999.
- [17] Bhattacharjee D, Kothari VK. Heat transfer through woven textiles. *Int J Heat Mass Transf* 2009; 52: 2155–2160.
- [18] Hollies RS, Bogaty H. Some thermal properties of fabrics: part II: the influence of water content. *Text Res J* 1965; 35: 187–190.
- [19] Mangat MM, Hes L, Bajzík V. Thermal resistance models of selected fabrics in wet state and their experimental verification. *Text Res J* 2015; 85: 200–210.
- [20] Boughattas A, Benltoufa S, Hes L, et al. Thermo-physiological properties of woven structures in wet state. *Ind Textila* 2018; 69: 298–303.
- [21] Wang F, Lai D, Shi W, et al. Effects of fabric thickness and material on apparent ‘wet’ conductive thermal resistance of knitted fabric ‘skin’ on sweating manikins. *J Therm Biol* 2017; 70: 69–76.
- [22] Oglakcioglu N, Marmarali A. Thermal comfort properties of cotton knitted fabrics in dry and wet states. *Tekst ve Konfeksiyon* 2010; 20: 213–217.
- [23] Chen YS, Fan J, Zhang W. Clothing thermal insulation during sweating. *Text Res J* 2003; 73: 152–157.
- [24] Kuklane K, Holmér I. Effect of sweating on insulation of footwear. *Int J Occup Saf Ergon* 1998; 4: 123–136.
- [25] Bogusławska-Baczek M, Hes L. Effective water vapour permeability of wet wool fabric and blended fabrics. *Fibres Text East Eur* 2013; 97: 67–71.
- [26] Kuklane K, Holmer I, Giesbrecht G. Change of footwear insulation at various sweating rates. *Appl Hum Sci* 1999; 18: 161–168.
- [27] Richards MGM, Rossi R, Meinander H, et al. Dry and wet heat transfer through clothing dependent on the clothing properties under cold conditions. *Int J Occup Saf Ergon* 2008; 14: 69–76.
- [28] Hes L, Offermann P, Dvorakova I. The effect of underwear on thermal contact feeling caused by dressing up and wearing of garments. In: *Proceedings of Tecnitex 2001 Autex Conference*. 2001, pp. 236–245.
- [29] Kawabata S. Development of a device for measuring heat-moisture transfer properties of apparel fabrics. *Sen’i Kikai Gakkaishi (Journal Text Mach Soc Japan)* 1984; 37: T130–T141.
- [30] Hes L, Dolezal I. New method and equipment for measuring thermal properties of textiles. *Sen’i Kikai Gakkaishi (Journal Text Mach Soc Japan)* 1989; 42: T124–T128.
- [31] Hes L. Fast determination of surface moisture absorptivity of smart underwear knits.

- In: *Internatinal Textile Conference, Terassa*. 2001.
- [32] L H. Thermal properties of nonwovens. In: *Proceedings of Congress Index 87*. Geneva, 1987, pp. 1–11.
- [33] Mangat A, Hes L, Bajzik V. Effect of biopolishing on warm–cool feeling of knitted fabric: a subjective and an objective evaluations. *Autex Res J* 2017; 17: 95–102.
- [34] Mangat AE, Hes L, Bajzik V, et al. Model of thermal absorptivity of knitted rib in dry state and its experimental authentication. *Ind Textila* 2017; 68: 263.
- [35] Matusiak M, Fracczak L. Comfort-related properties of seersucker fabrics in dry and wet state. *Int J Cloth Sci Technol* 2017; 29: 366–379.
- [36] Bogusławska-Bączek M, Hes L. Thermophysiological Properties of Dry and Wet Functional Sportswear Made of Synthetic Fibres. *Tekstilec* 2017; 60: 331–338.
- [37] Jhanji Y, Gupta D, Kothari VK. Comfort properties of plated knitted fabrics with varying fibre type. *Indian J Fibre Text Res* 2015; 40: 11–18.
- [38] Afzal A, Ahmad S, Rasheed A, et al. Influence of fabric parameters on thermal comfort performance of double layer knitted interlock fabrics. *Autex Res J* 2017; 17: 20–26.
- [39] Rengasamy RS, Das BR, Patil YB. Bending and compression behaviour of polyester air-jet-textured and cotton-yarn fabrics. *Open Text J* 2009; 2: 48–52.
- [40] Oğlakcioğlu N, Marmarali A. Thermal comfort properties of some knitted structures. *Fibres Text East Eur* 2007; 15: 64–65.
- [41] ISO 8503-1. Surface roughness characteristics of blast-cleaned steel substrates. *Int Organ Stand*; 2012.
- [42] ASTM. D7127-13. Standard test method for measurement of surface roughness of abrasive blast cleaned metal surfaces using a portable stylus instrument. *ASTM Int* 2014; 1–6.
- [43] Hes L, Dolezal I. Indirect measurement of moisture absorptivity of functional textile fabrics. In: *Journal of Physics: Conference Series*. IOP Publishing, 2018, p. 122026.
- [44] Mangat AE, Hes L, Bajzik V, et al. Thermal absorptivity model of knitted rib fabric and its experimental verification. *Autex Res J* 2018; 18: 20–27.
- [45] Hes L. An indirect method for fast evaluation of surface moisture absorptivity of shirt and underwear fabrics. *Vlakna a Text* 2000; 7: 178–185.
- [46] Hes L. Optimisation of shirt fabrics' composition from the point of view of their appearance and thermal comfort. *Int J Cloth Sci Technol* 1999; 11: 105–119.
- [47] Ren YJ, Ruckman JE. Water vapour transfer in wet waterproof breathable fabrics. *J*

- Ind Text* 2003; 32: 165–175.
- [48] Hes L, Dolezal I. Precise measurement of water vapour permeability of wet fabrics. In: *Proceedings of the AUTEX International Textile Conference*, Tampere. 2007.
- [49] Hes L, de Araujo M. Simulation of the Effect of Air Gaps between the Skin and a Wet Fabric on Resulting Cooling Flow. *Text Res J* 2010; 80: 1488–1497.
- [50] Kuklane K. Protection of feet in cold exposure. *Ind Health* 2009; 47: 242–253.
- [51] Błażejczyk K, Kazandjiev V, Degórski M, et al. Assessment of occupational heat stress risk among agriculture workers in Poland and Bulgaria. *Europa* 2015; 21: 59–72.
- [52] Martini L. Vitriols do guarantee an efficacious reduction of the human sweat when secreted from eccrine glands. *Our Dermatology Online/Nasza Dermatologia Online*; 7.
- [53] Smith CJ, Machado-Moreira CA, Plant G, et al. Design data for footwear: sweating distribution on the human foot. *Int J Cloth Sci Technol* 2013; 25: 43–58.
- [54] West AM, TARRIER J, Hodder S, et al. Sweat distribution and perceived wetness across the human foot: the effect of shoes and exercise intensity. *Ergonomics* 2019; 62: 1450–1461.
- [55] Young AJ, Roberts DE, Scott DP, et al. *Sustaining health and performance in the cold: A pocket guide to environmental medicine aspects of cold-weather operations*. Army Research Inst of Environmental Medicine Natick Ma, 1992.
- [56] Mangat MM, Hes L. Thermal resistance of denim fabric under dynamic moist conditions and its investigational confirmation. *Fibres Text East Eur* 2014; 22: 101–105.
- [57] Naka S, Kamata Y. Thermal conductivity of wet fabrics. *J Text Mach Soc Japan* 1977; 23: 114–119.
- [58] Dias T, Delkumburewatte GB. The influence of moisture content on the thermal conductivity of a knitted structure. *Meas Sci Technol* 2007; 18: 1304.
- [59] Fricke H. A mathematical treatment of the electric conductivity and capacity of disperse systems I. The electric conductivity of a suspension of homogeneous spheroids. *Phys Rev* 1924; 24: 575.
- [60] Wei J, Xu S, Liu H, et al. Simplified model for predicting fabric thermal resistance according to its microstructural parameters. *Fibres Text East Eur* 2015; 23: 57–60.
- [61] Schuhmeister J. *Ber. K Akad Wien (Math-Naturw Klasse)* 1877; 76: 283.
- [62] Baxter S t. The thermal conductivity of textiles. *Proc Phys Soc* 1946; 58: 105.
- [63] Militky J, Kremenakova D. Prediction of fabrics thermal conductivity. In: *5th*

- International textile, clothing & design conference–Magic World of Textiles*. 2010, pp. 1–6.
- [64] Militký J, Becker C. Selected topics of textile and material Science. *Sel Top Text Mater Sci* 2011; 404.
- [65] Maxwell JC. *A treatise on electricity and magnetism*. Dover, 1954.
- [66] Eucken A. Allgemeine gesetzmäßigkeiten für das wärmeleitvermögen verschiedener stoffarten und aggregatzustände. *Forsch auf dem Gebiet des Ingenieurwesens A* 1940; 11: 6–20.
- [67] Howard E, Oakley N. The design and function of military footwear: a review following experiences in the South Atlantic. *Ergonomics* 1984; 27: 631–637.
- [68] Li Y. The science of clothing comfort. *Text Prog* 2001; 31: 1–135.
- [69] Jaeger JC, Carslaw HS. *Conduction of heat in solids*. Clarendon P, 1959.
- [70] Cleland AC. *Food refrigeration processes*. Elsevier applied science, 1990.
- [71] Cleland AC, Earle RL. A comparison of analytical and numerical methods of predicting the freezing times of foods. *J Food Sci* 1977; 42: 1390–1395.
- [72] Mangat AE, Bajzik V, Lubos H, et al. The use of artificial neural networks to estimate thermal resistance of knitted fabrics. *Tekst ve Konfeksiyon* 2015; 25: 304–312.
- [73] Kanat ZE, Özdil N. Application of artificial neural network (ANN) for the prediction of thermal resistance of knitted fabrics at different moisture content. *J Text Inst* 2018; 109: 1247–1253.
- [74] Akyol U, Erhan Akan A, Durak A. Simulation and thermodynamic analysis of a hot-air textile drying process. *J Text Inst* 2015; 106: 260–274.
- [75] Qian X, Fan J. Prediction of clothing thermal insulation and moisture vapour resistance of the clothed body walking in wind. *Ann Occup Hyg* 2006; 50: 833–842.
- [76] Das A, Alagirusamy R, Kumar P. Study of heat transfer through multilayer clothing assemblies: a theoretical prediction. *Autex Res J* 2011; 11: 54–60.
- [77] Bogaty H, Hollies NRS, Harris M. Some thermal properties of fabrics: part I: The effect of fiber arrangement. *Text Res J* 1957; 27: 445–449.
- [78] Biron M. *Thermoplastics and thermoplastic composites*. William Andrew, 2018.
- [79] Rengasamy RS, Kawabata S. Computation of thermal conductivity of fibre from thermal conductivity of twisted yarn.
- [80] Hearle JWS, Morton WE. *Physical properties of textile fibres*. Elsevier, 2008.
- [81] Haghi AK. Thermal analysis of drying process: A theoretical approach. *J Therm Anal Calorim* 2003; 74: 827–842.

- [82] Brailsford AD, Major KG. The thermal conductivity of aggregates of several phases, including porous materials. *Br J Appl Phys* 1964; 15: 313.
- [83] Wang J, Carson JK, North MF, et al. A new approach to modelling the effective thermal conductivity of heterogeneous materials. *Int J Heat Mass Transf* 2006; 49: 3075–3083.
- [84] Carson JK. Prediction of the thermal conductivity of porous foods: a thesis submitted in partial fulfilment of the requirements for the degree of Doctor of Philosophy in Food Engineering, Massey University, Palmerston North, New Zealand, 2002.
- [85] *ASTM International. (2013a). ASTM D 4850: Standard terminology relating to fabrics and fabric test methods. Annual Book of ASTM Standards (Vol. 7.02, 11 pp.). West Conshohocken, PA, USA.*
- [86] Oxarango L. *Transferts de chaleur et de masse dans des structures poreuses multi-échelles: application à l'étude des filtres à particules Diesel.* Institut National Polytechnique de Toulouse-INPT, 2004.
- [87] Algaba I, Riva A, Crews PC. Influence of fiber type and fabric porosity on the UPF of summer fabrics. *AATCC Rev* 2004; 4: 26–31.
- [88] Matusiak M. Application of artificial neural networks to predict the air permeability of woven fabrics. *Fibres Text East Eur* 2015; 23: 41–48.
- [89] Backer S. The relationship between the structural geometry of a textile fabric and its physical properties: Part IV: interstice geometry and air permeability. *Text Res J* 1951; 21: 703–714.
- [90] Robertson AF. Air porosity of open-weave fabrics part I: metallic meshes. *Text Res J* 1950; 20: 838–844.
- [91] Jordeva S, Čortoševa S, Mojsov K, et al. The influence of the structural characteristics of cotton and polyester knitted fabrics on the thermo-physiological comfort. *Adv Technol* 2017; 6: 88–92.
- [92] Cubric IS, Skenderi Z, Havenith G. Impact of raw material, yarn and fabric parameters, and finishing on water vapor resistance. *Text Res J* 2013; 83: 1215–1228.
- [93] Adanur S. *Wellington Sears handbook of industrial textiles. 1995.*
- [94] Siddique HF, Mazari AA, Havelka A, et al. Effect of elastic elongation on compression pressure and air-permeation of compression socks. *Vlakna a Text* 2018; 25: 35–43.
- [95] Mansoor T, Hes L, Skenderi Z, et al. Effect of preheat setting process on heat, mass and air transfer in plain socks. *J Text Inst* 2019; 110: 159–170.

- [96] Siddiqui MOR, Sun D. Porosity prediction of plain weft knitted fabrics. *Fibers* 2015; 3: 1–11.
- [97] Hes L, Promerova M. The effect of thermal resistance and absorptivity of various fabrics on their thermal contact characteristics. In: *21st Textile Res. Symp. At Mt. Fuji*. 1992.
- [98] Hes L. Non-destructive determination of comfort parameters during marketing of functional garments and clothing. *Indian J Fibre Text Res* 2008; 33: 239–245.
- [99] Akcagun E, Bogusławsk-Bączek M, Hes L. Thermal insulation and thermal contact properties of wool and wool/PES fabrics in wet state. *J Nat fibers* 2019; 16: 199–208.
- [100] Hes L. Thermal comfort properties of textile fabrics in wet state. In: *Proceedings of XI. International Textile and Apparel Symposium”, Turkey. İzmir*.
- [101] Wang L. Heat, Moisture and Air Transfer Properties of Selected Woven Fabrics in Wet State. *J Fiber Bioeng Informatics* 2009; 2: 141–149.
- [102] Oglakcioglu N, Celik P, Ute TB, et al. Thermal comfort properties of angora rabbit/cotton fiber blended knitted fabrics. *Text Res J* 2009; 79: 888–894.
- [103] Onofrei E, Maria Rocha A, Catarino A. Investigating the effect of moisture on the thermal comfort properties of functional elastic fabrics. *J Ind Text* 2012; 42: 34–51.
- [104] Gupta D, Chattopadhyay R, Bera M. Comfort properties of pressure garments in extended state. *Ind J Fibre Text Res* 2011; 36: 415–421.
- [105] Siddique HF, Mazari AA, Havelka A, et al. Analysis of thermal properties affected by different extension levels of compression socks. *Vlakna a Text* 2019; 26: 64–68.
- [106] Gorjanc DŠ, Dimitrovski K, Bizjak M. Thermal and water vapor resistance of the elastic and conventional cotton fabrics. *Text Res J* 2012; 82: 1498–1506.
- [107] Zhu G, Kremenakova D, Wang Y, et al. Study on air permeability and thermal resistance of textiles under heat convection. *Text Res J* 2015; 85: 1681–1690.
- [108] Das S. Study on comfort properties of different woven fabric. *Int J Manag Appl Sci* 2016; 2394–7926.
- [109] Kothari VK. Quality control: Fabric comfort. *Indian Ins. of Tech., Delhi, India*.
- [110] Mansoor T, Hes L, Bajzik V, et al. Effect of moisture content on thermophysiological properties of terry knitted socks followed by thermal resistance comparison among different skin models. In: *Fiber Society’s Fall 2018 Technical Meeting and Conference: Advanced, Smart, and Sustainable Fibers, Materials, and Textiles*. Fiber Society, 2018.
- [111] Hes L, Bogusławska-Bączek M, Geraldles MJ. Thermal comfort of bedsheets under

- real conditions of use. *J Nat Fibers* 2014; 11: 312–321.
- [112] Oğlakcioğlu N, Sari B, Üte TB, et al. A novel medical bandage with enhanced clothing comfort. In: *IOP Conference Series: Materials Science and Engineering*. IOP Publishing, 2016, p. 12021.
- [113] Arumugam V, Mishra R, Militky J, et al. Thermal and water vapor transmission through porous warp knitted 3D spacer fabrics for car upholstery applications. *J Text Inst* 2018; 109: 345–357.
- [114] Sampath MB, Senthilkumar M. Effect of moisture management finish on comfort characteristics of microdenier polyester knitted fabrics. *J Ind Text* 2009; 39: 163–173.
- [115] Rajwin AJ, Prakash C. Effect of air plasma treatment on thermal comfort properties of woven fabric. *Int J Thermophys* 2017; 38: 166.
- [116] Lenfeldova I, Hes L. Dependence of water vapor permeability of knitted samples on their wetting level. In: *Book of Abstracts*, p. 141.
- [117] Knapik JJ, Reynolds KL, Duplantis KL, et al. Friction blisters. *Sport Med* 1995; 20: 136–147.
- [118] Gerhardt L-C, Strässle V, Lenz A, et al. Influence of epidermal hydration on the friction of human skin against textiles. *J R Soc Interface* 2008; 5: 1317–1328.
- [119] Knapik JJ, Reynolds K, Barson J. Influence of an antiperspirant on foot blister incidence during cross-country hiking. *J Am Acad Dermatol* 1998; 39: 202–206.
- [120] Reynolds K, Darrigrand A, Roberts D, et al. Effects of an antiperspirant with emollients on foot-sweat accumulation and blister formation while walking in the heat. *J Am Acad Dermatol* 1995; 33: 626–630.
- [121] Costill DL. Sweating: its composition and effects on body fluids. *Ann N Y Acad Sci* 1977; 301: 160–174.
- [122] Tasron DN, Thurston TJ, Carré MJ. Frictional behaviour of running sock textiles against plantar skin. *Procedia Eng* 2015; 112: 110–115.
- [123] Liu X, Lu Z, Lewis R, et al. Feasibility of using optical coherence tomography to study the influence of skin structure on finger friction. *Tribol Int* 2013; 63: 34–44.
- [124] Tomlinson SE, Lewis R, Liu X, et al. Understanding the friction mechanisms between the human finger and flat contacting surfaces in moist conditions. *Tribol Lett* 2011; 41: 283–294.
- [125] Baussan E, Bueno MA, Rossi RM, et al. Analysis of current running sock structures with regard to blister prevention. *Text Res J* 2013; 83: 836–848.
- [126] Van Amber RR, Wilson CA, Laing RM, et al. Thermal and moisture transfer

- properties of sock fabrics differing in fiber type, yarn, and fabric structure. *Text Res J* 2015; 85: 1269–1280.
- [127] Bertaux E, Derler S, Rossi RM, et al. Textile, physiological, and sensorial parameters in sock comfort. *Text Res J* 2010; 80: 1803–1810.
- [128] Hursh DF, Johnston JB. *Anti-friction two-ply athletic sock*. Google Patents, 1989.
- [129] Baussan E, Bueno MA, Rossi RM, et al. Experiments and modelling of skin-knitted fabric friction. *Wear* 2010; 268: 1103–1110.
- [130] Sanders JE, Greve JM, Mitchell SB, et al. Material properties of commonly-used interface materials and their static coefficients of friction with skin and socks. *J Rehabil Res Dev* 1998; 35: 161–176.
- [131] Mathias A, Curry DG, Donnelly C, et al. Slip sliding away II - Slip resistance of dress socks on indoor flooring. *Proc Hum Factors Ergon Soc* 2010; 2: 1382–1386.
- [132] Ali WY. Frictional behaviour of bare foot and foot wearing socks sliding against marble flooring tiles. *J King Abdulaziz Univ Eng Sci* 2010; 149: 1–44.
- [133] Dai X-Q, Li Y, Zhang M, et al. Effect of sock on biomechanical responses of foot during walking. *Clin Biomech* 2006; 21: 314–321.
- [134] Euler RD. Creating “comfort” socks for the US consumer. *Knitt Times* 1985; 54: 47.
- [135] Herring KM, Richie Jr DH. Friction blisters and sock fiber composition. A double-blind study. *J Am Podiatr Med Assoc* 1990; 80: 63–71.
- [136] Jeddi AAA, Shams S, Nosraty H, et al. Relations between fabric structure and friction: Part i: Woven fabrics. *J Text Inst* 2003; 94: 223–234.
- [137] Kenins P. Influence of fiber type and moisture on measured fabric-to-skin friction. *Text Res J* 1994; 64: 722–728.
- [138] Gwosdow AR, Stevens JC, Berglund LG, et al. Skin friction and fabric sensations in neutral and warm environments. *Text Res J* 1986; 56: 574–580.
- [139] Sommerville P. Fundamental principles of fibre fineness measurement. *Technol Meas fineness wool fibres, part* 2002; 3: 1–5.
- [140] Burleigh EG, Wakeham H, Honold E, et al. Pore-Size Distribution in Textiles. *Text Res J* 1949; 19: 547–555.
- [141] Neckár B, Das D. *Theory of structure and mechanics of yarns*. Woodhead Publishing India PVT. Limited, 2019.
- [142] Ishtiaque SM, Das A. A new approach of prediction of yarn diameter. *Fibers Polym* 2013; 14: 838–843.
- [143] Neckar B, Das D. *Theory of structure and mechanics of fibrous assemblies*. WPI

- Publishing, 2012.
- [144] Mansoor T, Siddique HF, Ali A, et al. Wrinkle free plaited knitted fabrics without pre-heat setting. *J Text Inst* 2018; 109: 307–311.
- [145] AATCC Technical Manual 2014. 80–88.
- [146] Yoon HN, Buckley A. Improved comfort polyester: Part I: Transport properties and thermal comfort of polyester/cotton blend fabrics. *Text Res J* 1984; 54: 289–298.
- [147] Bories S, Mojtabi A, Prat M, et al. *Transferts de chaleur dans les milieux poreux*. Ed. Techniques Ingénieur, 1995.
- [148] Dubois A. *Porosite des tissus: correlations entre les methodes de determination de la permeabilite a l'air*. Eurédia, 1999.
- [149] Guidoin R, King M, Marceau D, et al. Textile arterial prostheses: Is water permeability equivalent to porosity? *J Biomed Mater Res* 1987; 21: 65–87.
- [150] Hsieh Y-L. Liquid transport in fabric structures. *Text Res J* 1995; 65: 299–307.
- [151] Dyck V. Desktop X-ray microscopy and microtomography. *J Microsc* 1998; 191: 151–158.
- [152] SKYSCAN 1272 - Videos - X-ray Micro-CT - SKYSCAN 1272 | Bruker, <https://www.bruker.com/products/microtomography/micro-ct-for-sample-scanning/skyscan-1272/videos.html> (accessed 20 June 2020).
- [153] *Pressure measuring device for medical compression and support stockings (Salzman, Group Switzerland)*, [https://www.swisslastic.ch/files/Druckmessgeraete/MST-MK\\_V-EN\\_SP\\_JP\\_CN-2014-4p.pdf](https://www.swisslastic.ch/files/Druckmessgeraete/MST-MK_V-EN_SP_JP_CN-2014-4p.pdf).
- [154] van Bemmelen JM. Die Absorption. Das Wasser in den Kolloiden, besonders in dem Gel der Kieselsäure. *Zeitschrift für Anorg Chemie* 1897; 13: 233–356.
- [155] Zsigmondy R. Structure of gelatinous silicic acid. Theory of dehydration. *Z anorg Chem* 1911; 71: 356.
- [156] Caurie M. Hysteresis phenomenon in foods. *Int J food Sci Technol* 2007; 42: 45–49.
- [157] Hes L, Dolezal I. A new computer-controlled skin model for fast determination of water vapour and thermal resistance of fabrics. In: *7th Asian Textile Conference, New Delhi*. 2003.
- [158] Gorica S. *Foot Manikin Technical Specifications*. 2010.
- [159] Wiley-VCH (ed). *Ullmann's Fibers, 2 Volumes*. Wiley, <https://books.google.cz/books?id=R9c8wgEACAAJ> (2008).
- [160] Bobeth W. Thermisches Verhalten. In: *Textile Faserstoffe*. Springer, 1993, pp. 253–284.

- [161] Geschke D. *Physical Properties of Polymers Handbook*. Springer New York. Epub ahead of print 1997. DOI: 10.1524/zpch.1997.199.part\_1.128.
- [162] Meloun M, Militky J. *Statistical data analysis: A practical guide*. Woodhead Publishing, Limited, 2011. Epub ahead of print 2011. DOI: 10.1533/9780857097200.
- [163] Lowther J, Keller G, Warwick B. *Statistics for Management and Economics*. Cengage Learning, 1997. Epub ahead of print 1997. DOI: 10.2307/3010500.
- [164] Fan J. Physiological comfort of fabrics and garments. *Eng Appar Fabr Garments* 2009; 1: 201–250.
- [165] Lubos HES, Marmarali A, Oezdil N, et al. The effect of moisture on friction coefficient of elastic knitted fabrics. *Tekst ve Konfeksiyon* 2008; 18: 206–210.
- [166] Tasron D, Maiti R, Hemming M, et al. Frictional interaction between running sock fabrics and plantar aspect of first metatarsal head in different moisture conditions. *Procedia Eng* 2016; 147: 753–758.
- [167] Dreby EC. A friction meter for determining the coefficient of kinetic friction of fabrics. *J Res Natl Bur Stand (1934)* 1943; 31: 237–246.
- [168] D1894. Standard test method for static and kinetic coefficients of friction of plastic film and sheeting. *Astm* 2014; 08: 1–8.
- [169] Classification P. ( 12 ) Patent Application Publication ( 10 ) Pub . No .: US 2013 / 0148102 A1 N-40 Patent Application Publication. 1.
- [170] Visualization of local thickness in 3D (Bruker Micro CT Academ). 2014; 1: 2–3.
- [171] Abdolmaleki S, Jeddi AAA, Amani M. Estimation on the 3D porosity of plain knitted fabric under uniaxial extension. *Fibers Polym* 2012; 13: 535–541.
- [172] Doczyova K, Glombikova V, Komarkova P. Application of microtomography in textile metrology. *Tekstilec*; 57.
- [173] Kanat Z, ÖZDİL N, Marmarali A. Prediction of thermal resistance of the knitted fabrics in wet state by using multiple regression analysis. *J Text Apparel/Tekstil ve Konfeksiyon*; 24.
- [174] Finck JL. Mechanism of heat flow in fibrous materials. *Bur Stand J Res* 1930; 5: 973–984.
- [175] Reddy KS, Karthikeyan P. Combinatory models for predicting the effective thermal conductivity of frozen and unfrozen food materials. *Adv Mech Eng* 2010; 2: 901376.
- [176] Mao N, Russell SJ. The thermal insulation properties of spacer fabrics with a mechanically integrated wool fiber surface. *Text Res J* 2007; 77: 914–922.
- [177] Supuren G, Oglakcioglu N, Ozdil N, et al. Moisture management and thermal

- absorptivity properties of double-face knitted fabrics. *Text Res J* 2011; 81: 1320–1330.
- [178] Bajzik V, Lubos HES. The effect of finishing treatment on thermal insulation and thermal contact properties of wet fabrics. *Tekst ve Konfeksiyon* 2012; 22: 26–31.
- [179] Bivainyte A, Mikučioniene D. Influence of shrinkage on air and water vapour permeability of double-layered weft knitted fabrics. *Medziagotyra* 2012; 18: 271–274.
- [180] Jhanji Y, Gupta D, Kothari VK. Moisture management properties of plated knit structures with varying fiber types. *J Text Inst* 2015; 106: 663–673.
- [181] Öner E, Atasagun HG, Okur A, et al. Evaluation of moisture management properties on knitted fabrics. *J Text Inst* 2013; 104: 699–707.
- [182] Chatterjee PK. *Textile Science and Technology*. 1994. Epub ahead of print 1994. DOI: 10.1016/B978-0-444-88224-0.50001-1.
- [183] Li Y, Zhu Q, Yeung KW. Influence of thickness and porosity on coupled heat and liquid moisture transfer in porous textiles. *Text Res J* 2002; 72: 435–446.
- [184] Lin C-M, Lou C-W, Lin J-H. Manufacturing and properties of fire-retardant and thermal insulation nonwoven fabrics with FR-polyester hollow fibers. *Text Res J* 2009; 79: 993–1000.
- [185] Barker RL, Heniford RC. Factors affecting the thermal insulation and abrasion resistance of heat resistant hydro-entangled nonwoven batting materials for use in firefighter turnout suit thermal liner systems. *J Eng Fiber Fabr* 2011; 6: 155892501100600100.
- [186] Frydrych I, Dziworska G, Biliska J. Comparative analysis of the thermal insulation properties of fabrics made of natural and man-made cellulose fibres. *Fibres Text East Eur* 2002; 10: 40–44.
- [187] Gnanauthayan G, Rengasamy RS, Kothari VK. Heat insulation characteristics of high bulk nonwovens. *J Text Inst* 2017; 108: 2173–2179.
- [188] Abdel-Rehim ZS, Saad MM, El-Shakankery M, et al. Textile fabrics as thermal insulators. *AUTEX Res J* 2006; 6: 148–161.
- [189] Arai K. Wearing comfort of water absorbent acrylic fibers. *J Text Mach Soc Japan* 1984; 30: 72–81.
- [190] Tasron D, Nasir SH, Troynikov O, et al. Thermo-physiological comfort and frictional characteristics of running socks in different moisture conditions. In: *Proceedings of the 9th Conference of the Textile Bioengineering and Informatics Symposium*. 2016.
- [191] Kozłowski RM, Mackiewicz-Talarczyk M, Wielgusz K, et al. Bast fibres: flax. In: *Handbook of Natural Fibres*. Elsevier, 2020, pp. 93–162.

- [192] Rotaru G-M, Pille D, Lehmeier FK, et al. Friction between human skin and medical textiles for decubitus prevention. *Tribol Int* 2013; 65: 91–96.
- [193] Varadaraju R, Srinivasan J. Design of polyester-elastane-cotton plated knitted components for hot and dry environment. *Int J Cloth Sci Technol* 2018; 30: 657–667.
- [194] Ke W, Rotaru G-M, Hu JY, et al. In vivo measurement of the friction between human skin and different medical compression stockings. *Tribol Lett* 2015; 60: 4.
- [195] Van Amber RR, Lowe BJ, Niven BE, et al. The effect of fiber type, yarn structure and fabric structure on the frictional characteristics of sock fabrics. *Text Res J* 2015; 85: 115–127.
- [196] Mogahzy Y. Friction and surface characteristics of synthetic fibers. In: *Friction in Textile Materials*. Elsevier, 2008, pp. 292–328.
- [197] Suchatlampong C, Davies E, von Fraunhofer JA. Frictional characteristics of resilient lining materials. *Dent Mater* 1986; 2: 135–138.
- [198] Aboalasaad ARR, Skenderi Z, Kolčavová SB, et al. Analysis of factors affecting thermal comfort properties of woven compression bandages. *Autex Res J* 2020; 20: 178–185.
- [199] Mansoor T, Hes L, Bajzik V, et al. Novel method on thermal resistance prediction and thermo-physiological comfort of socks in a wet state. *Text Res J* 2020; 0040517520902540.
- [200] Yu C-Y, Tu H-H. Foot surface area database and estimation formula. *Appl Ergon* 2009; 40: 767–774.

## Author's publications

1. Mansoor, T., Hes, L., Bajzik, V., & Noman, M. T. (2020). Novel method on thermal resistance prediction and thermo-physiological comfort of socks in a wet state. *Textile Research Journal*, 0040517520902540. **Impact factor: 1.613**
2. Mansoor, T., Hes, L., & Bajzik, V. (2020). A New Approach for Thermal Resistance Prediction of Different Composition Plain Socks in Wet State (Part 2). *Autex Research Journal*, 1(ahead-of-print). **Impact factor: 0.85**
3. Mansoor, T., Siddique, H. F., Ali, A., Komarkova, P., Havelka, A., & Hussain, Z. (2018). Wrinkle free plaited knitted fabrics without pre-heat setting. *The Journal of the Textile Institute*, 109(3), 307-311. **Impact factor: 1.36**

4. Mansoor, T., Hes, L., Skenderi, Z., Siddique, H. F., Hussain, S., & Javed, A. (2018). Effect of preheat setting process on heat, mass and air transfer in plain socks. *The Journal of the Textile Institute*, 1-12. **Impact factor: 1.36**
5. Ali, A., Nguyen, N. H., Baheti, V., Ashraf, M., Militky, J., Mansoor, T., & Ahmad, S. (2018). Electrical conductivity and physiological comfort of silver coated cotton fabrics. *The Journal of the Textile Institute*, 109(5), 620-628. **Impact factor: 1.36.**
6. Azeem, M., Hes, L., Wiener, J., Noman, M. T., Ali, A., & Mansoor, T. (2018). Comfort properties of nano-filament polyester fabrics: thermo-physiological evaluation. *Industria Textila*, 69(4), 315-321. **Impact factor: 0.90**
7. Hussain, S., Glombikova, V., Akhtar, N., Mazari, A., Mansoor, T., & Khan, K. A. H. (2019). Liquid moisture transportation properties of functional underwears: Part 1. *Autex Research Journal*, 19(2), 97-103. **Impact factor: 0.85**
8. Siddique, H. F., Mazari, A. A., Havelka, A., Mansoor, T., Ali, A., & Azeem, M. (2018). Development of V-Shaped Compression Socks on Conventional Socks Knitting Machine. *Autex Research Journal*, 18(4), 377-384. **Impact factor: 0.85**
9. Siddique, H. F., Mazari, A. A., Havelka, A., Hussain, S., & Mansoor, T. (2018). Effect of elastic elongation on compression pressure and air-permeation of compression socks. *Vlákna a Textil (Fibres and Textiles)*, 25(1). **Impact factor: 0.20**
10. Ahmad, I., M. Iftikhar., N. Mehmood and T. Mansoor. 2006. Comparative Study Of Some Reactive Dyes Performance On Cotton Fabric Under The Processing Variables Dyeing Time And Temperature. *The Indus Cotton* 3(2):372-283.

### **Author's publications in international conferences**

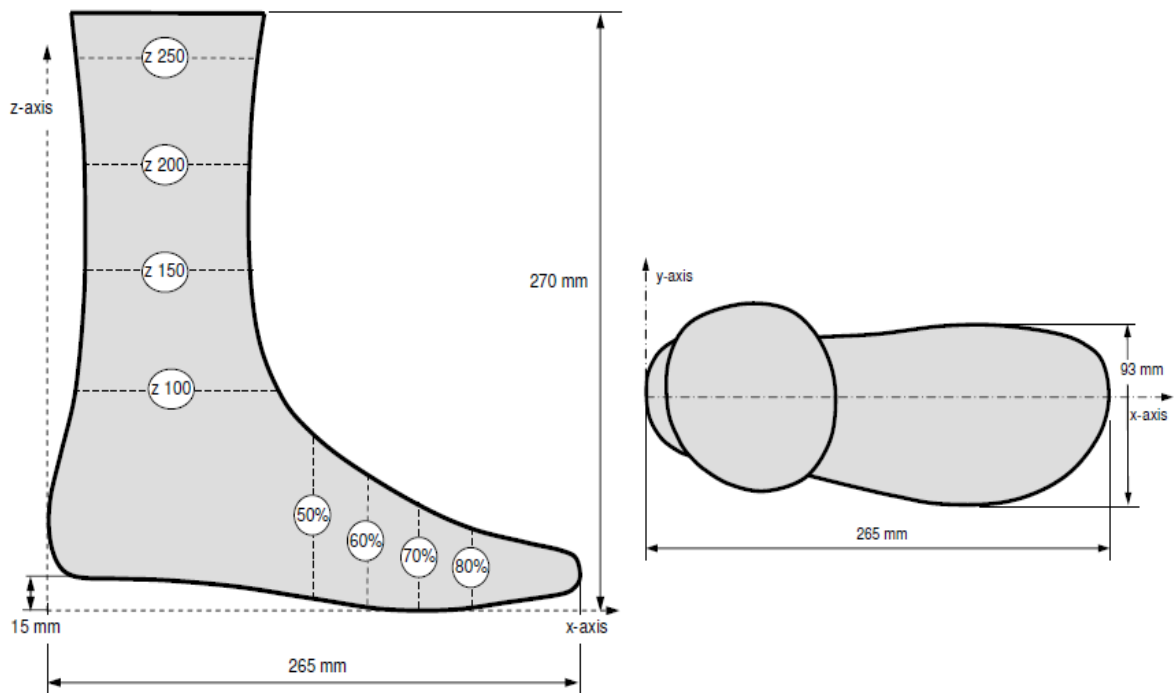
1. Mansoor, T., Hes, L., & Bajzik, V., Effect of moisture content on Thermophysiological Properties of Terry Knitted Socks followed by Thermal resistance comparison among different Skin Models. Fibre Society Conference October, 2018 UC Davis United States.
2. Mansoor, T., Hes, L., Zenun, S., & Javed, M.A., Effect of moisture content on Thermophysiological Properties of Plain Knitted Socks followed by Thermal resistance comparison among different Skin Models. STRUTEX 22nd International Conference December, 2018 Liberec Czech Republic.

# Appendixes

## Appendix 1

### Specifications of the Thermal Foot Model [158]

Segment	Nr. of heaters	Nr. of sw. glands	Max. heating power [w]	Min sweating rate [ml/min]	Max sweating rate [ml/min]	Sweating group	Segment Area [mm <sup>2</sup> ]
1	2	3	66	0.003	0.3	A	6720
2	4	3	33	0.003	0.3	A	12510
3	2	3	66	0.003	0.3	B	6520
4	3	3	46	0.003	0.3	B	7770
5	2	3	66	0.003	0.3	B	5910
6	2	3	66	0.003	0.3	B	5730
7	2	2	50	0.002	0.2	B	7570
8	2	3	44	0.003	0.3	A	8560
9	2	0	66	0	0	-	4380
10	3	4	30	0.004	0.4	B	11590
11	2	3	44	0.003	0.3	A	6960
12	2	2	45	0.002	0.2	A	8350
13	2	0	66	0	0	-	3880
<b>total</b>	<b>30</b>	<b>32</b>	<b>688</b>	<b>-</b>	<b>-</b>	<b>-</b>	<b>96450</b>



## Appendix 2

### Specifications of the wooden Leg (Salzmann MST Switzerland)

Foot dimensions		Value
Maximum foot length [mm]		235
Maximum foot width [mm]		97.5
Maximum foot girth [mm]		260
Minimum foot girth [mm]		230
Foot surface area [mm <sup>2</sup> ]	Predicted [200] $FSA_{\text{male}} = 1.06 \times MFL \times BG$ MFL = maximum foot length BG =ball girth	64766
	Measured	60375

For more detail see the specifications for medium size (24cm) in standard test method (RAL-GZ-381/1).



## Appendix 3

### Validation of models for other fabrics

Fabric type	Fibre composition [%]	GSM [gm <sup>-2</sup> ]	Thickness [mm]	Moisture content [%]	Thermal resistance [m <sup>2</sup> KW <sup>-1</sup> ]			
					ME-2 modified	Schuhmeister Modified	Militky modified	Experimental
1/1 plain woven fabric	Polyester 100%	154.41	0.46	4.53	0.0056	0.0071	0.0057	0.0078
				13.69	0.0046	0.0063	0.0050	0.0059
				28.22	0.0031	0.0050	0.0039	0.0053
	Cotton 100%	144.04	0.46	12.97	0.0042	0.0064	0.0050	0.0079
				29.57	0.0028	0.0051	0.0039	0.0049
				46.24	0.00168	0.0037	0.00284	0.0035
	Polyester 51.35%, Cotton 48.65%	154.12	0.44	15.20	0.0037	0.0056	0.0044	0.0066
				27.15	0.0027	0.0047	0.0036	0.0053
				41.29	0.0017	0.0036	0.0028	0.0039
Single jersey knitted fabrics	Cotton 55.29%, Polypropylene 44.71%	281.30	0.73	12.69	0.0078	0.0115	0.0092	0.01099
				30.71	0.0046	0.0082	0.0063	0.00632
				46.40	0.0025	0.0058	0.0044	0.0049
	Viscose 59.12%, Polypropylene 40.88%	287.20	0.82	9.83	0.0101	0.0142	0.0114	0.0119
				25.25	0.0067	0.0109	0.0085	0.0089
				45.39	0.0034	0.0072	0.0054	0.0059
	Cotton 53.02%, Polypropylene 25.23%, Polyester 21.75%	305.37	0.95	18.18	0.0095	0.0140	0.0111	0.013
				38.14	0.0054	0.0099	0.0076	0.0086
				51.23	0.0032	0.0074	0.0056	0.0069

## Appendix 4

### GSM and thickness of the plain (single jersey) socks without extension

Socks code	GSM [ $\text{gm}^{-2}$ ]	Thickness [mm]
P1	276.42	1.08
P2	315.98	1.12
P3	252.03	1.01
P4	227.64	1.09
P5	211.38	1.04
P6	268.29	1.32
P7	390.24	1.55

## Appendix 5

### Coding for thermal resistance prediction in Matlab/ Freemmat

For prediction of the models (ME-2, Militky & Schuhmeister modified) along with experimental values to moisture content, FreeMat is used for writing scripts. FreeMat is a free-access software, almost having the same coding as Matlab. By changing the values of (g, g1, g2.....) areal density, fibre content, (T) thickness, and thermal conductivity of the used fibres, thermal resistance could be predicted for any other fabric. Below is an example of a complete code for ME-2 thermal resistance prediction model (Sample P1).

```
function rct=ME_model(MC)
%MC=[0:1:60]
% MC is moisture content
MR=MC/(1-(MC/100)); % Moisture Regain

g=305.37;           % Fabric areal density
g1= g*0.5302;      % 1st Yarn areal density
g2=g*0.2175;      % 2nd Yarn areal density
g3=g*0.0105;      % 3rd Yarn areal density
g4=(g*MR)/100;    % Water areal density

T=0.95;           % Fabric Thickness
B1=g1/T;          % 1st Yarn Bulk density
B2=g2/T;          % 2nd Yarn Bulk density
B3=g3/T;          % 3rd Yarn Bulk density
B4=g4/T;          % Water Bulk density
```

```

F1=B1/1540;          % 1st Yarn Filling Coefficient
F2=B2/1360;          % 2nd Yarn Filling Coefficient
F3=B3/1200;          % 3rd Yarn Filling Coefficient
F4=B4/1000;          % Water Filling Coefficient
Fp=F1+F2+F3+F4;     % Wet polymer Filling Coefficient
Fa=1-Fp              % air Filling Coefficient

%% Thermal Resistance Prediction
k1=(0.50*F1+0.40*F2+0.20*F3+0.60*F4)/(F1+F2+F3+F4); %fibre thermal conductivity
k2=0.026;           %air thermal conductivity

a=k2*Fa+k1*Fp*((3*k2)/2*k2+k1); %1st factor
b=Fa+Fp*((3*k2)/(2*k2+k1));     %2nd factor

TC=a/b;
rct=(T/1000/TC);
%plot(rct,mcc)ME

```

For Schuhmeister and Militky modified models all the script will same like ME-2 except their formulas as given below;

For Schuhmeister;

```

a = 0.3*(k1*Fp+k2*Fa);          %1st factor
b = 0.7*(k1*k2)/(k1*Fa+k2*Fp); %2nd factor

rct=(T/1000)/(a+b)
%plot(rct,mcc)

```

and for Militky;

```

a = 0.5*(k1*Fp+k2*Fa);          %1st factor
b = 0.5*(k1*k2)/(k1*Fa+k2*Fp); %2nd factor

rct=(T/1000)/(a+b)
%plot(rct,mcc)

```

For loading the experimental thermal resistance values at specific moisture content, another script is needed as shown in the second column. This should be written in a matrix.

```

mo_rc=[11.12  0.0189
        23.18  0.0167
        31.87  0.0104
        39.139 0.0094
        50.02  0.0084];

```

The above code will result in only one value. After the above function, a script is needed in a different window for plotting the thermal resistance by different models by changing the moisture. Since all the parameters are scalars except moisture content (%) that is a vector. The following shows the plotting script for the model and experimental results.

```

%ploting different values

```

```

i=0
for MC=0:1:60
i=i+1
rct_Mi(i)=Mi_model(MC);
rct_ME(i)=ME_model(MC);
rct_Sc(i)=Sc_model(MC);
mcc(i)=MC;
MR=MC/(1-(MC/100));
end

%rct
%mcc

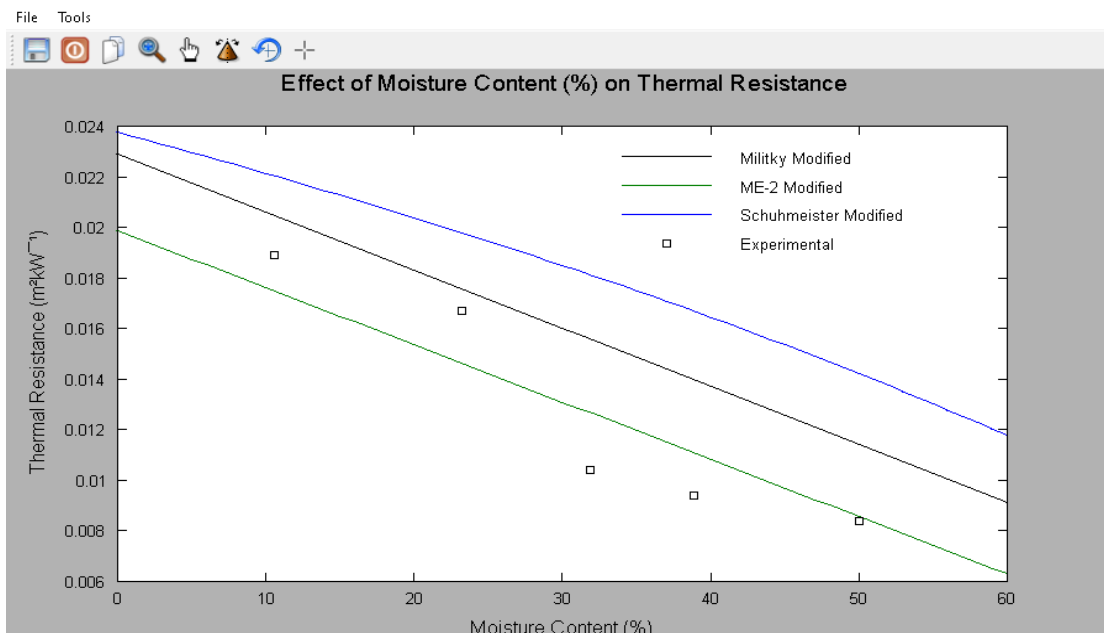
plot(mcc,rct_Mi,'k.-') ; hold on
plot(mcc,rct_ME,'o.-') ; hold on
plot(mcc,rct_Sc,'b.-') ; hold on

% load the experimental data
Experimental_data
plot(mo_rc(:,1),mo_rc(:,2),'ks') ; hold on

legend('Militky Modified','ME-2 Modified','Schuhmeister
Modified','Experimental'); hold on
legend('boxoff')
% labels
xlabel('Moisture Content (%)','fontSize',12)
ylabel('Thermal Resistance (m2kW-1)','fontSize',12)
title('Effect of Moisture Content (%) on Thermal
Resistance')
title('Effect of Moisture Content (%) on Thermal
Resistance','fontSize',14)
set(gca,'fontSize',10)

```

By running this code, below graph will be plotted for all three models along with their experimental values at specific moisture content.



## Appendix 6

<<<<< Begin of workflow >>>>>

CT Analyser, Version: 1.18.4.0  
Dataset name, F:\DATA\Tarik\P-1\P-1\_Rec\P-1\_rec00000867.bmp  
File postfix length, 8  
File type, BMP  
Image size (W/H), 2452, 2452  
Total number of images, 503  
Total Z-position range, 617, 1119  
Number of images inside VOI, 301  
Z-position range of VOI, 660, 960  
Z spacing, 1  
Pixel size (um), 3.000147

-----  
[ 06/05/20 09:19:41 ]      Thresholding  
Mode, Global  
Lower grey threshold, 33  
Upper grey threshold, 255  
[ 06/05/20 09:19:47 ]      Thresholding done

-----  
[ 06/05/20 09:19:47 ]      Despeckle  
Type: Remove white speckles (3D space)  
Volume : less than 10 voxels  
Apply to: Image  
299371 speckles removed  
[ 06/05/20 09:20:26 ]      Despeckle done

-----  
[ 06/05/20 09:20:26 ]      Despeckle  
Type: Remove black speckles (3D space)  
Volume : less than 10 voxels  
Apply to: Image  
2164 speckles removed  
[ 06/05/20 09:23:02 ]      Despeckle done

-----  
[ 06/05/20 09:23:02 ]      Bitwise operations  
<Image> = <Image> AND <Region of Interest>  
[ 06/05/20 09:23:04 ]      Bitwise operations done

-----  
[ 06/05/20 09:23:04 ]      3D analysis  
Destination folder of images of Structure separation: F:\DATA\Tarik\P-1\P-1\_Rec\TBSP  
Date and time,05.06.2020 09:23  
Operator identity,oem  
Computer name,T7610  
Computation time,00:05:51  
Dataset,p-1\_rec  
Location,F:\DATA\Tarik\P-1\P-1\_Rec\

### MORPHOMETRY RESULTS

-----  
Description,Abbreviation,Value,Unit  
Number of layers,,301  
Lower vertical position,,1.98009702,mm  
Upper vertical position,,2.88014113,mm  
Pixel size,,3.00014701,um

Lower grey threshold,,33  
Upper grey threshold,,255

Total VOI volume,TV,14.81359450,mm<sup>3</sup>  
Object volume,Obj.V,3.57728043,mm<sup>3</sup>  
Percent object volume,Obj.V/TV,24.14863208,%  
Total VOI surface,TS,47.40659594,mm<sup>2</sup>  
Object surface,Obj.S,939.84538343,mm<sup>2</sup>  
Intersection surface,i.S,6.16710206,mm<sup>2</sup>  
Object surface / volume ratio,Obj.S/Obj.V,262.72622490,1/mm  
Object surface density,Obj.S/TV,63.44478942,1/mm  
Centroid (x),Crd.X,-0.04255805,mm  
Centroid (y),Crd.Y,0.08958559,mm  
Centroid (z),Crd.Z,2.43044838,mm  
Structure separation,St.Sp,0.04418313,mm  
Number of objects,Obj.N,12624,  
Number of closed pores,Po.N(cl),64,  
Volume of closed pores,Po.V(cl),0.00003363,mm<sup>3</sup>  
Surface of closed pores,Po.S(cl),0.02546847,mm<sup>2</sup>  
Closed porosity (percent),Po(cl),0.00094004,%  
Volume of open pore space,Po.V(op),11.23628044,mm<sup>3</sup>  
Open porosity (percent),Po(op),75.85114091,%  
Total volume of pore space,Po.V(tot),11.23631406,mm<sup>3</sup>  
Total porosity (percent),Po(tot),75.85136792,%  
Euler number,Eu.N,-367145,  
Connectivity,Conn,379833,  
Connectivity density,Conn.Dn,0.00069240,1/mm<sup>3</sup>

Structure separation distribution, St. Sp  
Range, Mid-range, Volume, Percent volume in range  
mm, mm, mm<sup>3</sup>, %

0.00300 - <0.00900,0.00600,0.10210700,0.9121  
0.00900 - <0.01500,0.01200,0.91223281,8.1486  
0.01500 - <0.02100,0.01800,1.49080160,13.3168  
0.02100 - <0.02700,0.02400,1.72756406,15.4317  
0.02700 - <0.03300,0.03000,1.14826017,10.2570  
0.03300 - <0.03900,0.03600,0.75824173,6.7731  
0.03900 - <0.04500,0.04200,0.75316882,6.7278  
0.04500 - <0.05100,0.04800,0.63581985,5.6795  
0.05100 - <0.05700,0.05400,0.54497588,4.8681  
0.05700 - <0.06300,0.06000,0.49645642,4.4347  
0.06300 - <0.06900,0.06600,0.45352648,4.0512  
0.06900 - <0.07500,0.07200,0.37291944,3.3311  
0.07500 - <0.08100,0.07800,0.33777070,3.0172  
0.08100 - <0.08700,0.08400,0.31496244,2.8134  
0.08700 - <0.09300,0.09000,0.25725907,2.2980  
0.09300 - <0.09900,0.09600,0.20215409,1.8058  
0.09900 - <0.10501,0.10200,0.17476102,1.5611  
0.10501 - <0.11101,0.10801,0.13045507,1.1653  
0.11101 - <0.11701,0.11401,0.11830782,1.0568  
0.11701 - <0.12301,0.12001,0.08865238,0.7919  
0.12301 - <0.12901,0.12601,0.06627409,0.5920  
0.12901 - <0.13501,0.13201,0.04788036,0.4277  
0.13501 - <0.14101,0.13801,0.02113004,0.1887  
0.14101 - <0.14701,0.14401,0.01590104,0.1420  
0.14701 - <0.15301,0.15001,0.01170795,0.1046  
0.15301 - <0.15901,0.15601,0.01163755,0.1040

Standard deviation of structure separation,SD(St.Sp),0.02897733,mm

3D-analysis summary

Dataset,Date and time,Pixel size,Unit,Lower grey threshold,Upper grey threshold>Total VOI volume,Object volume,Percent object volume>Total VOI surface,Object surface,Intersection surface,Object surface / volume ratio,Object surface density,Structure thickness,Structure separation,Structure linear density,Surface convexity index,Centroid (x),Centroid (y),Centroid (z),Structure model index,Degree of anisotropy,Eigenvalue 1,Eigenvalue 2,Eigenvalue 3,Fractal dimension,Number of objects,Number of closed pores,Volume of closed pores,Surface of closed pores,Closed porosity (percent),Volume of open pore space,Open porosity (percent),Total volume of pore space>Total porosity (percent),Euler number,Connectivity,Connectivity density,Standard deviation of structure thickness,Standard deviation of structure separation,Moment of inertia (x),Moment of inertia (y),Moment of inertia (z),Polar moment of inertia,Radius of gyration (x),Radius of gyration (y),Radius of gyration (z),Polar radius of gyration,Product of inertia (xy),Product of inertia (xz),Product of inertia (yz),

,,U,,,TV,Obj.V,Obj.V/TV,TS,Obj.S,i.S,Obj.S/Obj.V,Obj.S/TV,St.Th,St.Sp,St.Li.Dn,SCv.I,Crd.X,Crd.Y,Crd.Z, SMI,DA,,,FD,Obj.N,Po.N(cl),Po.V(cl),Po.S(cl),Po(cl),Po.V(op),Po(op),Po.V(tot),Po(tot),Eu.N,Conn,Conn.Dn, SD(St.Th),SD(St.Sp),MMI(x),MMI(y),MMI(z),MMI(polar),Gr.R(x),Gr.R(y),Gr.R(z),Gr.R(polar),Pr.In(xy),Pr.I n(xz),Pr.In(yz),

,,um,,,U^3,U^3,%U^2,U^2,U^2,1/U,1/U,U,U,1/U,1/U,U,U,U,,,,,,U^3,U^2,%U^3,%U^3,%,,,1/U^3,U,U,U^ 5,U^5,U^5,U^5,U,U,U,U,U^5,U^5,U^5,

F:\DATA\Tarik\P-1\P-1\_Rec\p-1\_rec,05.06.2020

09:23,3.00014701,mm,33,255,14.81359450,3.57728043,24.14863208,47.40659594,939.84538343,6.16710206, 262.72622490,63.44478942,,0.04418313,,,-

0.04255805,0.08958559,2.43044838,,,,,,12624,64,0.00003363,0.02546847,0.00094004,11.23628044,75.85114 091,11.23631406,75.85136792,-367145,379833,0.00069240,,0.02897733,,,,,,,

<<<<< End of task (c07b070e-4018-4ff5-9274-e0340bd992cd) >>>>>

## Appendix 7

<<<<< Begin of workflow >>>>>

CT Analyser, Version: 1.18.4.0

Dataset name, F:\DATA\Tarik\P-2\P-2\_Rec\P-2\_rec00000819.bmp

File postfix length, 8

File type, BMP

Image size (W/H), 2452, 2452

Total number of images, 535

Total Z-position range, 593, 1127

Number of images inside VOI, 301

Z-position range of VOI, 660, 960

Z spacing, 1

Pixel size (um), 3.000147

-----  
[ 06/04/20 14:38:18 ]      Thresholding

Mode, Global

Lower grey threshold, 33

Upper grey threshold, 255

[ 06/04/20 14:38:24 ]      Thresholding done

-----  
[ 06/04/20 14:38:25 ]      Despeckle

Type: Remove white speckles (3D space)

Volume : less than 10 voxels

Apply to: Image

550656 speckles removed

[ 06/04/20 14:39:02 ]      Despeckle done

[ 06/04/20 14:39:02 ] Despeckle  
Type: Remove black speckles (3D space)  
Volume : less than 10 voxels  
Apply to: Image  
9257 speckles removed  
[ 06/04/20 14:41:43 ] Despeckle done

-----  
[ 06/04/20 14:41:43 ] Bitwise operations  
<Image> = <Image> AND <Region of Interest>  
[ 06/04/20 14:41:45 ] Bitwise operations done

-----  
[ 06/04/20 14:41:45 ] 3D analysis

Destination folder of images of Structure separation: F:\DATA\Tarik\P-2\P-2\_Rec\TBSP

Date and time,04.06.2020 14:41  
Operator identity,oem  
Computer name,T7610  
Computation time,00:06:03  
Dataset,p-2\_rec  
Location,F:\DATA\Tarik\P-2\P-2\_Rec\

#### MORPHOMETRY RESULTS

-----  
Description,Abbreviation,Value,Unit

Number of layers,,301  
Lower vertical position,,1.98009702,mm  
Upper vertical position,,2.88014113,mm  
Pixel size,,3.00014701,um  
Lower grey threshold,,33  
Upper grey threshold,,255  
  
Total VOI volume,TV,14.81359450,mm<sup>3</sup>  
Object volume,Obj.V,3.89472976,mm<sup>3</sup>  
Percent object volume,Obj.V/TV,26.29159158,%  
Total VOI surface,TS,47.40659594,mm<sup>2</sup>  
Object surface,Obj.S,936.58713878,mm<sup>2</sup>  
Intersection surface,i.S,7.21755031,mm<sup>2</sup>  
Object surface / volume ratio,Obj.S/Obj.V,240.47551323,1/mm  
Object surface density,Obj.S/TV,63.22483979,1/mm  
Centroid (x),Crd.X,-0.12284217,mm  
Centroid (y),Crd.Y,0.01176283,mm  
Centroid (z),Crd.Z,2.45126185,mm  
Structure separation,St.Sp,0.04953284,mm  
Number of objects,Obj.N,16789,  
Number of closed pores,Po.N(cl),809,  
Volume of closed pores,Po.V(cl),0.00041230,mm<sup>3</sup>  
Surface of closed pores,Po.S(cl),0.34731052,mm<sup>2</sup>  
Closed porosity (percent),Po(cl),0.01058500,%  
Volume of open pore space,Po.V(op),10.91845243,mm<sup>3</sup>  
Open porosity (percent),Po(op),73.70562516,%  
Total volume of pore space,Po.V(tot),10.91886473,mm<sup>3</sup>  
Total porosity (percent),Po(tot),73.70840842,%  
Euler number,Eu.N,-400647,  
Connectivity,Conn,418245,  
Connectivity density,Conn.Dn,0.00076242,1/mm<sup>3</sup>

### Structure separation distribution,St.Sp

Range, Mid-range, Volume, Percent volume in range  
mm, mm, mm<sup>3</sup>, %

0.00300 - <0.00900, 0.00600, 0.22386204, 2.0551  
0.00900 - <0.01500, 0.01200, 1.20101893, 11.0258  
0.01500 - <0.02100, 0.01800, 1.11491467, 10.2353  
0.02100 - <0.02700, 0.02400, 1.02429642, 9.4034  
0.02700 - <0.03300, 0.03000, 0.82830312, 7.6041  
0.03300 - <0.03900, 0.03600, 0.67622338, 6.2080  
0.03900 - <0.04500, 0.04200, 0.75568000, 6.9374  
0.04500 - <0.05100, 0.04800, 0.68390620, 6.2785  
0.05100 - <0.05700, 0.05400, 0.60377187, 5.5428  
0.05700 - <0.06300, 0.06000, 0.56400418, 5.1778  
0.06300 - <0.06900, 0.06600, 0.50658520, 4.6506  
0.06900 - <0.07500, 0.07200, 0.42408270, 3.8932  
0.07500 - <0.08100, 0.07800, 0.39816154, 3.6553  
0.08100 - <0.08700, 0.08400, 0.35556858, 3.2642  
0.08700 - <0.09300, 0.09000, 0.27002606, 2.4789  
0.09300 - <0.09900, 0.09600, 0.23039187, 2.1151  
0.09900 - <0.10501, 0.10200, 0.19401631, 1.7811  
0.10501 - <0.11101, 0.10801, 0.16169094, 1.4844  
0.11101 - <0.11701, 0.11401, 0.14512921, 1.3323  
0.11701 - <0.12301, 0.12001, 0.11999495, 1.1016  
0.12301 - <0.12901, 0.12601, 0.10206709, 0.9370  
0.12901 - <0.13501, 0.13201, 0.07253037, 0.6659  
0.13501 - <0.14101, 0.13801, 0.05427169, 0.4982  
0.14101 - <0.14701, 0.14401, 0.04831869, 0.4436  
0.14701 - <0.15301, 0.15001, 0.02713056, 0.2491  
0.15301 - <0.15901, 0.15601, 0.02197397, 0.2017  
0.15901 - <0.16501, 0.16201, 0.02448072, 0.2247  
0.16501 - <0.17101, 0.16801, 0.00723245, 0.0664  
0.17101 - <0.17701, 0.17401, 0.00774768, 0.0711  
0.17701 - <0.18301, 0.18001, 0.01409340, 0.1294  
0.18301 - <0.18901, 0.18601, 0.01566878, 0.1438  
0.18901 - <0.19501, 0.19201, 0.00968792, 0.0889  
0.19501 - <0.20101, 0.19801, 0.00599566, 0.0550  
Standard deviation of structure separation, SD(St.Sp), 0.03405722, mm

### 3D-analysis summary

Dataset, Date and time, Pixel size, Unit, Lower grey threshold, Upper grey threshold, Total VOI volume, Object volume, Percent object volume, Total VOI surface, Object surface, Intersection surface, Object surface / volume ratio, Object surface density, Structure thickness, Structure separation, Structure linear density, Surface convexity index, Centroid (x), Centroid (y), Centroid (z), Structure model index, Degree of anisotropy, Eigenvalue 1, Eigenvalue 2, Eigenvalue 3, Fractal dimension, Number of objects, Number of closed pores, Volume of closed pores, Surface of closed pores, Closed porosity (percent), Volume of open pore space, Open porosity (percent), Total volume of pore space, Total porosity (percent), Euler number, Connectivity, Connectivity density, Standard deviation of structure thickness, Standard deviation of structure separation, Moment of inertia (x), Moment of inertia (y), Moment of inertia (z), Polar moment of inertia, Radius of gyration (x), Radius of gyration (y), Radius of gyration (z), Polar radius of gyration, Product of inertia (xy), Product of inertia (xz), Product of inertia (yz),  
,,U,,,TV,Obj.V,Obj.V/TV,TS,Obj.S,i.S,Obj.S/Obj.V,Obj.S/TV,St.Th,St.Sp,St.Li.Dn,SCv.I,Crd.X,Crd.Y,Crd.Z, SMI,DA,,,,FD,Obj.N,Po.N(cl),Po.V(cl),Po.S(cl),Po(cl),Po.V(op),Po(op),Po.V(tot),Po(tot),Eu.N,Conn,Conn.Dn, SD(St.Th),SD(St.Sp),MMI(x),MMI(y),MMI(z),MMI(polar),Gr.R(x),Gr.R(y),Gr.R(z),Gr.R(polar),Pr.In(xy),Pr.I n(xz),Pr.In(yz),  
,,um,,,,U<sup>3</sup>,U<sup>3</sup>,%,U<sup>2</sup>,U<sup>2</sup>,U<sup>2</sup>,1/U,1/U,U,U,1/U,1/U,U,U,U,,,,,,U<sup>3</sup>,U<sup>2</sup>,%,U<sup>3</sup>,%,U<sup>3</sup>,%,,,1/U<sup>3</sup>,U,U,U<sup>5</sup>,U<sup>5</sup>,U<sup>5</sup>,U<sup>5</sup>,U,U,U,U,U<sup>5</sup>,U<sup>5</sup>,U<sup>5</sup>,

F:\DATA\Tarik\P-2\P-2\_Rec\p-2\_rec,04.06.2020  
14:41,3.00014701,mm,33,255,14.81359450,3.89472976,26.29159158,47.40659594,936.58713878,7.21755031,  
240.47551323,63.22483979,,0.04953284,,,-  
0.12284217,0.01176283,2.45126185,,,,,,16789,809,0.00041230,0.34731052,0.01058500,10.91845243,73.7056  
2516,10.91886473,73.70840842,-400647,418245,0.00076242,,0.03405722,,,,,,  
<<<<< End of task (5743edf2-fe77-424f-bcfd-5bb5859a631a) >>>>>

## Appendix 8

<<<<< Begin of workflow >>>>>

CT Analyser, Version: 1.18.4.0

Dataset name, F:\DATA\Tarik\P-3\P-3\_Rec\P-3\_rec00000891.bmp

File postfix length, 8

File type, BMP

Image size (W/H), 2452, 2452

Total number of images, 675

Total Z-position range, 584, 1258

Number of images inside VOI, 271

Z-position range of VOI, 650, 920

Z spacing, 1

Pixel size (um), 3.000147

-----  
[ 06/04/20 13:49:24 ]      Thresholding  
Mode, Global  
Lower grey threshold, 33  
Upper grey threshold, 255  
[ 06/04/20 13:49:31 ]      Thresholding done  
-----

[ 06/04/20 13:49:31 ]      Despeckle  
Type: Remove white speckles (3D space)  
Volume : less than 10 voxels  
Apply to: Image  
263496 speckles removed  
[ 06/04/20 13:49:59 ]      Despeckle done  
-----

[ 06/04/20 13:49:59 ]      Despeckle  
Type: Remove black speckles (3D space)  
Volume : less than 10 voxels  
Apply to: Image  
2191 speckles removed  
[ 06/04/20 13:52:53 ]      Despeckle done  
-----

[ 06/04/20 13:52:53 ]      Bitwise operations  
<Image> = <Image> AND <Region of Interest>  
[ 06/04/20 13:52:56 ]      Bitwise operations done  
-----

[ 06/04/20 13:52:56 ]      3D analysis  
Destination folder of images of Structure separation: F:\DATA\Tarik\P-3\P-3\_Rec\TBSP  
Date and time,04.06.2020 13:52  
Operator identity,oem  
Computer name,T7610  
Computation time,00:06:31  
Dataset,p-3\_rec  
Location,F:\DATA\Tarik\P-3\P-3\_Rec\  
-----

MORPHOMETRY RESULTS  
-----

Description,Abbreviation,Value,Unit  
 Number of layers,,271  
 Lower vertical position,,1.95009555,mm  
 Upper vertical position,,2.76013525,mm  
 Pixel size,,3.00014701,um  
 Lower grey threshold,,33  
 Upper grey threshold,,255  
 Total VOI volume,TV,13.33715287,mm<sup>3</sup>  
 Object volume,Obj.V,2.38846422,mm<sup>3</sup>  
 Percent object volume,Obj.V/TV,17.90835152,%  
 Total VOI surface,TS,45.94876940,mm<sup>2</sup>  
 Object surface,Obj.S,661.93564114,mm<sup>2</sup>  
 Intersection surface,i.S,3.81877957,mm<sup>2</sup>  
 Object surface / volume ratio,Obj.S/Obj.V,277.13860464,1/mm  
 Object surface density,Obj.S/TV,49.63095552,1/mm  
 Centroid (x),Crd.X,0.01818211,mm  
 Centroid (y),Crd.Y,0.05840082,mm  
 Centroid (z),Crd.Z,2.37937522,mm  
 Structure separation,St.Sp,0.07336386,mm  
 Number of objects,Obj.N,6099,  
 Number of closed pores,Po.N(cl),99,  
 Volume of closed pores,Po.V(cl),0.00004739,mm<sup>3</sup>  
 Surface of closed pores,Po.S(cl),0.03927785,mm<sup>2</sup>  
 Closed porosity (percent),Po(cl),0.00198421,%  
 Volume of open pore space,Po.V(op),10.94864126,mm<sup>3</sup>  
 Open porosity (percent),Po(op),82.09129313,%  
 Total volume of pore space,Po.V(tot),10.94868866,mm<sup>3</sup>  
 Total porosity (percent),Po(tot),82.09164848,%  
 Euler number,Eu.N,-269819,  
 Connectivity,Conn,276017,  
 Connectivity density,Conn.Dn,0.00055885,1/mm<sup>3</sup>

Structure separation distribution,St.Sp  
 Range,Mid-range,Volume,Percent volume in range  
 mm,mm,mm<sup>3</sup>,%  
 0.00300 - <0.00900,0.00600,0.09766758,0.8944  
 0.00900 - <0.01500,0.01200,0.78946663,7.2300  
 0.01500 - <0.02100,0.01800,0.88874541,8.1392  
 0.02100 - <0.02700,0.02400,0.79349884,7.2669  
 0.02700 - <0.03300,0.03000,0.58001059,5.3118  
 0.03300 - <0.03900,0.03600,0.46965906,4.3012  
 0.03900 - <0.04500,0.04200,0.52709880,4.8272  
 0.04500 - <0.05100,0.04800,0.48959096,4.4837  
 0.05100 - <0.05700,0.05400,0.44578261,4.0825  
 0.05700 - <0.06300,0.06000,0.44574731,4.0822  
 0.06300 - <0.06900,0.06600,0.44686444,4.0924  
 0.06900 - <0.07500,0.07200,0.41107670,3.7647  
 0.07500 - <0.08100,0.07800,0.41595300,3.8093  
 0.08100 - <0.08700,0.08400,0.40088551,3.6713  
 0.08700 - <0.09300,0.09000,0.36492052,3.3420  
 0.09300 - <0.09900,0.09600,0.32482899,2.9748  
 0.09900 - <0.10501,0.10200,0.32214126,2.9502  
 0.10501 - <0.11101,0.10801,0.28320507,2.5936  
 0.11101 - <0.11701,0.11401,0.28179449,2.5807  
 0.11701 - <0.12301,0.12001,0.23948416,2.1932  
 0.12301 - <0.12901,0.12601,0.23437747,2.1465  
 0.12901 - <0.13501,0.13201,0.20078801,1.8388

0.13501 - <0.14101,0.13801,0.16221500,1.4856  
0.14101 - <0.14701,0.14401,0.15898052,1.4560  
0.14701 - <0.15301,0.15001,0.14321474,1.3116  
0.15301 - <0.15901,0.15601,0.13627572,1.2480  
0.15901 - <0.16501,0.16201,0.11661005,1.0679  
0.16501 - <0.17101,0.16801,0.10130639,0.9278  
0.17101 - <0.17701,0.17401,0.10433286,0.9555  
0.17701 - <0.18301,0.18001,0.09237521,0.8460  
0.18301 - <0.18901,0.18601,0.06883277,0.6304  
0.18901 - <0.19501,0.19201,0.06875108,0.6296  
0.19501 - <0.20101,0.19801,0.03816946,0.3496  
0.20101 - <0.20701,0.20401,0.04113677,0.3767  
0.20701 - <0.21301,0.21001,0.03582911,0.3281  
0.21301 - <0.21901,0.21601,0.04477328,0.4100  
0.21901 - <0.22501,0.22201,0.03434446,0.3145  
0.22501 - <0.23101,0.22801,0.03539162,0.3241  
0.23101 - <0.23701,0.23401,0.02491232,0.2281  
0.23701 - <0.24301,0.24001,0.01056141,0.0967  
0.24301 - <0.24901,0.24601,0.00184902,0.0169  
0.24901 - <0.25501,0.25201,0.00177735,0.0163  
0.25501 - <0.26101,0.25801,0.00199746,0.0183  
0.26101 - <0.26701,0.26401,0.00218157,0.0200  
0.26701 - <0.27301,0.27001,0.01345062,0.1232  
0.27301 - <0.27901,0.27601,0.00104349,0.0096  
0.27901 - <0.28501,0.28201,0.00126765,0.0116  
0.28501 - <0.29101,0.28801,0.00142465,0.0130  
0.29101 - <0.29701,0.29401,0.00253697,0.0232  
0.29701 - <0.30301,0.30001,0.00205446,0.0188  
0.30301 - <0.30902,0.30601,0.00237802,0.0218  
0.30902 - <0.31502,0.31202,0.01573975,0.1441

Standard deviation of structure separation,SD(St.Sp),0.05311607,mm

3D-analysis summary

Dataset,Date and time,Pixel size,Unit,Lower grey threshold,Upper grey threshold>Total VOI volume,Object volume,Percent object volume>Total VOI surface,Object surface,Intersection surface,Object surface / volume ratio,Object surface density,Structure thickness,Structure separation,Structure linear density,Surface convexity index,Centroid (x),Centroid (y),Centroid (z),Structure model index,Degree of anisotropy,Eigenvalue 1,Eigenvalue 2,Eigenvalue 3,Fractal dimension,Number of objects,Number of closed pores,Volume of closed pores,Surface of closed pores,Closed porosity (percent),Volume of open pore space,Open porosity (percent),Total volume of pore space>Total porosity (percent),Euler number,Connectivity,Connectivity density,Standard deviation of structure thickness,Standard deviation of structure separation,Moment of inertia (x),Moment of inertia (y),Moment of inertia (z),Polar moment of inertia,Radius of gyration (x),Radius of gyration (y),Radius of gyration (z),Polar radius of gyration,Product of inertia (xy),Product of inertia (xz),Product of inertia (yz),  
,,,U,,,TV,Obj.V,Obj.V/TV,TS,Obj.S,i.S,Obj.S/Obj.V,Obj.S/TV,St.Th,St.Sp,St.Li.Dn,SCv.I,Crd.X,Crd.Y,Crd.Z, SMI,DA,,,,FD,Obj.N,Po.N(cl),Po.V(cl),Po.S(cl),Po(cl),Po.V(op),Po(op),Po.V(tot),Po(tot),Eu.N,Conn,Conn.Dn, SD(St.Th),SD(St.Sp),MMI(x),MMI(y),MMI(z),MMI(polar),Gr.R(x),Gr.R(y),Gr.R(z),Gr.R(polar),Pr.In(xy),Pr.I n(xz),Pr.In(yz),  
,,um,,,,U^3,U^3,%,U^2,U^2,U^2,1/U,1/U,U,U,1/U,1/U,U,U,,,,,,U^3,U^2,%,U^3,%,U^3,%,,,,1/U^3,U,U,U^ 5,U^5,U^5,U^5,U,U,U,U,U^5,U^5,U^5,

F:\DATA\Tarik\P-3\P-3\_Rec\p-3\_rec,04.06.2020

13:52,3.00014701,mm,33,255,13.33715287,2.38846422,17.90835152,45.94876940,661.93564114,3.81877957, 277.13860464,49.63095552,,0.07336386,,0.01818211,0.05840082,2.37937522,,,,,,6099,99,0.00004739,0.0392 7785,0.00198421,10.94864126,82.09129313,10.94868866,82.09164848,- 269819,276017,0.00055885,,0.05311607,,,,,,

<<<<< End of task (ac7b0d9d-b6bd-4490-9df1-2d1e4648a655) >>>>>

## Appendix 9

<<<<< Begin of workflow >>>>>

CT Analyser, Version: 1.18.4.0  
Dataset name, F:\DATA\Tarik\P-4\P-4\_Rec\P-4\_rec00000923.bmp  
File postfix length, 8  
File type, BMP  
Image size (W/H), 2452, 2452  
Total number of images, 639  
Total Z-position range, 584, 1222  
Number of images inside VOI, 341  
Z-position range of VOI, 630, 970  
Z spacing, 1  
Pixel size (um), 3.000120

-----  
[ 06/04/20 11:25:25 ]      Thresholding  
Mode, Global  
Lower grey threshold, 33  
Upper grey threshold, 255  
[ 06/04/20 11:25:32 ]      Thresholding done

-----  
[ 06/04/20 11:25:35 ]      Despeckle  
Type: Remove white speckles (3D space)  
Volume : less than 10 voxels  
Apply to: Image  
258261 speckles removed  
[ 06/04/20 11:26:04 ]      Despeckle done

-----  
[ 06/04/20 11:26:05 ]      Despeckle  
Type: Remove black speckles (3D space)  
Volume : less than 10 voxels  
Apply to: Image  
1300 speckles removed  
[ 06/04/20 11:28:47 ]      Despeckle done

-----  
[ 06/04/20 11:28:47 ]      Bitwise operations  
<Image> = <Image> AND <Region of Interest>  
[ 06/04/20 11:28:49 ]      Bitwise operations done

-----  
[ 06/04/20 11:28:49 ]      3D analysis  
Destination folder of images of Structure separation: F:\DATA\Tarik\P-4\P-4\_Rec\TBSP  
Date and time,04.06.2020 11:28  
Operator identity,oem  
Computer name,T7610  
Computation time,00:07:16  
Dataset,p-4\_rec  
Location,F:\DATA\Tarik\P-4\P-4\_Rec\

### MORPHOMETRY RESULTS

-----  
Description,Abbreviation,Value,Unit  
Number of layers,,341  
Lower vertical position,,1.89007560,mm  
Upper vertical position,,2.91011640,mm  
Pixel size,,3.00012000,um  
Lower grey threshold,,33

Upper grey threshold,,255

Total VOI volume,TV,16.78173019,mm<sup>3</sup>  
Object volume,Obj.V,2.91788393,mm<sup>3</sup>  
Percent object volume,Obj.V/TV,17.38726517,%  
Total VOI surface,TS,49.34947632,mm<sup>2</sup>  
Object surface,Obj.S,670.30777904,mm<sup>2</sup>  
Intersection surface,i.S,3.57735881,mm<sup>2</sup>  
Object surface / volume ratio,Obj.S/Obj.V,229.72393540,1/mm  
Object surface density,Obj.S/TV,39.94270980,1/mm  
Centroid (x),Crd.X,0.13502830,mm  
Centroid (y),Crd.Y,0.00622892,mm  
Centroid (z),Crd.Z,2.41662020,mm  
Structure separation,St.Sp,0.06759425,mm  
Number of objects,Obj.N,10425,  
Number of closed pores,Po.N(cl),21,  
Volume of closed pores,Po.V(cl),0.00000870,mm<sup>3</sup>  
Surface of closed pores,Po.S(cl),0.00723877,mm<sup>2</sup>  
Closed porosity (percent),Po(cl),0.00029801,%  
Volume of open pore space,Po.V(op),13.86383757,mm<sup>3</sup>  
Open porosity (percent),Po(op),82.61268301,%  
Total volume of pore space,Po.V(tot),13.86384626,mm<sup>3</sup>  
Total porosity (percent),Po(tot),82.61273483,%  
Euler number,Eu.N,-131231,  
Connectivity,Conn,141677,  
Connectivity density,Conn.Dn,0.00022797,1/mm<sup>3</sup>

Structure separation distribution, St. Sp  
Range, Mid-range, Volume, Percent volume in range  
mm, mm, mm<sup>3</sup>, %

0.00300 - <0.00900, 0.00600, 0.03372802, 0.2439  
0.00900 - <0.01500,0.01200,0.29331276,2.1209  
0.01500 - <0.02100,0.01800,0.56181092,4.0624  
0.02100 - <0.02700,0.02400,1.00922175,7.2976  
0.02700 - <0.03300,0.03000,1.05684504,7.6420  
0.03300 - <0.03900,0.03600,0.92279599,6.6727  
0.03900 - <0.04500,0.04200,1.05657703,7.6400  
0.04500 - <0.05100,0.04800,0.96590469,6.9844  
0.05100 - <0.05700,0.05400,0.85395609,6.1749  
0.05700 - <0.06300,0.06000,0.80625084,5.8299  
0.06300 - <0.06900,0.06600,0.75622850,5.4682  
0.06900 - <0.07500,0.07200,0.64287160,4.6486  
0.07500 - <0.08100,0.07800,0.61428432,4.4418  
0.08100 - <0.08700,0.08400,0.55047769,3.9805  
0.08700 - <0.09300,0.09000,0.46477370,3.3607  
0.09300 - <0.09900,0.09600,0.42810802,3.0956  
0.09900 - <0.10500,0.10200,0.37379576,2.7029  
0.10500 - <0.11100,0.10800,0.35607577,2.5748  
0.11100 - <0.11700,0.11400,0.32166749,2.3260  
0.11700 - <0.12300,0.12000,0.27978389,2.0231  
0.12300 - <0.12901,0.12601,0.23307661,1.6854  
0.12901 - <0.13501,0.13201,0.19590648,1.4166  
0.13501 - <0.14101,0.13801,0.17559667,1.2697  
0.14101 - <0.14701,0.14401,0.14962663,1.0819  
0.14701 - <0.15301,0.15001,0.13212488,0.9554  
0.15301 - <0.15901,0.15601,0.09832776,0.7110  
0.15901 - <0.16501,0.16201,0.09267896,0.6702

0.16501 - <0.17101,0.16801,0.07045324,0.5094  
0.17101 - <0.17701,0.17401,0.07028366,0.5082  
0.17701 - <0.18301,0.18001,0.06818121,0.4930  
0.18301 - <0.18901,0.18601,0.04610919,0.3334  
0.18901 - <0.19501,0.19201,0.03940213,0.2849  
0.19501 - <0.20101,0.19801,0.03602248,0.2605  
0.20101 - <0.20701,0.20401,0.01573409,0.1138  
0.20701 - <0.21301,0.21001,0.02071986,0.1498  
0.21301 - <0.21901,0.21601,0.01233527,0.0892  
0.21901 - <0.22501,0.22201,0.02442513,0.1766  
Standard deviation of structure separation,SD(St.Sp),0.04074372,mm

### 3D-analysis summary

Dataset,Date and time,Pixel size,Unit,Lower grey threshold,Upper grey threshold>Total VOI volume,Object volume,Percent object volume>Total VOI surface,Object surface,Intersection surface,Object surface / volume ratio,Object surface density,Structure thickness,Structure separation,Structure linear density,Surface convexity index,Centroid (x),Centroid (y),Centroid (z),Structure model index,Degree of anisotropy,Eigenvalue 1,Eigenvalue 2,Eigenvalue 3,Fractal dimension,Number of objects,Number of closed pores,Volume of closed pores,Surface of closed pores,Closed porosity (percent),Volume of open pore space,Open porosity (percent),Total volume of pore space>Total porosity (percent),Euler number,Connectivity,Connectivity density,Standard deviation of structure thickness,Standard deviation of structure separation,Moment of inertia (x),Moment of inertia (y),Moment of inertia (z),Polar moment of inertia,Radius of gyration (x),Radius of gyration (y),Radius of gyration (z),Polar radius of gyration,Product of inertia (xy),Product of inertia (xz),Product of inertia (yz),  
,,,U,,,TV,Obj.V,Obj.V/TV,TS,Obj.S,i.S,Obj.S/Obj.V,Obj.S/TV,St.Th,St.Sp,St.Li.Dn,SCv.I,Crd.X,Crd.Y,Crd.Z, SML,DA,,,,,FD,Obj.N,Po.N(cl),Po.V(cl),Po.S(cl),Po(cl),Po.V(op),Po(op),Po.V(tot),Po(tot),Eu.N,Conn,Conn.Dn, SD(St.Th),SD(St.Sp),MMI(x),MMI(y),MMI(z),MMI(polar),Gr.R(x),Gr.R(y),Gr.R(z),Gr.R(polar),Pr.In(xy),Pr.I n(xz),Pr.In(yz),  
,,um,,,U^3,U^3,%,U^2,U^2,U^2,1/U,1/U,U,U,1/U,1/U,U,U,U,,,,,,,U^3,U^2,%,U^3,%,U^3,%,,,,1/U^3,U,U,U^ 5,U^5,U^5,U^5,U,U,U,U,U^5,U^5,U^5,

F:\DATA\Tarik\P-4\P-4\_Rec\p-4\_rec,04.06.2020  
11:28,3.00012000,mm,33,255,16.78173019,2.91788393,17.38726517,49.34947632,670.30777904,3.57735881, 229.72393540,39.94270980,,0.06759425,,,0.13502830,0.00622892,2.41662020,,,,,,10425.21,0.00000870,0.007 23877,0.00029801,13.86383757,82.61268301,13.86384626,82.61273483,- 131231,141677,0.00022797,,0.04074372,,,,,,

<<<<< End of task (7fd156c2-c6b8-4879-ba36-1196ea18b638) >>>>>

## Appendix 10

<<<<< Begin of workflow >>>>>

CT Analyser, Version: 1.18.4.0  
Dataset name, F:\DATA\Tarik\P-5\P-5\_Rec\P-5\_rec00000843.bmp  
File postfix length, 8  
File type, BMP  
Image size (W/H), 2452, 2452  
Total number of images, 541  
Total Z-position range, 575, 1115  
Number of images inside VOI, 301  
Z-position range of VOI, 660, 960  
Z spacing, 1  
Pixel size (um), 3.000120

-----  
[ 06/04/20 09:04:08 ]      Thresholding  
Mode, Global  
Lower grey threshold, 33  
Upper grey threshold, 255  
[ 06/04/20 09:04:15 ]      Thresholding done  
-----

[ 06/04/20 09:04:16 ]      Despeckle  
Type: Remove white speckles (3D space)  
Volume : less than 10 voxels  
Apply to: Image  
281153 speckles removed  
[ 06/04/20 09:04:48 ]      Despeckle done  
-----

[ 06/04/20 09:04:48 ]      Despeckle  
Type: Remove black speckles (3D space)  
Volume : less than 10 voxels  
Apply to: Image  
1758 speckles removed  
[ 06/04/20 09:07:26 ]      Despeckle done  
-----

[ 06/04/20 09:07:26 ]      Bitwise operations  
<Image> = <Image> AND <Region of Interest>  
[ 06/04/20 09:07:28 ]      Bitwise operations done  
-----

[ 06/04/20 09:07:28 ]      3D analysis  
-----

Destination folder of images of Structure separation: F:\DATA\Tarik\P-5\P-5\_Rec\TBSP

Date and time,04.06.2020 09:07  
Operator identity,oem  
Computer name,T7610  
Computation time,00:06:39  
Dataset,p-5\_rec  
Location,F:\DATA\Tarik\P-5\P-5\_Rec\  
-----

#### MORPHOMETRY RESULTS

-----

Description,Abbreviation, Value,Unit

Number of layers,,301  
Lower vertical position,,1.98007920,mm  
Upper vertical position,,2.88011520,mm  
Pixel size,,3.00012000,um  
Lower grey threshold,,33  
Upper grey threshold,,255  
  
Total VOI volume,TV,14.81319452,mm<sup>3</sup>  
Object volume,Obj.V,2.62724637,mm<sup>3</sup>  
Percent object volume,Obj.V/TV,17.73585278,%  
Total VOI surface,TS,47.40574259,mm<sup>2</sup>  
Object surface,Obj.S,636.80495090,mm<sup>2</sup>  
Intersection surface,i.S,4.50329846,mm<sup>2</sup>  
Object surface / volume ratio,Obj.S/Obj.V,242.38493872,1/mm  
Object surface density,Obj.S/TV,42.98903590,1/mm  
Centroid (x),Crd.X,0.06650615,mm  
Centroid (y),Crd.Y,-0.05042121,mm

Centroid (z),Crd.Z,2.44939039,mm  
Structure separation,St.Sp,0.06295957,mm  
Number of objects,Obj.N,7955,  
Number of closed pores,Po.N(cl),124,  
Volume of closed pores,Po.V(cl),0.00006574,mm<sup>3</sup>  
Surface of closed pores,Po.S(cl),0.05034633,mm<sup>2</sup>  
Closed porosity (percent),Po(cl),0.00250200,%  
Volume of open pore space,Po.V(op),12.18588241,mm<sup>3</sup>  
Open porosity (percent),Po(op),82.26370345,%  
Total volume of pore space,Po.V(tot),12.18594814,mm<sup>3</sup>  
Total porosity (percent),Po(tot),82.26414722,%  
Euler number,Eu.N,-123992,  
Connectivity,Conn,132071,  
Connectivity density,Conn.Dn,0.00024075,1/mm<sup>3</sup>

Structure separation distribution,St.Sp

Range,Mid-range,Volume,Percent volume in range  
mm,mm,mm<sup>3</sup>,%

0.00300 - <0.00900,0.00600,0.03329826,0.2740  
0.00900 - <0.01500,0.01200,0.29976648,2.4667  
0.01500 - <0.02100,0.01800,0.64081163,5.2731  
0.02100 - <0.02700,0.02400,1.07330419,8.8320  
0.02700 - <0.03300,0.03000,1.03397589,8.5084  
0.03300 - <0.03900,0.03600,0.86429919,7.1122  
0.03900 - <0.04500,0.04200,0.94373465,7.7658  
0.04500 - <0.05100,0.04800,0.83392746,6.8623  
0.05100 - <0.05700,0.05400,0.73340776,6.0351  
0.05700 - <0.06300,0.06000,0.67759474,5.5758  
0.06300 - <0.06900,0.06600,0.64086720,5.2736  
0.06900 - <0.07500,0.07200,0.53501047,4.4025  
0.07500 - <0.08100,0.07800,0.52502994,4.3204  
0.08100 - <0.08700,0.08400,0.46565970,3.8318  
0.08700 - <0.09300,0.09000,0.38520930,3.1698  
0.09300 - <0.09900,0.09600,0.35564420,2.9265  
0.09900 - <0.10500,0.10200,0.34462205,2.8358  
0.10500 - <0.11100,0.10800,0.27880162,2.2942  
0.11100 - <0.11700,0.11400,0.23693666,1.9497  
0.11700 - <0.12300,0.12000,0.22251764,1.8311  
0.12300 - <0.12901,0.12601,0.18963709,1.5605  
0.12901 - <0.13501,0.13201,0.13947873,1.1477  
0.13501 - <0.14101,0.13801,0.14434058,1.1878  
0.14101 - <0.14701,0.14401,0.10377669,0.8540  
0.14701 - <0.15301,0.15001,0.09878398,0.8129  
0.15301 - <0.15901,0.15601,0.06314476,0.5196  
0.15901 - <0.16501,0.16201,0.06768891,0.5570  
0.16501 - <0.17101,0.16801,0.04315771,0.3551  
0.17101 - <0.17701,0.17401,0.06187371,0.5091  
0.17701 - <0.18301,0.18001,0.03177417,0.2615  
0.18301 - <0.18901,0.18601,0.02675994,0.2202  
0.18901 - <0.19501,0.19201,0.01275355,0.1049  
0.19501 - <0.20101,0.19801,0.01379190,0.1135  
0.20101 - <0.20701,0.20401,0.00357499,0.0294  
0.20701 - <0.21301,0.21001,0.01540821,0.1268  
0.21301 - <0.21901,0.21601,0.01202522,0.0990  
Standard deviation of structure separation,SD(St.Sp),0.03827974,mm

### 3D-analysis summary

Dataset, Date and time, Pixel size, Unit, Lower grey threshold, Upper grey threshold, Total VOI volume, Object volume, Percent object volume, Total VOI surface, Object surface, Intersection surface, Object surface / volume ratio, Object surface density, Structure thickness, Structure separation, Structure linear density, Surface convexity index, Centroid (x), Centroid (y), Centroid (z), Structure model index, Degree of anisotropy, Eigenvalue 1, Eigenvalue 2, Eigenvalue 3, Fractal dimension, Number of objects, Number of closed pores, Volume of closed pores, Surface of closed pores, Closed porosity (percent), Volume of open pore space, Open porosity (percent), Total volume of pore space, Total porosity (percent), Euler number, Connectivity, Connectivity density, Standard deviation of structure thickness, Standard deviation of structure separation, Moment of inertia (x), Moment of inertia (y), Moment of inertia (z), Polar moment of inertia, Radius of gyration (x), Radius of gyration (y), Radius of gyration (z), Polar radius of gyration, Product of inertia (xy), Product of inertia (xz), Product of inertia (yz),  
,,U,,,TV,Obj.V,Obj.V/TV,TS,Obj.S,i.S,Obj.S/Obj.V,Obj.S/TV,St.Th,St.Sp,St.Li.Dn,SCv.I,Crd.X,Crd.Y,Crd.Z, SMI,DA,,,FD,Obj.N,Po.N(cl),Po.V(cl),Po.S(cl),Po(cl),Po.V(op),Po(op),Po.V(tot),Po(tot),Eu.N,Conn,Conn.Dn, SD(St.Th),SD(St.Sp),MMI(x),MMI(y),MMI(z),MMI(polar),Gr.R(x),Gr.R(y),Gr.R(z),Gr.R(polar),Pr.In(xy),Pr.In(xz),Pr.In(yz),  
,,um,,,U^3,U^3,% ,U^2,U^2,U^2,1/U,1/U,U,U,1/U,1/U,U,U,U,,,,,,,U^3,U^2,% ,U^3,% ,U^3,% ,,,,1/U^3,U,U,U^5,U^5,U^5,U^5,U,U,U,U,U^5,U^5,U^5,

F:\DATA\Tarik\P-5\P-5\_Rec\p-5\_rec,04.06.2020  
09:07,3.00012000,mm,33,255,14.81319452,2.62724637,17.73585278,47.40574259,636.80495090,4.50329846, 242.38493872,42.98903590,,0.06295957,,0.06650615,-  
0.05042121,2.44939039,,,,,7955,124,0.00006574,0.05034633,0.00250200,12.18588241,82.26370345,12.1859 4814,82.26414722,-123992,132071,0.00024075,,0.03827974,,,,,,

<<<<< End of task (076f25ff-745b-4d3a-b7dd-442f67c94018) >>>>>

## Appendix 11

<<<<< Begin of workflow >>>>>

CT Analyser, Version: 1.18.4.0  
Dataset name, F:\DATA\Tarik\P-6\P-6\_Rec\P-6\_rec00000945.bmp  
File postfix length, 8  
File type, BMP  
Image size (W/H), 2452, 2452  
Total number of images, 791  
Total Z-position range, 582, 1372  
Number of images inside VOI, 361  
Z-position range of VOI, 650, 1010  
Z spacing, 1  
Pixel size (um), 3.000120

-----  
[ 06/03/20 13:17:10 ]      Thresholding  
Mode, Global  
Lower grey threshold, 33  
Upper grey threshold, 255  
[ 06/03/20 13:17:18 ]      Thresholding done  
-----

[ 06/03/20 13:17:19 ]      Despeckle  
Type: Remove white speckles (3D space)  
Volume : less than 10 voxels  
Apply to: Image  
266842 speckles removed  
[ 06/03/20 13:17:56 ]      Despeckle done

-----  
[ 06/03/20 13:17:56 ] Despeckle  
Type: Remove black speckles (3D space)  
Volume : less than 10 voxels  
Apply to: Image  
2886 speckles removed  
[ 06/03/20 13:21:02 ] Despeckle done  
-----

[ 06/03/20 13:21:03 ] Bitwise operations  
<Image> = <Image> AND <Region of Interest>  
[ 06/03/20 13:21:05 ] Bitwise operations done  
-----

[ 06/03/20 13:21:05 ] 3D analysis  
-----

Destination folder of images of Structure separation: F:\DATA\Tarik\P-6\P-6\_Rec\TBSP

Date and time,03.06.2020 13:21  
Operator identity,oem  
Computer name,T7610  
Computation time,00:10:03  
Dataset,p-6\_rec  
Location,F:\DATA\Tarik\P-6\P-6\_Rec\  
-----

#### MORPHOMETRY RESULTS

-----  
Description,Abbreviation,Value,Unit

Number of layers,,361  
Lower vertical position,,1.95007800,mm  
Upper vertical position,,3.03012120,mm  
Pixel size,,3.00012000,um  
Lower grey threshold,,33  
Upper grey threshold,,255  
  
Total VOI volume,TV,17.76599664,mm<sup>3</sup>  
Object volume,Obj.V,3.19554471,mm<sup>3</sup>  
Percent object volume,Obj.V/TV,17.98685868,%  
Total VOI surface,TS,52.78377983,mm<sup>2</sup>  
Object surface,Obj.S,612.91716678,mm<sup>2</sup>  
Intersection surface,i.S,5.49796572,mm<sup>2</sup>  
Object surface / volume ratio,Obj.S/Obj.V,191.80365877,1/mm  
Object surface density,Obj.S/TV,34.49945305,1/mm  
Centroid (x),Crd.X,0.11110951,mm  
Centroid (y),Crd.Y,0.07578002,mm  
Centroid (z),Crd.Z,2.52416854,mm  
Structure separation,St.Sp,0.09631893,mm  
Number of objects,Obj.N,17802,  
Number of closed pores,Po.N(cl),175,  
Volume of closed pores,Po.V(cl),0.00008345,mm<sup>3</sup>  
Surface of closed pores,Po.S(cl),0.06718609,mm<sup>2</sup>  
Closed porosity (percent),Po(cl),0.00261127,%  
Volume of open pore space,Po.V(op),14.57036848,mm<sup>3</sup>  
Open porosity (percent),Po(op),82.01267162,%  
Total volume of pore space,Po.V(tot),14.57045193,mm<sup>3</sup>  
Total porosity (percent),Po(tot),82.01314132,%  
Euler number,Eu.N,-95331,  
Connectivity,Conn,113308,

Connectivity density,Conn.Dn,0.00017222,1/mm<sup>3</sup>

Structure separation distribution,St.Sp

Range,Mid-range,Volume,Percent volume in range  
mm,mm,mm<sup>3</sup>,%

0.00300 - <0.00900,0.00600,0.04859060,0.3341  
0.00900 - <0.01500,0.01200,0.34328763,2.3601  
0.01500 - <0.02100,0.01800,0.55908440,3.8436  
0.02100 - <0.02700,0.02400,0.86475217,5.9451  
0.02700 - <0.03300,0.03000,0.82623316,5.6803  
0.03300 - <0.03900,0.03600,0.69598419,4.7848  
0.03900 - <0.04500,0.04200,0.76455354,5.2562  
0.04500 - <0.05100,0.04800,0.67528407,4.6425  
0.05100 - <0.05700,0.05400,0.59928183,4.1200  
0.05700 - <0.06300,0.06000,0.56308577,3.8711  
0.06300 - <0.06900,0.06600,0.54377246,3.7384  
0.06900 - <0.07500,0.07200,0.47358115,3.2558  
0.07500 - <0.08100,0.07800,0.47835411,3.2886  
0.08100 - <0.08700,0.08400,0.44836429,3.0824  
0.08700 - <0.09300,0.09000,0.39963680,2.7475  
0.09300 - <0.09900,0.09600,0.38811657,2.6683  
0.09900 - <0.10500,0.10200,0.39076087,2.6864  
0.10500 - <0.11100,0.10800,0.34845829,2.3956  
0.11100 - <0.11700,0.11400,0.35962000,2.4723  
0.11700 - <0.12300,0.12000,0.34452011,2.3685  
0.12300 - <0.12901,0.12601,0.33176780,2.2809  
0.12901 - <0.13501,0.13201,0.28701955,1.9732  
0.13501 - <0.14101,0.13801,0.29839855,2.0515  
0.14101 - <0.14701,0.14401,0.26405089,1.8153  
0.14701 - <0.15301,0.15001,0.25521543,1.7546  
0.15301 - <0.15901,0.15601,0.26573873,1.8269  
0.15901 - <0.16501,0.16201,0.26437690,1.8176  
0.16501 - <0.17101,0.16801,0.24894957,1.7115  
0.17101 - <0.17701,0.17401,0.23471165,1.6136  
0.17701 - <0.18301,0.18001,0.17917328,1.2318  
0.18301 - <0.18901,0.18601,0.21024177,1.4454  
0.18901 - <0.19501,0.19201,0.17402846,1.1964  
0.19501 - <0.20101,0.19801,0.17114613,1.1766  
0.20101 - <0.20701,0.20401,0.13747763,0.9451  
0.20701 - <0.21301,0.21001,0.13843948,0.9518  
0.21301 - <0.21901,0.21601,0.10358810,0.7122  
0.21901 - <0.22501,0.22201,0.11212310,0.7708  
0.22501 - <0.23101,0.22801,0.10011738,0.6883  
0.23101 - <0.23701,0.23401,0.07496356,0.5154  
0.23701 - <0.24301,0.24001,0.06801987,0.4676  
0.24301 - <0.24901,0.24601,0.07632261,0.5247  
0.24901 - <0.25501,0.25201,0.04684290,0.3220  
0.25501 - <0.26101,0.25801,0.05036509,0.3463  
0.26101 - <0.26701,0.26401,0.02981541,0.2050  
0.26701 - <0.27301,0.27001,0.02055497,0.1413  
0.27301 - <0.27901,0.27601,0.03367488,0.2315  
0.27901 - <0.28501,0.28201,0.05509344,0.3788  
0.28501 - <0.29101,0.28801,0.01707504,0.1174  
0.29101 - <0.29701,0.29401,0.01274818,0.0876  
0.29701 - <0.30301,0.30001,0.03932290,0.2703  
0.30301 - <0.30901,0.30601,0.02932128,0.2016  
0.30901 - <0.31501,0.31201,0.02183582,0.1501

0.31501 - <0.32101,0.31801,0.03810352,0.2620  
0.32101 - <0.32701,0.32401,0.01576600,0.1084  
0.32701 - <0.33301,0.33001,0.00119454,0.0082  
0.33301 - <0.33901,0.33601,0.02280958,0.1568  
Standard deviation of structure separation,SD(St.Sp),0.06763297,mm

### 3D-analysis summary

Dataset,Date and time,Pixel size,Unit,Lower grey threshold,Upper grey threshold>Total VOI volume,Object volume,Percent object volume>Total VOI surface,Object surface,Intersection surface,Object surface / volume ratio,Object surface density,Structure thickness,Structure separation,Structure linear density,Surface convexity index,Centroid (x),Centroid (y),Centroid (z),Structure model index,Degree of anisotropy,Eigenvalue 1,Eigenvalue 2,Eigenvalue 3,Fractal dimension,Number of objects,Number of closed pores,Volume of closed pores,Surface of closed pores,Closed porosity (percent),Volume of open pore space,Open porosity (percent),Total volume of pore space>Total porosity (percent),Euler number,Connectivity,Connectivity density,Standard deviation of structure thickness,Standard deviation of structure separation,Moment of inertia (x),Moment of inertia (y),Moment of inertia (z),Polar moment of inertia,Radius of gyration (x),Radius of gyration (y),Radius of gyration (z),Polar radius of gyration,Product of inertia (xy),Product of inertia (xz),Product of inertia (yz),  
,,U,,,TV,Obj.V,Obj.V/TV,TS,Obj.S,i.S,Obj.S/Obj.V,Obj.S/TV,St.Th,St.Sp,St.Li.Dn,SCv.I,Crd.X,Crd.Y,Crd.Z, SMI,DA,,,FD,Obj.N,Po.N(cl),Po.V(cl),Po.S(cl),Po(cl),Po.V(op),Po(op),Po.V(tot),Po(tot),Eu.N,Conn,Conn.Dn, SD(St.Th),SD(St.Sp),MMI(x),MMI(y),MMI(z),MMI(polar),Gr.R(x),Gr.R(y),Gr.R(z),Gr.R(polar),Pr.In(xy),Pr.I n(xz),Pr.In(yz),  
,,um,,,U^3,U^3,%U^2,U^2,U^2,1/U,1/U,U,U,1/U,1/U,U,U,U,,,,,,,U^3,U^2,%U^3,%U^3,%,,,1/U^3,U,U,U^ 5,U^5,U^5,U^5,U,U,U,U,U^5,U^5,U^5,

F:\DATA\Tarik\P-6\P-6\_Rec\p-6\_rec,03.06.2020  
13:21,3.00012000,mm,33,255,17.76599664,3.19554471,17.98685868,52.78377983,612.91716678,5.49796572, 191.80365877,34.49945305,,0.09631893,,,0.11110951,0.07578002,2.52416854,,,,,,17802,175,0.00008345,0.06 718609,0.00261127,14.57036848,82.01267162,14.57045193,82.01314132,- 95331,113308,0.00017222,,0.06763297,,,,,,

<<<<< End of task (bd0efc3c-513c-4a85-992f-eb7bf3994651) >>>>>

## Appendix 12

<<<<< Begin of workflow >>>>>

CT Analyser, Version: 1.18.4.0  
Dataset name, F:\DATA\Tarik\test1\test1\_Rec\test1\_rec00001043.bmp  
File postfix length, 8  
File type, BMP  
Image size (W/H), 2452, 2452  
Total number of images, 895  
Total Z-position range, 559, 1453  
Number of images inside VOI, 361  
Z-position range of VOI, 650, 1010  
Z spacing, 1  
Pixel size (um), 3.000120

-----  
[ 06/03/20 11:20:22 ]      Thresholding  
Mode, Global  
Lower grey threshold, 33  
Upper grey threshold, 255  
[ 06/03/20 11:20:33 ]      Thresholding done

-----  
[ 06/03/20 11:20:33 ] Despeckle  
Type: Remove white speckles (3D space)  
Volume : less than 10 voxels  
Apply to: Image  
456372 speckles removed  
[ 06/03/20 11:21:29 ] Despeckle done  
-----

[ 06/03/20 11:21:30 ] Despeckle  
Type: Remove black speckles (3D space)  
Volume : less than 10 voxels  
Apply to: Image  
2292 speckles removed  
[ 06/03/20 11:25:47 ] Despeckle done  
-----

[ 06/03/20 11:25:47 ] Bitwise operations  
<Image> = <Image> AND <Region of Interest>  
[ 06/03/20 11:25:50 ] Bitwise operations done  
-----

[ 06/03/20 11:25:50 ] 3D analysis  
-----

Destination folder of images of Structure separation: F:\DATA\Tarik\test1\test1\_Rec\TBSP

Date and time,03.06.2020 11:25  
Operator identity,oem  
Computer name,T7610  
Computation time,00:07:18  
Dataset,test1\_rec  
Location,F:\DATA\Tarik\test1\test1\_Rec\

#### MORPHOMETRY RESULTS

-----

Description,Abbreviation,Value,Unit

Number of layers,,361  
Lower vertical position,,1.95007800,mm  
Upper vertical position,,3.03012120,mm  
Pixel size,,3.00012000,um  
Lower grey threshold,,33  
Upper grey threshold,,255  
  
Total VOI volume,TV,17.76599803,mm<sup>3</sup>  
Object volume,Obj.V,4.16806427,mm<sup>3</sup>  
Percent object volume,Obj.V/TV,23.46090697,%  
Total VOI surface,TS,50.32134319,mm<sup>2</sup>  
Object surface,Obj.S,1037.16488620,mm<sup>2</sup>  
Intersection surface,i.S,6.40057773,mm<sup>2</sup>  
Object surface / volume ratio,Obj.S/Obj.V,248.83610688,1/mm  
Object surface density,Obj.S/TV,58.37920755,1/mm  
Centroid (x),Crd.X,0.02521433,mm  
Centroid (y),Crd.Y,0.21374499,mm  
Centroid (z),Crd.Z,2.54877554,mm  
Structure separation,St.Sp,0.05277577,mm  
Number of objects,Obj.N,14247,  
Number of closed pores,Po.N(cl),104,  
Volume of closed pores,Po.V(cl),0.00004561,mm<sup>3</sup>  
Surface of closed pores,Po.S(cl),0.03771759,mm<sup>2</sup>

Closed porosity (percent),Po(cl),0.00109425,%  
Volume of open pore space,Po.V(op),13.59788815,mm<sup>3</sup>  
Open porosity (percent),Po(op),76.53883630,%  
Total volume of pore space,Po.V(tot),13.59793376,mm<sup>3</sup>  
Total porosity (percent),Po(tot),76.53909303,%  
Euler number,Eu.N,-344407,  
Connectivity,Conn,358758,  
Connectivity density,Conn.Dn,0.00054529,1/mm<sup>3</sup>

Structure separation distribution,St.Sp

Range,Mid-range,Volume,Percent volume in range  
mm,mm,mm<sup>3</sup>,%

0.00300 - <0.00900,0.00600,0.08855696,0.6533  
0.00900 - <0.01500,0.01200,1.02828844,7.5863  
0.01500 - <0.02100,0.01800,1.64948094,12.1691  
0.02100 - <0.02700,0.02400,1.64246906,12.1174  
0.02700 - <0.03300,0.03000,1.21932130,8.9956  
0.03300 - <0.03900,0.03600,0.89937151,6.6352  
0.03900 - <0.04500,0.04200,0.92132177,6.7971  
0.04500 - <0.05100,0.04800,0.78481947,5.7901  
0.05100 - <0.05700,0.05400,0.66003812,4.8695  
0.05700 - <0.06300,0.06000,0.59399689,4.3822  
0.06300 - <0.06900,0.06600,0.55462344,4.0918  
0.06900 - <0.07500,0.07200,0.45674674,3.3697  
0.07500 - <0.08100,0.07800,0.42154370,3.1100  
0.08100 - <0.08700,0.08400,0.36603678,2.7005  
0.08700 - <0.09300,0.09000,0.29737170,2.1939  
0.09300 - <0.09900,0.09600,0.26785032,1.9761  
0.09900 - <0.10500,0.10200,0.25019174,1.8458  
0.10500 - <0.11100,0.10800,0.20846898,1.5380  
0.11100 - <0.11700,0.11400,0.19346374,1.4273  
0.11700 - <0.12300,0.12000,0.16786540,1.2384  
0.12300 - <0.12901,0.12601,0.12915247,0.9528  
0.12901 - <0.13501,0.13201,0.10515451,0.7758  
0.13501 - <0.14101,0.13801,0.09425864,0.6954  
0.14101 - <0.14701,0.14401,0.08110418,0.5984  
0.14701 - <0.15301,0.15001,0.06733512,0.4968  
0.15301 - <0.15901,0.15601,0.06078894,0.4485  
0.15901 - <0.16501,0.16201,0.03886655,0.2867  
0.16501 - <0.17101,0.16801,0.03945919,0.2911  
0.17101 - <0.17701,0.17401,0.05029902,0.3711  
0.17701 - <0.18301,0.18001,0.03759985,0.2774  
0.18301 - <0.18901,0.18601,0.03313160,0.2444  
0.18901 - <0.19501,0.19201,0.01953676,0.1441  
0.19501 - <0.20101,0.19801,0.01563868,0.1154  
0.20101 - <0.20701,0.20401,0.01471218,0.1085  
0.20701 - <0.21301,0.21001,0.01526820,0.1126  
0.21301 - <0.21901,0.21601,0.00776259,0.0573  
0.21901 - <0.22501,0.22201,0.02049268,0.1512  
0.22501 - <0.23101,0.22801,0.00339517,0.0250  
0.23101 - <0.23701,0.23401,0.01072091,0.0791  
0.23701 - <0.24301,0.24001,0.01933121,0.1426  
0.24301 - <0.24901,0.24601,0.00941519,0.0695  
0.24901 - <0.25501,0.25201,0.00936759,0.0691  
Standard deviation of structure separation,SD(St.Sp),0.04012633,mm

### 3D-analysis summary

Dataset, Date and time, Pixel size, Unit, Lower grey threshold, Upper grey threshold, Total VOI volume, Object volume, Percent object volume, Total VOI surface, Object surface, Intersection surface, Object surface / volume ratio, Object surface density, Structure thickness, Structure separation, Structure linear density, Surface convexity index, Centroid (x), Centroid (y), Centroid (z), Structure model index, Degree of anisotropy, Eigenvalue 1, Eigenvalue 2, Eigenvalue 3, Fractal dimension, Number of objects, Number of closed pores, Volume of closed pores, Surface of closed pores, Closed porosity (percent), Volume of open pore space, Open porosity (percent), Total volume of pore space, Total porosity (percent), Euler number, Connectivity, Connectivity density, Standard deviation of structure thickness, Standard deviation of structure separation, Moment of inertia (x), Moment of inertia (y), Moment of inertia (z), Polar moment of inertia, Radius of gyration (x), Radius of gyration (y), Radius of gyration (z), Polar radius of gyration, Product of inertia (xy), Product of inertia (xz), Product of inertia (yz),  
,,U,,,TV,Obj.V,Obj.V/TV,TS,Obj.S,i.S,Obj.S/Obj.V,Obj.S/TV,St.Th,St.Sp,St.Li.Dn,SCv.I,Crd.X,Crd.Y,Crd.Z, SMI,DA,,,FD,Obj.N,Po.N(cl),Po.V(cl),Po.S(cl),Po(cl),Po.V(op),Po(op),Po.V(tot),Po(tot),Eu.N,Conn,Conn.Dn, SD(St.Th),SD(St.Sp),MMI(x),MMI(y),MMI(z),MMI(polar),Gr.R(x),Gr.R(y),Gr.R(z),Gr.R(polar),Pr.In(xy),Pr.I n(xz),Pr.In(yz),  
,,um,,,U^3,U^3%,U^2,U^2,U^2,1/U,1/U,U,U,1/U,1/U,U,U,,,,,,U^3,U^2%,U^3%,U^3%,,,,1/U^3,U,U,U^5, U^5,U^5,U,U,U,U,U^5,U^5,U^5,

F:\DATA\Tarik\test1\test1\_Rec\test1\_rec.03.06.2020  
11:25.3.00012000,mm,33,255,17.76599803,4.16806427,23.46090697,50.32134319,1037.16488620,6.40057773 ,248.83610688,58.37920755,,0.05277577,,,0.02521433,0.21374499,2.54877554,,,,,,14247,104,0.00004561,0.0 3771759,0.00109425,13.59788815,76.53883630,13.59793376,76.53909303,-  
344407,358758,0.00054529,,0.04012633,,,,,,,

<<<<< End of task (0f48d623-c2e8-4ae6-9af1-e19f735d1a36) >>>>>

## Appendix 13

[System]

Scanner=SkyScan1272  
Instrument S/N=13B09011  
Software Version=1.1.9  
Home Directory=C:\SkyScan1272  
Source Type=HAMAMATSU\_L11871\_20  
Camera Type=XIMEA xiRAY16  
Camera Pixel Size (um)=7.4  
Camera X/Y Ratio=1.0149

[User]

User Name=1272 Control PC  
Computer Name=1272CONTROLPC

[Acquisition]

Data Directory=C:\data\Tarik\P-1  
Filename Prefix=P-1  
Filename Index Length=8  
Number Of Files= 940  
Number Of Rows= 1640  
Number Of Columns= 2452  
Partial Width=OFF  
Image crop origin X=0  
Image crop origin Y=0  
Camera binning=2x2  
Image Rotation=0.03400  
Optical Axis (line)= 781

Camera to Source (mm)=273.71121  
Object to Source (mm)=55.37252  
Source Voltage (kV)= 50  
Source Current (uA)= 200  
Image Pixel Size (um)=3.000149  
Scaled Image Pixel Size (um)=3.000149  
Image Format=TIFF  
Depth (bits)=16  
Reference Intensity=57000  
Exposure (ms)=672  
Rotation Step (deg)=0.200  
Use 360 Rotation=NO  
Scanning position=4.900 mm  
Frame Averaging=ON (3)  
Random Movement=OFF (20)  
Flat Field Correction=ON  
Geometrical Correction=ON  
Filter=No Filter  
Gantry direction=CC  
Rotation Direction=CC  
Type of Detector Motion=STEP AND SHOOT  
Scanning Trajectory=ROUND  
Number Of Horizontal Offset Positions=1  
Study Date and Time=04 Jun 2020 15h:38m:50s  
Scan duration=1h:5m:23s  
Maximum vertical TS=5.0

[Reconstruction]

Reconstruction Program=NRecon  
Program Version=Version: 1.6.10.4  
Program Home Directory=C:\Skyscan\nrecon 2016  
Reconstruction engine=GPUREconServer  
Engine version=Version: 1.6.10  
Reconstruction from batch=No  
Postalignment=-19.00  
Reconstruction servers= T7610  
Dataset Origin=SkyScan1272  
Dataset Prefix=P-1  
Dataset Directory=F:\DATA\Tarik\P-1  
Output Directory=F:\DATA\Tarik\P-1\P-1\_Rec  
Time and Date=Jun 08, 2020 09:34:32  
First Section=617  
Last Section=1119  
Reconstruction duration per slice (seconds)=0.268390  
Total reconstruction time (503 slices) in seconds=135.000000  
Section to Section Step=1  
Sections Count=503  
Result File Type=BMP  
Result File Header Length (bytes)=1134  
Result Image Width (pixels)=2452  
Result Image Height (pixels)=2452  
Pixel Size (um)=3.00015  
Reconstruction Angular Range (deg)=188.00  
Use 180+=OFF  
Angular Step (deg)=0.2000  
Smoothing=0  
Ring Artifact Correction=20

Draw Scales=OFF  
 Object Bigger than FOV=OFF  
 Reconstruction from ROI=OFF  
 Filter cutoff relative to Nyquist frequency=100  
 Filter type=0  
 Filter type description=Hamming (Alpha=0.54)  
 Undersampling factor=1  
 Threshold for defect pixel mask (%)=0  
 Beam Hardening Correction (%)=0  
 CS Static Rotation (deg)=0.00  
 Minimum for CS to Image Conversion=0.000000  
 Maximum for CS to Image Conversion=0.224093  
 HU Calibration=OFF  
 BMP LUT=0  
 Cone-beam Angle Horiz.(deg)=7.600709  
 Cone-beam Angle Vert.(deg)=5.087794

## Appendix 14

### Socks biaxial extension on the wooden leg

Socks were loaded on the wooden leg (Salzmann MST Switzerland, size =24cm) and marked with a known length in both wale and course directions name as (final length). After removing and relaxing, these measurements were measured again and considered as initial (length). The extension is calculated as per below equation;

$$\text{Extension [\%]} = \frac{\text{final length} - \text{initial length}}{\text{initial length}} \times 100$$

Sock code	Extension [%]	
	Wale	Course
P1	28.57	32.15
P2	37.14	57.38
P3	11.63	37.14
P4	27.50	39.09
P5	36.61	52.24
P6	24.14	46.94
P7	33.04	44.34

## Appendix 15

### Sock's washing recipe

Liquor ratio	1:20
Temperature [°C]	40
Time [min]	20
Machine speed [rpm]	10
Tubingal RGH from CHT [%]	1
Jinsofeco TWM-2 from Jintex [%]	2
pH	5.5
Citric acid for adjusting pH	